

PA 1002193

REC'D 22 OCT 2003

WIPO

PCT

# THE UNITED STATES OF AMERICA

TO ALL TO WHOM THESE PRESENTS SHALL COME:

UNITED STATES DEPARTMENT OF COMMERCE

United States Patent and Trademark Office

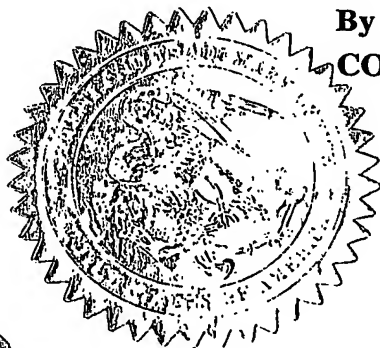
May 01, 2003

THIS IS TO CERTIFY THAT ANNEXED HERETO IS A TRUE COPY FROM THE RECORDS OF THE UNITED STATES PATENT AND TRADEMARK OFFICE OF THOSE PAPERS OF THE BELOW IDENTIFIED PATENT APPLICATION THAT MET THE REQUIREMENTS TO BE GRANTED A FILING DATE UNDER 35 USC 111.

APPLICATION NUMBER: 60/413,162

FILING DATE: September 25, 2002

PRIORITY DOCUMENT  
SUBMITTED OR TRANSMITTED IN  
COMPLIANCE WITH  
RULE 17.1(a) OR (b)



By Authority of the  
COMMISSIONER OF PATENTS AND TRADEMARKS

A handwritten signature in cursive script, reading 'E. Bornett', is positioned above the printed name.

E. BORNETT  
Certifying Officer

BEST AVAILABLE COPY

60413162.092502

A/ pre

**PROVISIONAL APPLICATION FOR PATENT COVER SHEET**  
This is a request for filing a PROVISIONAL APPLICATION FOR PATENT under 37 CFR 1.53(c).

INVENTOR(S)					
Given Name (first and middle (if any))	Family or Surname		Residence (City and either State or Foreign Country)		
1 Roger	Guevremont		Ottawa, Ontario, Canada		
2 Yves	Baribeau		Ottawa, Ontario, Canada		
3 Lucien	Potvin		Ottawa, Ontario, Canada		
<input type="checkbox"/> Additional inventors are being named on the sheet attached hereto.					
TITLE OF THE INVENTION (280 characters max)					
Waveform Generator, Waveform Optimization, and New Electrode Geometry for High-Field Asymmetric Waveform Ion Mobility Spectrometry					
Direct all correspondence to: CORRESPONDENCE ADDRESS					
<input checked="" type="checkbox"/> Customer Number 25,319					
Firm or Individual Name		Freedman & Associates			
Address		117 Centrepointhe Drive			
Address		Suite 350			
City	Nepean	Province	Ontario	Postal Code	K2G 5X3
Country	Canada	Telephone	(613) 274-7272	Fax	(613) 274-7414
ENCLOSED APPLICATION PARTS (check all that apply)					
<input checked="" type="checkbox"/>	Specification	Number of pages:	109		
<input checked="" type="checkbox"/>	Drawing(s)	Number of Sheets:	32		
<input type="checkbox"/>	Other	(Specify):			
METHOD OF PAYMENT OF FILING FEES FOR THIS PROVISIONAL APPLICATION FOR PATENT					
<input checked="" type="checkbox"/> Applicant claims small entity status See 37 CFR 1.27.					FILING FEE AMOUNT (4)
<input checked="" type="checkbox"/> The Commissioner is hereby authorized to charge filing fees or credit any overpayment to Deposit Account Number: 50-1142					\$80.00
The invention was made by an agency of the United States Government or under a contract with an agency of the United States Government.					
<input checked="" type="checkbox"/> No.					
<input type="checkbox"/> Yes, the name of the U.S. Government agency and the government contract number are:.....					

Respectfully submitted,

DATE: September 24, 2002

SIGNATURE:



TYPED or PRINTED NAME: Gordon Freedman

DOCKET NO: 151-02 US Prov

REGISTRATION NO : 41,553

EMAIL: gordon@ipatent4u.com

TELEPHONE: (613) 274-7272

FAX: (613) 274-7414

09/25/02  
JC923 U.S. PTO

60413162  
JC923 U.S. PTO

**Waveform Generator, Waveform Optimization, and New Electrode  
Geometry for High-Field Asymmetric Waveform Ion Mobility  
Spectrometry**

**Inventors: Roger Guevremont, Yves Baribeau and Lucien Potvin  
Ionalytics Corporation  
Ottawa, ON  
Canada.**

Addresses (as of September 24, 2002):

Roger Guevremont (Canadian, employee of Ionalytics, inventions assigned to Ionalytics)  
2059 Gatineau View Cr.,  
Ottawa, Ontario, Canada

Yves Baribeau (Canadian, employee of Ionalytics, inventions assigned to Ionalytics)  
1124 St. Emmanuel Terrace,  
Ottawa, Ontario, Canada

Lucien Potvin (Canadian, contract with Ionalytics, inventions assigned to Ionalytics)  
29 Goulding Crescent,  
Ottawa, Ontario, Canada

## Table of Contents:

Table of Contents:	2
1. Introduction	4
1.1 Operation of Drift Tube Ion Mobility Spectrometry (DTIMS)	9
1.1.1 Recent Advances in Drift Tube Ion Mobility Spectrometry	10
1.2 High-Field Asymmetric Waveform Ion Mobility Spectrometry (FAIMS)	12
1.3 Recent advances in FAIMS	17
1.4 Literature Cited in the Introduction Section	28
1.5 Publications and Patents Closely Related to FAIMS	31
2. Objectives of the Inventions in this Provisional Patent Submission	39
3. Invention #1: Waveform Generator Electronics Based on Tuned LC Circuits	43
4. Inventions #2 and #3: Algorithms for Automated Optimization of the Asymmetric Waveform Generator LC Tuning Electronics	51
4.1 Algorithm for Control of the Asymmetric Waveform: INVENTION #2	53
4.1.1 Waveform Feedback and Control Algorithm	59
4.2 Algorithm for Control of the Asymmetric Waveform: INVENTION #3	63
4.2.1 Waveform Feedback and Control Algorithm	67
5.1 New FAIMS Electrode Assembly based on Stacked Parallel Plates, INVENTION #4	71
5.2 New FAIMS Electrode Assembly based on Stacked Parallel Plates facing a Flat Surface, INVENTION #5	75
5.3 Ion Motions in the FAIMS Electrode Assemblies Based on Layered Plates	76
6. Invention #6: New Version of the FAIMS Electrodes: Parallel Rods	83



6.1	A FAIMS Electrode Based upon an Array of Parallel Rods. ....	84
6.2	Ion Motions in the FAIMS Electrode Assemblies Based on Parallel Rods.....	86
7.	Invention #7: Operation of FAIMS Electrodes in Quadrupole Configuration.....	90
	Figure Captions (incomplete descriptions) .....	106

## 1. Introduction

Literature cited in this introduction section is indicated by brackets (x) and the expanded literature citation appears in section 1.4, page 27. Previous literature and patents filed by the present inventors and others appears in section 1.5 beginning on page 31.

The origins of high-field asymmetric waveform ion mobility spectrometry (FAIMS) date back to at least 1982 and a Russian inventor's certificate(1). Since that time, FAIMS has undergone several technological advancements and has become a powerful analytical tool, particularly for processing ions prior to their introduction into mass spectrometers. A brief discussion of the principles of operation of a FAIMS device will follow with emphasis on the properties particularly relevant to this patent application. This section also describes several key advances in the FAIMS technology.

Ion mobility spectrometry is a global term used to identify a technology in which ions are traveling through a bath gas that is at sufficiently high pressure that the ion rapidly reaches constant velocity when driven by the force of a constant (in time and location) electric field. This is to be clearly distinguished from those techniques, most of which are related to mass spectrometry, in which the gas pressure is sufficiently low that, if under the influence of a constant electric field, the ion will continue to accelerate. Because this indefinite acceleration is usually undesirable within the confines of a vacuum chamber of a mass spectrometer, in mass spectrometry the ions are generally exposed to electric fields of a transient nature (in either time or physical location), which may even reverse directions intermittently, in order that the ion velocity not increase indefinitely.

Drift tube ion mobility experiments (prior to FAIMS) generally operate with a uniform in space, constant-in-time electric field to cause the ion drifting through a (high pressure) gas to reach a constant velocity. The magnitude of this constant velocity is related to a property of the ion called 'ion mobility', which is the proportionality constant between the ion velocity and the strength of the electric field. For example, at low electric fields and high gas pressure (low  $E/N$ ) where  $E$  is the strength of the electric field and  $N$  is the number density of the gas, the doubling of the ion mobility will result in doubling of the velocity of the ion (in a constant  $E/N$ ). Similarly, at low electric fields and high gas pressure, the doubling of the strength of the electric field will double the velocity of the ion, if the ion mobility is constant under the applied conditions of field strength and gas density. Note that the 'ion mobility constant' usually shown as  $K$ , is not actually constant in all conditions, but may vary with temperature, electric field strength, type of gas, gas pressure and other ambient conditions. Naturally, since FAIMS is a type of ion mobility (characterized by a sufficiently high gas pressure that the ions come to constant velocity in a constant field), the gas pressures suitable for operation of FAIMS correspond to the same ranges of pressures in which drift tube ion mobility spectrometers will operate.

At pressures higher than that necessary for the ion to achieve constant velocity, as the ion drifts in a constant (in time) electric field ( $E/N$ ), in a time less than 0.01 microseconds, the previous (literature and patents) discussions of FAIMS are a good approximation to the behavior of the ions, and all of the FAIMS technology previously discussed is applicable at these and higher pressures. This pressure range will therefore be called "high pressure". At very low pressures (below  $10^{-5}$  torr), the mean free path between collisions is long and FAIMS cannot function in the manner previously described. Clearly there is an intermediate range of pressures

wherein the ion requires significant distance/time to reach constant velocity (for example, distances over 5% of the size of the distances between electrodes and/or over 5% of the duration of the cycle of the waveform). Although FAIMS will function in this pressure region, some changes in the details of the mechanism of separation must be considered (acceleration and deceleration distances/times required by the ion). For emphasis on this point, the reason that the ion mobility changes with  $E/N$  is related to collisions with the bath gas. The longer range ion-dipole attractive force and the close range repulsions between the ion and the gas molecule contribute to different degrees to the collision as a function of the relative velocity between the ion and molecule when the collision takes place. At high relative collision velocity (ion moving in fields with higher  $E/N$ ) the long range attractive effects are less significant than they would be for lower velocity collisions. This is apparent if we consider a low relative velocity encounter between the ion and the gas molecule. Assume that the ion is on a path that would bring the ion close to, but not into collision with, the gas molecule. Nevertheless, the collision does take place because the ion-dipole attractive interaction created by the influence of the ion on the electrons of the gas molecule pulls the ion from its original straight line trajectory towards the gas molecule. If the same original trajectory of ion and molecule was repeated at high relative velocity, the ion and the molecule do not collide because the attractive ion-dipole interaction is not strong enough to pull the two together to create the collision. This is an example in which the size (collision cross section) of the ion appears to decrease as the ion energy, i.e., the relative velocity difference between the ion and the bath gas molecule increases. Since this fast moving ion seems to avoid some collisions, the ion mobility appears higher than it would be at low velocity. In this case the ion mobility is seen to increase at the higher  $E/N$ . In summary therefore, if there are interactions between the ion and the bath gas molecules, these interactions

may have an effect on the apparent size of the ion, and as a result of this apparent size change, the ion mobility may change as a function of the speed of the ion, or alternately stated, as a function of the electric field ( $E/N$ ).

For simplicity the ratio ( $E/N$ ) which describes the electric field strength at gas pressures with number density  $N$ , will be replaced by  $E$  in this document. It is well known that the velocity of an ion drifting in an electric field will be proportional to  $E/N$ , i.e., if the gas pressure is decreased ( $N$  decreased) by a factor of two the ion velocity will double if the voltage applied to the electrodes remains constant (as long as  $E/N$  remains "low"). In order to avoid discussions of the effect of gas pressure, the ratio  $E/N$  will often be used interchangeably with the "electric field" or  $E$ . If limitations of pressure, other than the pressure range generally considered appropriate for ion mobility spectrometry, are important, these limitations and conditions will be discussed separately.

The three types of 'ion mobility' spectrometers that are described here are well known in the literature. The design and the hardware of 'ion mobility spectrometers' can be very different from each other and deducing the design of one type from the design of another type of ion mobility spectrometer is not obvious. Although the devices are all considered under the generic name 'ion mobility', the design of the hardware, the mechanism of operation, and the applicability to specific ion separation problems is very distinctive in each case. The techniques share the name 'ion mobility', and share the feature that they operate at sufficiently high gas pressure that the ion velocity is constant in a constant electric field, but the similarities usually do not extend any further.

The three types of an 'ion mobility spectrometer' include:

(1) Drift tube ion mobility spectrometry (DTIMS) was developed in the 1970's and detailed descriptions of this technique can be found in two well known books by Eiceman(2) and Mason and McDaniel(3). Commercial systems are available from vendors including Barringer Research (Mississauga), Barringer Instruments Inc. (New Jersey), and PCP Inc. (Florida).

(2) A second system based on the perpendicular combination of gas flow and electric field is called Transverse Gas Flow Ion Mobility Spectrometry (TGFIMS). Although it has been described in the patent literature, there is no commercial exploitation of this concept at present.

(3) A third, newer type of ion mobility spectrometer is presently under development. The new system is called High-Field Asymmetric Waveform Ion Mobility Spectrometry (FAIMS).

In the following sections, the operation of DTIMS and FAIMS will be reviewed. Although the descriptions are not intended to be comprehensive and thorough overviews of each technology, they are included below to eliminate possible misunderstanding of the technology that could arise through the use (or mis-use) of the names applied to the devices. Because the names of various technology may change in time, we define the name and approach of these technologies below, and it is understood that although other names are used in the scientific literature, the commercial literature, and elsewhere in the world, an expert in this field will recognize the technology from the description below and will understand the naming scheme used in this provisional patent.

## **1.1 Operation of Drift Tube Ion Mobility Spectrometry (DTIMS)**

In brief, a drift tube ion mobility spectrometer separates ions as a function of the drift velocity of ions in a high pressure gas. The gas is at sufficiently high pressure that the ions drift at a constant velocity while under the influence of a uniform, fixed in time, constant strength electric field. In one possible embodiment, the electric field is generated using a set of parallel flat plates each having an aperture through which ions pass, and each of which is connected to a dc power supply. The plates are aligned so that the ions will drift down the channel created by the alignment of the apertures in each of the parallel plates. The voltages applied to the individual plates are adjusted so that a uniform, constant strength field is generated along the set of plates. The voltages applied to the plates do not change as a function of time while the ions are drifting through the flight tube. For example, in a system composed of a set of uniformly spaced plates, a constant voltage difference from plate to plate will generate an (approximately) uniform electric field. An ion that is located in the channel through the plates will drift along the channel at a constant velocity that is determined by the field strength, direction, and the mobility of the ion at the particular conditions of temperature, gas pressure, electric field strength, and type of bath gas. Typically a mixture of ions is gated (or injected) into this device as a small, physically compact, cloud of ions. The ions drift at velocities characteristic of each ion type, and therefore arrive at a detector at various times after their injection, the fast moving ions arriving after a short time, and the slow moving ions after a longer time. The drift times are dependent on the ion velocity, and hence the ion mobility of each type of ion, and are characteristic of each ion type. This type of ion mobility spectrometer can only separate ions having differences in the magnitude of the 'mobility constant' (i.e., the types of ions that are to be separated must drift

through the gas, in a constant electric field, at different velocities). This type of ion mobility spectrometer cannot separate two types of ions (for example) that have identical ion mobilities at the operating conditions of the drift tube, irrespective of whether the ion mobilities of these species increase or decrease differently when the ions are exposed to very strong electric fields. DTIMS generally only operates at low fields.

### **1.1.1 Recent Advances in Drift Tube Ion Mobility Spectrometry**

In the early 1980's, during the development of electrospray ionization (ESI), drift tube ion mobility spectrometry was used by Dole and his co-workers(4) for the separation of electrospray-generated ions. More recently, ESI-DTIMS has been used in conjunction with mass spectrometry(5-11). Guevremont et al.(12) described the first combination of ESI-IMS-TOFMS (time-of-flight mass spectrometer) and have demonstrated this system with several electrospray-generated ions. More recently, Jarrold and Clemmer(9-11, 13, 14) have described systems that are capable of determining the cross sections of proteins and peptides by measuring the drift time of these ions in drift tubes (operated below atmospheric pressure) combined with quadrupole and time-of-flight mass spectrometers. This technology offers significant promise for the rapid determination of the peptides resulting from enzymatic protein digestion. The data from a tandem combination of a drift tube ion mobility separation and TOFMS can be viewed as a 2-dimensional array, a technique described by Clemmer(10).

Drift tube ion mobility spectrometry suffers two significant limitations: First, the ions arrive at the detector (e.g., electrometer-based electric current measurement, or alternatively a mass spectrometer) in a short pulse; and, secondly, the ion transmission efficiency of a DTIMS is low. These limitations are considered briefly below.



The transient ion signal from a DTIMS system is ideally suited to target-compound analysis, but is unsuitable for some types of ion detectors, including those that scan over a wide mass-range. For example, the transient of ions from the DTIMS separation is too short to permit a reasonable mass range scan with a quadrupole mass spectrometer. This limitation is overcome by using of a Time-of-Flight mass spectrometer (TOFMS) for ion detection. However, this tandem system of DTIMS-TOFMS is a combination of two transient-based instruments and the resulting overall efficiency is exceedingly low. In this system, the TOFMS is idle for the periods of time between the arrivals of DTIMS-separated pulses of ions. Even during the arrival of a pulse of ions, the TOFMS samples ions intermittently because a delay is required while the ions drift to the detector. Nevertheless, due to the enormous quantity of data that results from the collection of this 2-dimensional array (drift time versus mass-to-charge), the future of this technology for rapid, high-throughput analysis of proteins and protein tryptic digests is exciting.

The DTIMS lacks a mechanism for confining the ions in space. The ions disperse and spread out in space due to diffusion and space-charge ion-ion repulsion, and dispersion increases with increasing drift time. Since the ion beam is not physically focused along the center axis of the drift tube, the transfer of ions into the orifice leading to the MS is not efficient because only a limited number of the ions within the spreading ion beam remain in a location appropriate to land directly on the orifice. This beam spreads with time and with the distance that the beam is required to travel. In practice, this problem is addressed by minimizing the ion drift time. A minimized drift time will result in less spreading of the pulse of ions, with the realization of improved intensity (i.e., more of the ions are near the center axis of the orifice) and better resolution (i.e., the ions arrive in a narrow time-period).

## **1.2 High-Field Asymmetric Waveform Ion Mobility Spectrometry (FAIMS)**

The two limitations of drift tube ion mobility spectrometry discussed above are overcome by the new FAIMS technology that will be described briefly in this provisional patent. The FAIMS separation system operates continuously and permits quadrupole-based mass spectrometers to collect wide mass-range scans. Moreover, FAIMS has the capability to focus and confine ions in space by overcoming diffusion and space-charge ion-ion repulsion. The ion transmission efficiency of a combined ESI-FAIMS-MS system can be high.

Although the FAIMS is a type of ion mobility based technology, it is readily distinguished from all other types of ion mobility spectrometers by two main features. First, the applied electric fields are variable in time (i.e., a waveform is applied) whereas all other types of ion mobility rely on constant applied voltages. Second, FAIMS in a cylindrical geometry (as well as other geometries) can focus ions to prevent spreading in space and time. No other ion mobility spectrometer has ever had this beneficial property.

FAIMS separates ions by taking advantage of differences in the 'ion mobility',  $K$ , of ions under the influence of weak electric fields, and the 'ion mobility' of ions under the influence of strong electric fields. The mobility of the ion at sufficiently high fields such that it has changed from  $K$  will be referred to as  $K_h$ , for simplification of the discussion here. FAIMS will function under the same conditions of gas pressure, gas temperature and gas composition as conventional drift tube ion mobility spectrometry and thus retains the generic name "ion mobility".

Note however, that FAIMS does not separate ions of high mobility from those of low mobility (as was discussed above for DTIMS). Instead, FAIMS separates ions whose mobility increases (or decreases) more rapidly at high field strength ( $E/N$ ) from those whose mobility

increases (or decreases) less rapidly at high field. The difference in separation mechanism of DTIMS and FAIMS means that one technology may be capable of separating a given set of compounds from each other while the other cannot. If two compounds can be separated by DTIMS, it cannot be predicted whether or not they can be separated by FAIMS. Similarly, FAIMS may separate pairs of ions that cannot be separated by DTIMS systems. The independence of these types of separations is important both from a commercial applications point of view as well as from a patent point of view. A given separation by FAIMS is not predictable or obvious, from any analogous separation previously accomplished (or not accomplished) by DTIMS.

Since FAIMS is relatively new, a description of the technique is appropriate. The principles of the operation of a flat parallel plate geometry of FAIMS have been described by Buryakov et. al.(15). Some description of the mechanism of ion separation using FAIMS is outlined below, since FAIMS has previously been called by other terminology. This will avoid ambiguity introduced by differing nomenclature.

The mobility of a given ion under the influence of a high electric field can be expressed by:

$$K_h(E/N) = K[1+f(E/N)]$$

Where K is the ion mobility at low electric field,  $K_h$  is the ion mobility at high electric field, and where  $f(E/N)$  describes the functional dependence of the ion mobility on field strength. When both high and low electric fields are applied at the same fixed conditions of temperature, gas pressure, gas composition etc., we simplify this equation to  $K_h(E) = K[1+f(E)]$ .

Figure INTRO1 illustrates three possible examples of the change in ion mobility with electric field. The separation of ions in FAIMS is based upon these changes in mobility.

To illustrate how FAIMS separates ions, consider a positively charged type A ion (type A defined by the curves in Figure INTRO1) that is being carried by a gas stream between two parallel plates shown in Figure INTRO2. One of the plates is maintained at ground potential while the other has an asymmetric waveform, described by  $V(t)$  applied to it. The peak voltage applied during the waveform is called the dispersion voltage (DV). The waveform is synthesized so that the electric fields during the two time periods  $t_{\text{high}}$  and  $t_{\text{low}}$  are not equal. If  $K_h$  and  $K$  are identical at high and low fields, the ion will be returned to its original position relative to the plates at the completion of one cycle of the waveform. However, under conditions of sufficiently high electric fields,  $K_h$  is greater than  $K$  and the distances traveled during  $t_{\text{high}}$  and  $t_{\text{low}}$  are no longer identical. The ion will experience a net displacement from its original position relative to the plates as illustrated by the dashed line in Figure INTRO2.

If a type A ion (type A defined in Figure INTRO1) is migrating away from the upper plate, a constant negative dc voltage ("compensation voltage", CV) can be applied to this plate to reverse or "compensate" for this offset drift. At an appropriately selected applied CV voltage, the ion will not travel toward either plate. If two types of ions respond differently to the applied high electric field (i.e., their ratios of  $K_h$  to  $K$  are not identical), the compensation voltages necessary to prevent their drift toward either plate will be different. If the CV voltage is set to be appropriate to prevent the first ion from hitting the plates, the second ion will drift to a plate and be lost, similarly, at the appropriate CV voltage to prevent the second ion from hitting the plates, the first ion will be lost. To analyze a mixture of ions, the compensation voltage can be scanned

to transmit each of the components of the mixture in turn. This produces a compensation voltage spectrum (CV spectrum).

It is important to note from Figure INTRO2 that the ion is being carried by a gas stream, and the time that the ions spend between the plates (assuming that the applied voltages are selected to prevent drift to one of the plates), is only a function of the velocity of the flow of gas. All types of ions, of all sizes and mobilities, will spend identical time between the plates shown in Figure INTRO2. For example, if CV and DV are selected so that a type A ion (for example  $\text{Cs}^+$ ) does not drift to the plates shown in Figure INTRO2, then the time required to travel from the left side of the plates in Figure INTRO2 is  $v_g/d$  where  $v_g$  is the velocity of the flow of the gas, and  $d$  is the distance from the left edge (ion entrance) of the plates in Figure INTRO2 to the right edge of the plates (ion exit). Similarly if the DV and CV are selected so that a type C ion (for example a cytochrome c ion with a charge of +16) will not drift to the plates, this ion will also spend a time of  $v_g/d$  between the plates. In both cases the ions spend time equal to  $v_g/d$  between the plates. By contrast, in a drift tube ion mobility spectrometer, the various ions spend differing times in the drift tube, because the drift time is dependent on the mobility of each type of ion being separated. In DTIMS, the  $\text{Cs}^+$  ion (which has a high ion mobility) will spend a shorter time in the drift tube than the cytochrome c ion with a charge of +16. Note that both types of ion mobility spectrometers, DTIMS and FAIMS are capable of separating  $\text{Cs}^+$  and the cytochrome c ion with a charge of +16. In DTIMS these ions are separated because they have differing drift velocities (a function of the size and charge state of the ion), whereas in FAIMS they are separated because the ion mobility changes differently in strong electric fields (i.e.,  $\text{Cs}^+$  is a type A ion, and a cytochrome c ion with a charge of +16 is a type C ion, where A and C are defined in Figure INTRO1). It is very important to also note that using DTIMS itself, identification of the

type of ion (Figure INTRO1) is not feasible, and that the type of ion (Figure INTRO1) cannot be defined '*a priori*' on the basis of the ion mobility defined by the drift of the ion in a DTIMS.

The introduction of a concentric cylinder-FAIMS by Carnahan et al. (16) provided an increase in sensitivity over the flat plate geometry used by Buryakov et al. (15). Mine Safety Appliances Company (Pittsburgh, PA) (MSA) developed an instrument called a "Field Ion Spectrometer" or FIS for trace gas analysis. Their instrument consisted of a FAIMS device using electrometer based detection (FAIMS-E) rather than mass spectrometric detection. The FAIMS-E was shown to be capable of separating compounds having the same low-field mobility constant(17). This technology was limited in that several of the peaks appearing in the CV spectra (ionogram) could not be identified unambiguously(17-19). In a collaborative project between the National Research Council of Canada (NRCC) and MSA, the elimination of this shortcoming of FAIMS-E through the interfacing of FAIMS to a mass spectrometer (now referred to as FAIMS-MS), was described (20).

Guevremont and Purves(21-23) have described the reason for the high sensitivity achieved with a cylindrical geometry FAIMS. Theoretical ion trajectory calculations and experimental results support a model based on atmospheric pressure ion focusing within the FAIMS analyzer. Ions that are transmitted through FAIMS under suitable DV and CV conditions fall into a potential well that is located between the concentric cylinders of FAIMS. This focusing field acts to reverse the effects of diffusion, space charge repulsion and turbulence, thereby significantly reducing the loss of ions to the walls of the device. In general, the compounds that are transmitted at high magnitudes of CV appear to have the highest ion transmission efficiency through FAIMS.

As a consequence of ion focusing in a cylindrical FAIMS apparatus, the instrument operates in four distinct modes: namely P1, P2, N1 and N2 where P and N describe ion polarity (positive and negative), and "1" and "2" are indicative of the polarity of the asymmetric waveform(20, 24). Spectra collected using a positive DV are of type P1 or N2 while spectra collected using a negative DV are of type P2 or N1. In each case the compensation voltage can be positive or negative. The conditions wherein the ion is at a stable (non drifting) trajectory, and is focused (to minimize loss to the walls) are dependent on the ionic charge polarity and the behavior of the ion in strong electric fields as shown in Figure INTRO1.

### **1.3 Recent advances in FAIMS**

The first reports describing FAIMS discussed hardware development and the theory of ion motion in this device(15, 20, 23, 25). The first study using ESI-FAIMS-MS was reported by Guevremont and Purves in early 1999(26). In this report, the electrospray-generated ions of the peptide leucine enkephalin were separated by FAIMS and analyzed by MS and MS/MS. Several types of isobaric ions, including  $[M + H]^+$  and  $[2M + 2H]^+$  ions, both with  $m/z$  556.5, were observed to be separated by FAIMS. Four complex ions  $[2M + H]^+$ ,  $[4M + 2H]^{2+}$ ,  $[6M + 3H]^{3+}$  and  $[8M + 4H]^{4+}$ , all with  $m/z$  1112, could also be separated.

A schematic of this FAIMS-MS system that was described previously is shown in Figure INTRO3. In brief, the apparatus was composed of two short inner cylinders, that were axially aligned and positioned about 5 mm apart, and a long outer cylinder that surrounded the two inner cylinders. The inner cylinders (12 mm inner diameter and 14 mm outer diameter) were about 3 and 9 cm long, respectively, whereas the outer cylinder (18 mm inner diameter) was about 125 mm long. Ion separation occurs in the 2 mm annular space of the FAIMS analyzer region

between the long inner cylinder and the outer cylinder. The ionization source was housed within the short inner cylinder terminating short of the gap between the two cylinders. Four gas connections to the apparatus (all adjustable) are shown. A gas was passed through a charcoal/molecular sieve purification cylinder (not shown) and into the FAIMS device through the carrier gas in and/or sample gas in ports. The gas exited the device through the carrier out and/or sample out ports. For the first study using a corona discharge needle(21), volatile analytes were introduced into the FAIMS through the sample in port. Later studies used an electrospray ionization source to introduce analytes into the FAIMS device.

Still referring to Figure INTRO3, positively charged ions formed within the short inner cylinder are driven radially outward by the electric field of the ionization needle (biased to +3000 volts, for example), whereas neutrals travel through the center of the long inner cylinder and exit via the sample out port. Neutrals are prevented from entering the annular FAIMS analyzer region by a portion of the carrier gas flow that is directed radially inward through the gap (or ion inlet) between the two inner cylinders and exits via the sample out port. This portion of the carrier gas flow that travels radially inward is counter-current to the ions being driven radially outward and acts to reduce the solvation of the ions. Some of the ions produced by the ionization source are carried by the gas stream along the length of the annular space between the outer cylinder and the long inner cylinder (i.e., the FAIMS analyzer region). If the combination of DV and CV are appropriate to prevent the ion from being lost to the walls, an opening (or ion outlet) near the downstream end of the outer cylinder allows some of the transmitted ions to be carried by the gas flow to the sampler cone where they are sampled by the mass spectrometer.

The first ESI-FAIMS-MS spectrum of a protein was reported by Purves and Guevremont in Analytical Chemistry in July 1999(24) using the system shown in Figure INTRO3. The ESI-



generated ions of the protein equine cytochrome c were transmitted through FAIMS at negative CV values using P2 mode. This study provided the first experimental data showing that the ion mobility of these multiply-charged protein ions decreases at high electric field (as illustrated by trace C in Figure INTRO1). The mass spectra of cytochrome c collected at two compensation voltages spaced about 1 volt apart showed slightly differing multiply-charged ion distributions suggesting that these ions can be differentiated using FAIMS. In addition, the FAIMS separation of a series of poly-glycine peptides showed that the short peptides containing up to 5 residues were transmitted in P1 mode, whereas the longer peptides were transmitted in modes P2 or N2. Mode 2 transmission was also observed for the positive ions of leucine enkephalin (i.e., P2 mode) and the negative ions of substance P (i.e., N2 mode). Mass spectra collected at the CV of optimum transmission of each of the polyglycine peptides revealed complete separation of each peptide from that of the lower and higher analogs. Moreover, the mass spectra of the peptide ions separated using FAIMS were greatly simplified and had significantly reduced background noise.

A report on the separation of the isomeric amino acids leucine and isoleucine was published in December 1999(27). The separation of leucine and isoleucine by FAIMS illustrates that significant benefits in analytical speed can be achieved relative to methods such as HPLC separation. This report showed that leucine and isoleucine were transmitted through FAIMS at slightly different CV. In practice therefore, the compensation voltage may be changed step-wise electronically to permit independent measurements of each ion. Because the time required for the ions to travel the length of FAIMS cylinders is a function of the gas flow rate through the analyzer and the signal at a new CV requires between 20 and 200 msec to stabilize, the minimum time for independent measurements of both ions would be about 500 msec (for example). The

separation by HPLC takes several minutes. This report also showed a comparison of ESI-MS and ESI-FAIMS-MS, and an improvement of the signal-to-background of over 50 was observed for the new ESI-FAIMS-MS technique. This improvement is a result of the separation of the analyte ions from the chemical background ions that characterize a conventional ESI-MS spectrum. The detection of leucine and isoleucine in nanomolar (nM) concentrations without sample preconcentration or condensed phase separation is possible using ESI-FAIMS-MS.

As part of a project supported by AWWARF (American Water Works Association Research Foundation) and the University of Alberta, the FAIMS separation and detection of chlorinated byproducts of drinking water disinfection has been studied(28). The detection limits for six haloacetic acids, a class of compounds regulated by the US EPA, ranged from between 0.5 and 4 ng/mL in a 9:1 methanol/water solvent mixture with no preconcentration, derivatization or chromatographic separation prior to ESI-FAIMS-MS analysis. A comparison of mass spectra acquired with conventional ESI-MS and with ESI-FAIMS-MS showed significant improvement in signal-to-background ratio using ESI-FAIMS-MS, with minimum signal intensity deterioration. A flow injection technique with a rate of replicate analytical measurement of about 2 minutes per sample was also demonstrated.

Parts-per-trillion detection limits of inorganic water contaminants using ESI-FAIMS-MS have been achieved(29). Because of the significant decrease in the background ion intensity, the measurement of chlorate, bromate and iodate was improved by 3 to 4 orders of magnitude compared with conventional ESI-MS. The background ion intensity was sufficiently low that the ions containing  $^{18}\text{O}$ , such as  $^{81}\text{Br}^{18}\text{O}^{16}\text{O}^-$ , were readily observed in the ESI-FAIMS-MS experiment.

An important advance in FAIMS-MS technology was the creation of the prototype shown in Figure INTRO4, which will be referred to as the “dome” prototype. The device in Figure INTRO4 is cylindrical, wherein the inner electrode is a solid cylindrical rod terminating in a smooth hemispherical 'dome' shape. The outer electrode is a hollow cylinder open at one end (left side of Figure INTRO4) but closed at the other end except for a small ion outlet orifice. Inside of the closed end, the outer electrode is machined with a curved internal spherical shape in such a way that the spacing between the inner and outer electrodes can be constant when the inner electrode is mounted inside of the outer electrode as shown in Figure INTRO4. Provision is also made to permit the inner electrode to slide a short distance longitudinally along the center of rotation of the cylindrical geometry to adjust the distance between the tip of the hemispherical surface of the inner electrode and the ion outlet orifice of the outer electrode. This geometry has key differences compared with the FAIMS-MS shown in Figure INTRO3. A critical difference is that the inner cylinder of the “dome” prototype ends in a hemispherical shape near the ion outlet. This geometry provides an advantage in sensitivity compared with the device shown in Figure INTRO3 because ions are more efficiently sampled by the mass spectrometer since all stable ions in the annular analyzer space are brought to the centre axis at the terminus of the inner electrode (i.e., extraction region) and are focused toward the orifice plate of the mass spectrometer. The previous device (Figure INTRO3) was only able to sample a small portion of the total ions in the annular space of the FAIMS device.

Figure INTRO4a shows a device in which the ionization source is placed external to the FAIMS device. In practice it is often necessary to include, as shown in Figure INTRO4b, a separate desolvation chamber between the ionization source and the ion inlet through the outer electrode into the FAIMS device. The only openings in the desolvation chamber are the curtain

gas inlet, the curtain plate orifice, and the ion inlet through the FAIMS outer electrode. A conductive curtain plate (having an opening referred to as the curtain plate orifice for allowing ions produced by the ionization source to enter the desolvation region) is electrically isolated and located between the ionization source and the ion inlet. In operation, the voltages applied to these conductive surfaces may be +4000 V (electrospray ionization source), +1000 V (curtain plate), and 0 V (outer electrode), for example. A gas (i.e., the curtain gas shown in Figure INTRO4b) is introduced into the desolvation chamber through an inlet (i.e., curtain gas in). As is shown schematically in the diagram, the curtain gas splits into two flows, i.e., the desolvation gas and the carrier gas entering the analyzer region. The desolvation gas exits the desolvation region through the curtain plate orifice in a direction approximately countercurrent to the ions entering the curtain plate orifice. This gas assists in desolvating the ions (i.e., reducing the solvent content) and functions to reduce the amount of neutral solvent and other gas impurities that pass into the desolvation chamber and eventually into the analyzer region of the FAIMS device through the ion inlet. Solvent and other gas impurities can have adverse affects on the performance of the FAIMS device and the desolvation gas functions to prevent these gases from entering the FAIMS device. The ions are able to pass through this countercurrent flow of gas and into the desolvation region because of the strong electric field produced by the high voltage difference between the ionization source and the curtain plate. The high voltage applied to the electrospray needle, in addition to producing an intensely strong electric field that creates conditions necessary to ionize the components of a liquid sample, also results in a strong electric field that directs electrosprayed ions (of the appropriate charge polarity) away from the source and toward the curtain plate. The carrier gas transports ions through the ion inlet in the outer electrode of the FAIMS device and into the analyzer region. The carrier gas flow will continue

ብሉይ ስራ ለማድረግ ለሚገባው ሰው ማዕከላዊ ስራ ማድረግ ይቻላል።

By operating a dome FAIMS device in near trapping conditions [PCT/CA99/00718], ions are more efficiently sampled by the mass spectrometer since all stable ions in the annular analyzer space are brought to the centre axis at the terminus of the inner electrode (extraction region) and are focused toward a region close to the orifice plate of the mass spectrometer. Ions at every location around the circumference of the inner electrode shown in Figure INTRO4 are brought to the center axis of the inner electrode at the tip of the hemispherical dome because the gas flow is converging from all directions towards the ion outlet (gas being pulled into the

vacuum chamber of the mass spectrometer). This type of a dome device first appeared in the literature in a study that examined the cross sections of gas-phase bovine ubiquitin conformers(31). The sensitivity of the device was illustrated by several publications that dealt with a variety of applications. For example, trace level determination of perchlorate in a water matrix was found to provide a detection limit of 50 ppt, whereas the current US EPA method for analyzing perchlorate in water using ion chromatography has a reporting limit of 4 ppb(32). The analysis of a tryptic digest of pig hemoglobin using ESI-FAIMS-MS showed a substantial decrease in the background ion intensity while maintaining comparable sensitivity to conventional ESI-MS(33).

Another important advance in the application of FAIMS technology was the discovery of the use of mixed carrier gases [PCT/CA01/00310]. A publication describing the separation of o-, m-, and p-phthalic acids using ESI-FAIMS-MS showed that these three isomers could not be separated using either pure nitrogen or carbon dioxide gases, but that they could be separated using a mixture of 95:5 nitrogen and carbon dioxide(34). The observed behavior of the three isomers in mixed carrier gases did not follow the theoretical predictions of the dependence of ion mobility on electric field in gas mixtures. Different combinations of mixed carrier gases have been used to improve sensitivity and detectability of various analytes including but not limited to nine chlorinated and brominated haloacetic acids(35) as well as morphine and codeine in human urine(36).

The dome FAIMS device carries ions from the ion inlet to the ion outlet of FAIMS by a gas flow in a direction along the length of the analyzer region (i.e., carrier gas flow as shown in Figure INTRO4), parallel to the longitudinal axis of the inner electrode then around the curved end of the hemispherical tip of the inner electrode. Finally the ions are pulled, by the flow of

gas, into the vacuum chamber of the mass spectrometer. In a general consideration of the direction of motion, the ions travel into the mass spectrometer in a direction approximately orthogonal to their original direction of motion as they traveled between the electrospray needle and the curtain plate orifice. Because of the difference in directions of travel of ions entering the ion inlet and the ions passing through the ion outlet to the detector, the FAIMS device shown in Figure INTRO4 cannot be immediately substituted for the original combination of the ionization source and the detector. For example, with a conventional electrospray ionization source for mass spectrometry, the ions travel in only one direction straight from the tip of the electrospray needle towards the orifice leading to the vacuum chamber of the mass spectrometer. The earlier dome FAIMS device (Figure INTRO4) is located at a distance and at an angle that would make it other than possible to mount the ESI-dome FAIMS device as a direct, simple replacement for ESI, if the electrospray needle was only translated directly away from the orifice of the mass spectrometer. A FAIMS geometry (Figure INTRO5) that overcomes this limitation [PCT/CA01/00308] involves a design wherein the gas flows through the analyzer region in a direction perpendicular to the length of the cylindrical inner electrode. In this device, the inner electrode is a solid cylinder (Figure INTRO5 shows the end view), and the outer electrode is a pipe through which the inner electrode is mounted such that the center axis of the inner and outer electrodes are aligned and in the same location. The ions enter through an entrance orifice on one side of the outer electrode, and exit at the same longitudinal position but at the opposite side of the circumference of the outer electrode. The geometry for the ESI-FAIMS-MS, shown in Figure INTRO5, has the advantage that the electrospray needle is oriented in the same direction and radial location as when used in the conventional ESI-MS experiment. The ions that leave the tip of the electrospray needle (in Figure INTRO5) begin to travel in a direction that is

approximately directly toward the orifice of the mass spectrometer. The FAIMS is located in such a way to accept these ions and to finally provide them to the orifice of the mass spectrometer. This FAIMS system permits a simple translation of the electrospray needle away from the mass spectrometer, followed by insertion of the FAIMS hardware, without further adjustment to the locations of the needle or the orifice of the mass spectrometer. The geometry shown in Figure INTRO5 will be referred to as the "side-to-side" FAIMS since the ions are carried from one side of the outer electrode to the other, perpendicular to the length of the electrode. To date, a side-to-side FAIMS device has not been reported in the refereed publications for use with ESI-MS on its own but recently it has been reported as part of a tandem FAIMS system as described below.

A tandem FAIMS-FAIMS device was coupled to a time-of-flight mass spectrometer (TOFMS) to investigate trapping of electrospray generated ions of gramicidin S (30). The tandem device can be used with two electrospray ionization sources as is shown schematically in Figure INTRO6. In the literature publication, the device was operated with the ion inlet to one of the side-to-side FAIMS devices plugged. For example, in Figure INTRO6, ion inlet<sub>2</sub> would be plugged and ions would not be able to enter through this ion inlet. Consequently, in operation, the system that was reported in the literature consisted of a side-to-side FAIMS device and a dome FAIMS device operating in series. The use of the side-to-side FAIMS device, with wider electrode diameters, and consequently better ion separation efficiency in front of the dome FAIMS device (narrower electrode diameters more suitable for trapping) was reported to lower the number of background ions captured in the trapping region of the dome FAIMS, and thus reduce the space charge effects in the trap. In addition, the tandem device allowed for a study of the decay kinetics of the cloud of trapped ions from the dome FAIMS since the side-to-side



Development of FAIMS for different applications has also been pursued. A PCT patent that described a micromachined FAIMS device (PCT/US00/17971) has been filed. The first published data presented using a micromachined FAIMS device was acquired with a FAIMS having a flat plate geometry and electrometer based detection(37). The system has since been extended to mass spectrometry(38), however, the sensitivity is low due in part to the use of a flat plate system that does not offer the ion focusing capabilities that were described earlier for devices of cylindrical geometry. The electric field strength in a parallel plate version of FAIMS is constant as a function of physical location along a perpendicular line taken from one plate to the other (at a given instant of time) and cannot create conditions necessary for formation of the potential well capable of focusing the ions nor prevent them from spreading in space due to diffusion and space charge repulsion. On the other hand, in cylindrical (and spherical) geometry devices, although the electrodes may be parallel to each other (see Figure INTRO3), the electric field strength changes with radial distance along a radial line taken perpendicular to the surface of the inner electrode and running from the inner electrode to the outer electrode. The magnitude of this change in electric field with radial distance decreases as the value of the radii of the electrodes increases (the space between the electrodes held constant) and goes to zero at large radii (thereby approximating parallel plates).

Development of FAIMS for different applications has also been pursued. A PCT patent that described a micromachined FAIMS device (PCT/US00/17971) has been filed. The first published data presented using a micromachined FAIMS device was acquired with a FAIMS having a flat plate geometry and electrometer based detection(37). The system has since been extended to mass spectrometry(38), however, the sensitivity is low due in part to the use of a flat plate system that does not offer the ion focusing capabilities that were described earlier for devices of cylindrical geometry. The electric field strength in a parallel plate version of FAIMS is constant as a function of physical location along a perpendicular line taken from one plate to the other (at a given instant of time) and cannot create conditions necessary for formation of the potential well capable of focusing the ions nor prevent them from spreading in space due to diffusion and space charge repulsion. On the other hand, in cylindrical (and spherical) geometry devices, although the electrodes may be parallel to each other (see Figure INTRO3), the electric field strength changes with radial distance along a radial line taken perpendicular to the surface of the inner electrode and running from the inner electrode to the outer electrode. The magnitude of this change in electric field with radial distance decreases as the value of the radii of the electrodes increases (the space between the electrodes held constant) and goes to zero at large radii (thereby approximating parallel plates).

#### 1.4 Literature Cited in the Introduction Section

1. Gorshkov, M. P. (1982) *SU 966583 (inventors certificate)* .
2. Eiceman, G. A., and Karpas, Z. (1994) *Ion mobility spectrometry*, CRC Press, Boca Raton, FL.
3. Mason, E. A., and McDaniel, E. W. (1988) *Transport properties of ions in gases*, John Wiley & Sons, Inc., New York.
4. Gieniec, J., Mack, L. L., Nakamae, K., Gupta, C., Kumar, V., and Dole, M. (1984) *Biomed. Mass Spectrom.* **11**, 259-268.
5. Wittmer, D., Chen, Y. H., Luckenbill, B. K., and Hill Jr., H. H. (1994) *Anal. Chem.* **66**, 2348-2355.
6. Chen, Y. H., Hill Jr., H. H., and Wittmer, D. P. (1996) *Int. J. Mass Spectrom. Ion Processes* **154**, 1-13.
7. Clemmer, D. E., Hudgins, R. R., and Jarrold, M. F. (1995) *J. Am. Chem. Soc.* **117**, 10141-10142.
8. Dugourd, P., Hudgins, R. R., Clemmer, D. E., and Jarrold, M. F. (1997) *Rev. Sci. Instrum.* **68**, 1122-1129.
9. Clemmer, D. E., and Jarrold, M. F. (1997) *J. Mass Spectrom.* **32**, 577-592.
10. Hoaglund, C. S., Valentine, S. J., Sporleder, C. R., Reilly, J. P., and Clemmer, D. E. (1998) *Anal. Chem.* **70**, 2236-2242.
11. Hudgins, R. R., Woenckhaus, J., and Jarrold, M. F. (1997) *Int. J. Mass Spectrom. Ion Processes* **165/166**, 497-507.
12. Guevremont, R., Siu, K. W. M., Wang, J., and Ding, L. (1997) *Anal. Chem.* **69**, 3959-65.

13. Shelimov, K. B., Clemmer, D. E., Hudgins, R. R., and Jarrold, M. F. (1997) *J. Am. Chem. Soc.* **119**, 2240-2248.
14. Valentine, S. J., Counterman, A. E., and Clemmer, D. E. (1997) *J. Am. Soc. Mass Spectrom.* **8**, 954-961.
15. Buryakov, I. A., Krylov, E. V., Nazarov, E. G., and Rasulev, U. K. (1993) *Int. J. Mass Spectrom. Ion Processes* **128**, 143-8.
16. Carnahan, B. L., and Tarassov, A. S. (1995) , United States Patent 5420424.
17. Riegner, D. E., Harden, C. S., Carnahan, B., and Day, S. (1997) , pp. 473, ASMS Conference, Palm Springs, California.
18. Riegner, D. E., Harden, C. S., Shoff, D. B., and Ewing, R. G. (1998) , pp. 1237, ASMS Conference, Orlando, Florida.
19. Carnahan, B., Day, S., Kouznetsov, V., Matyjaszczyk, M., and Tarassov, A. (1996), ISA Conference pp. 85-94, Framingham, MA.
20. Purves, R. W., Guevremont, R., Day, S., Pipich, C. W., and Matyjaszczyk, M. S. (1998) *Rev. Sci. Instrum.* **69**, 4094-4105.
21. Purves, R. W., Guevremont, R., Day, S., Matyjaszczyk, M., and Pipich, C. W. (1998) , pp. 430, ASMS Conference, Orlando, Florida.
22. Guevremont, R., Purves, R. W., Barnett, D. A., and Ding, L. (1999) *Int J. Mass Spectrom.* **193**, 45-56.
23. Guevremont, R., and Purves, R. W. (1999) *Rev. Sci. Instrum.* **70**, 1370-1383.
24. Purves, R. W., and Guevremont, R. (1999) *Anal. Chem.* **71**, 2346-2357.
25. Krylov, E. V. (1999) *Tech. Phys.* **44**, 113-116.
26. Guevremont, R., and Purves, R. W. (1999) *J. Am. Soc. Mass Spectrom.* **10**, 492-501.

27. Barnett, D. A., Ells, B., Purves, R. W., and Guevremont, R. (1999) *J. Am. Soc. Mass Spectrom.* **10**, 1279-1284.
28. Ells, B., Barnett, D. A., Froese, K., Purves, R. W., Hrudey, S., and Guevremont, R. (1999) *Anal. Chem.* **71**, 4747-4752.
29. Barnett, D. A., Purves, R. W., and Guevremont, R. (1999) *Appl. Spectrosc.* **53**, 1367-1374.
30. Guevremont, R., Ding, L., Ells, B., Barnett, D. A., and Purves, R. W. (2001) *J. Am. Soc. Mass Spectrom.* **12**, 1320-1330.
31. Purves, R. W., Barnett, D. A., Ells, B., and Guevremont, R. (2000) *J. Am. Soc. Mass Spectrom.* **11**, 738-745.
32. Ells, B., Barnett, D. A., Purves, R. W., and Guevremont, R. (2000) *J. Environ. Monitor.* **2**, 393-397.
33. Guevremont, R., Barnett, D. A., Purves, R. W., and Vandermeij, J. (2000) *Anal. Chem.* **72**, 4577-4584.
34. Barnett, D. A., Purves, R. W., Ells, B., and Guevremont, R. (2000) *J. Mass Spectrom.* **35**, 976-980.
35. Ells, B., Barnett, D. A., Purves, R. W., and Guevremont, R. (2000) *Anal. Chem.* **72**, 4555-4559.
36. McCooeye, M. A., Ells, B., Barnett, D. A., Purves, R. W., and Guevremont, R. (2001) *J. Anal. Toxicol.* **25**, 81-87.
37. Miller, R. A., Eiceman, G. A., Nazarov, E. G., and King, A. T. (2000) *Sensors Actuators B Chem* **67**, 300-306.

38. Miller, R. A., Nazarov, E. G., Eiceman, G. A., and King, A. T. (2001) *Sensors and Actuators A* 91, 307-318.

## **1.5 Publications and Patents Closely Related to FAIMS**

### **Known Refereed Publications in scientific journals (updated Aug 2002).**

**Title:** Quantitation of amphetamine, methamphetamine, and their methylenedioxy derivatives in urine by solid-phase microextraction coupled with electrospray ionization - high-field asymmetric waveform ion mobility spectrometry - mass spectrometry.  
**Author:** McCooeye, M.A.; Zoltan, M.; Ells, B.; Barnett, D.A.; Purves, R.W.; Guevremont, R.;  
**Publication:** Anal. Chem., 2002, v74, 3071-3075.

**Title:** Tandem mass spectra of tryptic peptides at signal-to-background ratios approaching unity using electrospray ionization high-field asymmetric waveform ion mobility spectrometry/hybrid quadrupole time-of-flight mass spectrometry.  
**Author:** Barnett, D.A.; Ding, L.; Ells, B.; Purves, R.W.; Guevremont, R.;  
**Publication:** Rapid Commun. Mass Spectrom. 2002, v16, 676-680.

**Title:** Application of mobility theory to the interpretation of data generated by linear and RF excited ion mobility spectrometers.  
**Author:** Spangler, G.E.; Miller, R.A.;  
**Publication:** Int. J. Mass Spectrom. 2002, v214, 95-104.

**Title:** Detection of explosive vapors in the air using an ion drift nonlinearity spectrometer.  
**Author:** Buryakov, I.A.; Kolomiets, Y.N.; Lupp, B.V.;  
**Publication:** Journal of Analytical Chemistry. 2001, v56, 336-40.

**Title:** Atmospheric pressure ion trapping in a tandem FAIMS-FAIMS coupled to a TOFMS: studies with electrospray generated gramicidin S ions  
**Author:** Guevremont, R.; Ding, L.; Ells, B.; Barnett, D. A.; Purves, R. W.  
**Publication:** Journal of the American Society for Mass Spectrometry 2001, v12, 1320-1330.

**Title:** Gas phase conformers of the  $[M+2H]^{2+}$  ion of bradykinin investigated by combining high-field asymmetric waveform ion mobility spectrometry, hydrogen/deuterium exchange, and energy-loss measurements.

**Author:** Purves, R. W.; Barnett, D. A.; Ells, B.; Guevremont, R.,

**Publication:** Rapid Communications in Mass Spectrometry 2001, v15, 1453-6.

**Title:** Miniature radio-frequency mobility analyzer as a gas chromatographic detector for oxygen-containing volatile organic compounds, pheromones and other insect attractants.

**Author:** Eiceman, G. A.; Tadjikov, B.; Krylov, E.; Nazarov, E. G.; Miller, R. A.; Westbrook, J.; Funk, P.,

**Publication:** Journal of Chromatography A, 2001, v917, 205-17.

**Title:** A MEMS radio-frequency ion mobility spectrometer for chemical vapour detection.

**Author:** Miller, R. A.; Nazarov, E. G.; Eiceman, G. A.; King, A. T.,

**Publication:** Sensors and Actuators A, 2001, v91, 307-318.

**Title:** Elongated conformers of charge states +11 to +15 of bovine ubiquitin studied using ESI-FAIMS-MS.

**Author:** Purves, R. W.; Barnett, D. A.; Ells, B.; Guevremont, R.,

**Publication:** Journal of the American Society for Mass Spectrometry 2001, v12, 894-901.

**Title:** Calculation of ion mobilities from electrospray ionization high-field asymmetric waveform ion mobility spectrometry mass spectrometry data.

**Author:** Guevremont, R.; Purves, R. W.; Barnett, D. A.; Viehland, L. A.,

**Publication:** Journal of Chemical Physics, 2001, v114, 10270-7.

**Title:** Quantitation of morphine and codeine in human urine using high-field asymmetric waveform ion mobility spectrometry (FAIMS) with mass spectrometric detection.

**Author:** McCooey, M.A.; Ells, B.; Barnett, D. A.; Purves, R. W.; Guevremont, R.,

**Publication:** Journal of Analytical Toxicology, 2001, v25, 81-87.

**Title:** Monitoring volatile organic compounds in ambient air inside and outside buildings with the use of a radio-frequency-based ion-mobility analyzer with a micromachined drift tube.

**Author:** Eiceman, G. A.; Nazarov, E. G.; Tadjikov, B.; Miller, R. A.,

**Publication:** Field Analytical Chemistry and Technology, 2000, v4, 297-308.

**Title:** Evaluation of carrier gases for use in high-field asymmetric waveform ion mobility spectrometry

**Author:** Barnett, D. A.; Ells, B.; Guevremont, R.; Purves, R. W.; Viehland, L. A.,

**Publication:** Journal of the American Society for Mass Spectrometry, 2000, v11, 1125-33.

**Title:** Fundamental considerations for the application of miniature ion mobility spectrometry to field analytical applications.

**Author:** Spangler, G. E.,

**Publication:** Field Analytical Chemistry and Technology, 2000, v4, 255-67.

**Title:** Analysis of a tryptic digest of pig hemoglobin using ESI-FAIMS-MS.

**Author:** Guevremont, R.; Barnett, D. A.; Purves, R. W.; Vandermeij, J.,

**Publication:** Analytical Chemistry, 2000, v72, 4577-84.

**Title:** Detection of nine chlorinated and brominated haloacetic acids at part-per-trillion levels using ESI-FAIMS-MS.

**Author:** Ells, B.; Barnett, D. A.; Purves, R. W.; Guevremont, R.,

**Publication:** Analytical Chemistry, 2000, v72, 4555-59.

**Title:** Trace level determination of perchlorate in water matrices and human urine using ESI-FAIMS-MS.

**Author:** Ells, B.; Barnett, D. A.; Purves, R. W.; Guevremont, R.,

**Publication:** Journal of Environmental Monitoring, 2000, v2, 393-397.

**Title:** A novel micromachined high-field asymmetric waveform - ion mobility spectrometer.

**Author:** Miller, R. A.; Eiceman, G. A.; Nazarov, E. G.; King, A. T.,

**Publication:** Sensors and Actuators B, 2000, v67, 300-306.

**Title:** Separation of *o*-, *m*-, and *p*-phthalic acids by high-field asymmetric waveform ion mobility spectrometry (FAIMS) using mixed carrier gases.

**Author:** Barnett, D. A.; Purves, R. W.; Ells, B.; Guevremont, R.,

**Publication:** Journal of Mass Spectrometry 2000, v35, 976-980.

**Title:** Determination of nanomolar levels of perchlorate in water using ESI-FAIMS-MS

**Author:** Handy, Russell; Barnett, David A.; Purves, Randy W.; Horlick, Gary; Guevremont, Roger,

**Publication:** Journal of Analytical Atomic Spectrometry, 2000, v15, 907 - 911.

**Title:** Detection of microcystins using electrospray ionization high-field asymmetric waveform ion mobility spectrometry / mass spectrometry

**Author:** Ells, Barbara; Froese, Kenneth; Hrudey, Steve E.; Purves, Randy W.; Guevremont, Roger; Barnett, David A.;

**Publication:** Rapid Communications in Mass Spectrometry 2000, v14, 1538-42.

**Title:** Isotope separation using high-field asymmetric waveform ion mobility spectrometry

**Author:** Barnett, David A.; Purves, Randy W.; Guevremont, Roger,

**Publication:** Nuclear Instruments and Methods in Physics Research A, 2000, v450, 179-85.

**Title:** Investigation of bovine ubiquitin conformers separated by high-field asymmetric waveform ion mobility spectrometry: Cross sections measurements using energy-loss experiments with a triple quadrupole mass spectrometer

**Author:** Purves, Randy W.; Barnett, David A.; Ells, Barbara.; Guevremont, Roger,

**Publication:** Journal of the American Society for Mass Spectrometry 2000, v11, 738-745.

**Title:** Separation of protein conformers using electrospray-high field asymmetric waveform ion mobility spectrometry-mass spectrometry

**Author:** Purves, Randy W.; Barnett, David A.; Guevremont, Roger;  
**Publication:** International Journal of Mass Spectrometry 2000, v197, p. 163-177.

**Title:** Comparison of high-field ion mobility obtained from drift tubes and a FAIMS apparatus  
**Author:** Viehland, Larry A.; Guevremont, Roger; Purves, Randy W.; Barnett, David A.,  
**Publication:** International Journal of Mass Spectrometry, 2000, v197, p. 123-130.

**Title:** Determination of parts-per-trillion levels of chlorate, bromate, and iodate by electrospray ionization/high-field asymmetric waveform ion mobility spectrometry/mass spectrometry  
**Author:** Barnett, David A.; Guevremont, Roger; Purves, Randy W.  
**Publication:** Applied Spectroscopy, 1999, v53, p. 1367-74.

**Title:** Ion trapping at atmospheric pressure (760 Torr) and room temperature with a high-field asymmetric waveform ion mobility spectrometer  
**Author:** Guevremont, Roger; Purves, Randy W.; Barnett, David A.; Ding, Luyi  
**Publication:** International Journal of Mass Spectrometry, 1999, v193, p. 45-56.

**Title:** Detection of chlorinated and brominated byproducts of drinking water disinfection using electrospray ionization high - field asymmetric waveform ion mobility spectrometry - mass spectrometry.  
**Author:** Ells, B.; Barnett, David A.; Froese, K.; Purves, Randy W.; Hrudey, S.; Guevremont, Roger  
**Publication:** Analytical Chemistry, 1999, v71, p. 4747-52.

**Title:** Separation of leucine and isoleucine by electrospray ionization high-field asymmetric waveform ion mobility spectrometry-mass spectrometry.  
**Author:** Barnett, David A.; Ells, B.; Guevremont, Roger; Purves, Randy W.  
**Publication:** Journal of the American Society for Mass Spectrometry, 1999, v10, 1279-1284.

**Title:** Electrospray ionization high-field asymmetric waveform ion mobility spectrometry-mass spectrometry.  
**Author:** Purves, Randy W; Guevremont, Roger  
**Publication:** Analytical Chemistry, 1999, v13, p.2346-2357.

**Title:** High field asymmetric waveform ion mobility spectrometry-mass spectrometry: an investigation of leucine enkephalin ions produced by electrospray ionization.  
**Author:** Guevremont, Roger; Purves, Randy W.  
**Publication:** Journal of the American Society for Mass Spectrometry, 1999, v.10, p492-501.

**Title:** Atmospheric pressure ion focusing in a high-field asymmetric waveform ion mobility spectrometer.  
**Author:** Guevremont, Roger; Purves, Randy W.  
**Publication:** Review of Scientific Instruments, 1999, v.70, n.2, p.1370, 14p.

**Title:** A method of reducing diffusion losses in a drift spectrometer.  
**Author:** Krylov, E. V.



**Publication:** Technical Physics, 1999, v44, p.113-6.

**Title:** Mass spectrometric characterization of a high-field asymmetric waveform ion mobility spectrometer.

**Author:** Purves, Randy W; Guevremont, Roger; Day, Stephen; Pipich, Charles W.; Matyjaszczyk, Matthew S.

**Publication:** Review of Scientific Instruments, 1998, v.69, n.12, p.4094, 12p.

**Title:** A new method of separation of multi-atomic ions by mobility at atmospheric pressure using a high-frequency amplitude-asymmetric strong electric field.

**Author:** Buryakov, I. A.; Krylov, E. V.; Nazarov, E. G.; Rasulev, U. K.

**Publication:** International Journal of Mass Spectrometry. Ion Processes, 1993, v128, p.143-8.

#### **Patents and patent applications.**

US patent 5,420,424. Ion mobility spectrometer, Carnahan and Tarassov. (1995)

US patent 6,124,592. Ion mobility Storage Trap and Method, Spangler. (2000).

US patent 5,801,379. High voltage waveform generator, V. Kouznetsov (1998).

Canada patent application, 2,273,322 filed May 28, 1999 (Apparatus and method for desolvating and focusing ions for introduction into a mass spectrometer).

Canada patent application, 2,339,548 filed August 5, 1999 (Apparatus and method for atmospheric pressure 3-dimensional ion trapping).

Canada patent application, 2,339,549 filed August 5, 1999 (Method for separation and Enrichment of Isotopes in Gaseous phase.

Canada patent application, 2,339,552 filed August 5, 1999 (Apparatus and method for desolvating and Focussing Ions for Introduction into a Mass Spectrometer).

Canada patent application, 2,339,553 filed August 5, 1999 (Method for separation of Isomers and different conformations of ions in gaseous phase).

US patent application, 09/321,820 filed May 28, 1999 (Apparatus and method for desolvating and focusing ions for introduction into a mass spectrometer).

US patent application, 09/762,236 filed August 5, 1999 (Method for separation of Isomers and different conformations of ions in gaseous phase).

US patent application, 09/762,237 filed August 5, 1999 (Apparatus and method for atmospheric pressure 3-dimensional ion trapping).

US patent application, 09/762,238 filed August 5, 1999 (Method for separation and Enrichment of Isotopes in Gaseous phase).

US patent application, 09/762,239 filed August 5, 1999 (Apparatus and method for desolvating and Focussing Ions for Introduction into a Mass Spectrometer).

Europe Common Market patent application, 1 102 984 filed August 5, 1999 (Method for separation of Isomers and different conformations of ions in gaseous phase).

Europe Common Market patent application, 1 102 985 filed August 5, 1999 (Method for separation and Enrichment of Isotopes in Gaseous phase).

Europe Common Market patent application, 1 102 986 filed August 5, 1999 (Apparatus and method for atmospheric pressure 3-dimensional ion trapping).

Japan patent application, 2000-564041 filed August 5, 1999 (Apparatus and method for atmospheric pressure 3-dimensional ion trapping).

**PCT applications describing FAIMS.**

PCT/CA00/00416 Mass Spectrometer, Including Coupling of an atmospheric pressure ion source to a low pressure mass analyzer, Published as: WO 00/63949 A1 (26.10.2000). (MDS Inc.)

PCT/US00/17971 Micromachined Field Asymmetric Ion Mobility Filter and Detection System, Published as: WO 01/08197 A1 (01.02.2001). (Draper Laboratory, Inc.)  
also WO 01/35441 from same group (Draper Laboratory, Inc.)

WO 01/22049, Haley et al, Canada (29.03.2001)

PCT/CA99/00714 Method for separation of isomers and different conformations of gas phase ions. Published as: WO 00/08454 (17.02.2000).

PCT/CA99/00715 Apparatus and method for desolvating and focusing ions for introduction into a mass spectrometer Published as: WO 00/08455 (17.02.2000).

PCT/CA99/00716 Method for separation and enrichment of isotopes in gaseous phase, Published as: WO 00/08455 (17.02.2000).

PCT/CA99/00718 Apparatus and method for atmospheric pressure 3-dimensional ion trapping, Published as: WO 00/08457 (17.02.2000).

PCT/CA01/00308 Improved Parallel Plate Geometry FAIMS apparatus and method, Published as: WO 01/69216 A2 (20.09.2001).

PCT/CA01/00309 FAIMS Apparatus and Method with Ion Diverting Device, Published as: WO 01/69217 A2 (20.09.2001).

PCT/CA01/00310 FAIMS Apparatus and Method Using Carrier gas of Mixed Composition,  
Published as: WO 01/69646 A2 (20.09.2001).

PCT/CA01/00311 Tandem FAIMS/Ion-Trapping Apparatus and Method, Published as: WO  
01/69218 A2 (20.09.2001).

PCT/CA01/00312 FAIMS apparatus and Method with Laser-Based Ionization Source, Published  
as: WO 01/69219 A2 (20.09.2001).

PCT/CA01/00313 Apparatus and Method for TANDEM ICP/FAIMS/MS, Published as: WO  
01/69220 A2 (20.09.2001).

PCT/CA01/00314 TANDEM High Field Asymmetric Waveform Ion Mobility Spectrometry  
(FAIMS)/Tandem Mass Spectrometry, Published as: WO 01/69647 A2 (20.09.2001).

PCT/CA01/00315 TANDEM High Field Asymmetric Waveform Ion Mobility Spectrometry  
(FAIMS)/Ion Mobility Spectrometry, Published as: WO 01/69221 A2 (20.09.2001).

## **2. Objectives of the Inventions in this Provisional Patent**

### **Submission**

Biochemical and pharmaceutical applications have requirements for rapid screening and detection of compounds in extremely complex mixtures. Advances in chemical analysis technology applied to these fields must achieve a high degree of specificity in separations and incorporate systems that avoid slow separations, especially those involving chromatography and electrophoresis.

At present, the compounds in complex mixtures may be separated and analyzed by chromatographic and electrophoretic methods combined with electrospray ionization - mass spectrometry (MS). In these separation techniques a portion of sample is introduced as a discrete pulse into the inlet of the instrument. The components in the sample are separated either through a component-specific interaction with mobile or stationary phases, or by differences in the drift velocities of components under the influence of electric fields. Because of the time necessary for the components to migrate chromatographic and electrophoretic methods require relatively large time periods for the separation (minutes) whereas analysis by mass spectrometric methods provides data almost immediately. In practice, therefore, the mass spectrometer spends significant periods of time waiting for the arrival of transient signals. This is inefficient since the separation technology is very much less expensive than the MS instrumentation. This problem would disappear if the separation technology were operated in a continuous mode, for example the mixture could be continuously delivered to the inlet of the separator and the selection of the separated components could be electronically controlled. In this manner the MS would make measurements of selected components in the mixture almost at full efficiency. The MS could also be used to continuously study any particular component in a mixture until sufficient

information was acquired. This is impossible with existing chromatographic and electrophoretic techniques because the component of interest only arrives as a transient at the end of the separation. This transient operation significantly limits the number and types of experiments that can be conducted during the lifetime of a given transient signal. If the information acquired during the transient is insufficient, a new sample must be injected and a delay is encountered during which the components are separated. These problems with transient signals do not occur with FAIMS because the component of interest can be continuously transmitted since the sample transmission is continuous and separation is electrically controlled.

Complex mixtures may be studied with tandem mass spectrometry (MS/MS). With this technology, the ions are selected by a first mass analyzer operating at low pressure (e.g.,  $1 \times 10^{-5}$  torr) inside the vacuum of a mass spectrometer and directed to enter a gas cell which is held at a higher bath gas pressure (e.g.,  $1 \times 10^{-3}$  torr). Upon entering this chamber, the ions collide with the molecules of bath gas and, if the kinetic energy of the ion is sufficient, the ion dissociates into some compound-specific fragments. The fragments pass out of the higher pressure gas cell and are analyzed by a second mass analyzer, operating at a lower pressure, similar to the first mass analyzer. The advantage of tandem mass spectrometry is that the specificity is exceedingly high because of compound-specific fragmentation patterns created during the collision induced dissociation. Tandem MS requires considerable method development time and the operator must have expertise to operate the instrument. Tandem MS cannot effectively quantify many kinds of isobaric isomeric ions (e.g., leucine and isoleucine) when both components coexist in the mixture. Tandem MS is most suited to applications based on target compound analysis, where the system is searching for a series of expected compounds and the identity of the expected fragment ions is known. Under these conditions the MS/MS experiment can detect ions at



However, to meet the ever-increasing demands for speed and sensitivity of chemical analysis, different combinations of FAIMS (or FAIMS with fast separation techniques) may eventually be most beneficial. FAIMS also lends itself to analyzing multiple samples simultaneously since the ion inlet location(s) is not restricted to a single orifice as is the case for a mass spectrometer. Some of the concepts discussed below relate to this simultaneous analysis of multiple samples using FAIMS. In addition, novel FAIMS geometries for improving ion transmission into the mass spectrometer are visualized and some of the devices are described below.

Because of the unique requirements of the asymmetric waveform applied to the FAIMS electrodes, existing technology for production of high voltage waveforms and high voltage pulses is not applicable to FAIMS. As a result of the unusual requirements of FAIMS a new system for producing the asymmetric waveform was required, and several innovative features of this waveform generator are described below. Automatic feedback for retaining stability of the asymmetry of the waveform is necessary for reliable long-term operation of FAIMS. Two methods of data processing from analog-to-digital (A/D) inputs are discussed. Simple data processing allows a real-time feedback under microprocessor control to establish and maintain constant operating conditions.



### 3. Invention #1: Waveform Generator Electronics Based on Tuned LC Circuits

Inventors: Lucien Potvin and Yves Baribeau

Operation of FAIMS requires: (a) an asymmetric waveform and (b) strong electric fields (high E/N). Separation of ions in FAIMS requires, in addition to the above, another dc electric field applied in superposition to the asymmetric waveform. The electrodes to which the actual voltages are applied is irrelevant, however the fields that exist between the electrodes are essential.

The shape of the waveform and the consequences of application of the asymmetric waveform on the motion of the ions between the FAIMS electrodes have been discussed in several places including:

"Atmospheric pressure ion trapping in a tandem FAIMS-FAIMS coupled to a TOFMS: studies with electrospray generated gramicidin S ions" by Guevremont, R.; Ding, L.; Ells, B.; Barnett, D. A.; Purves, R. W. in the Journal of the American Society for Mass Spectrometry 2001, v12, 1320-1330.

"Calculation of ion mobilities from electrospray ionization high-field asymmetric waveform ion mobility spectrometry mass spectrometry data" by Guevremont, R.; Purves, R. W.; Barnett, D. A.; Viehland, L. A., in the Journal of Chemical Physics, 2001, v114, 10270-7.

Briefly, the waveform must have a difference in the peak voltages in the positive and negative polarity portions of the waveform. In general this is accomplished by changing the relative periods of time of the high and low voltage portions of the waveform. For a square wave this means that  $V_1 t_1 = -V_2 t_2$  where  $V_1$  is a first voltage applied for a period of time  $t_1$  and  $V_2$  is a second, different, opposite polarity voltage applied for a second period of time  $t_2$ .

In practice this square waveform is difficult to produce and apply to the FAIMS electrodes because of electrical power consumption considerations. Without a tuned circuit the power which would be required to drive a capacitive load of capacitance  $C$ , at frequency  $f$ , with a peak voltage  $V$ , will be  $2(\pi)V^2fC$ . For example if a square wave at 750 kHz, 4000 V peak voltage is applied to a 20 picofarad load, the power consumption will be 240 Watts. If, on the other hand, a waveform is applied via a tuned circuit, the power consumption will be reduced since the power will be  $P\cos(\phi)$  where  $\phi$  is the angle between the current and the voltage applied to the capacitive load, and  $P$  is the power described by  $2(\pi)V^2fC$ . The function  $P\cos(\phi)$  approaches zero if the current and voltage are out of phase by 90 degrees (as they would be in a perfectly tuned LC circuit).

Since a tuned circuit cannot provide a square wave, an approximation of a square wave can be taken as the first terms of a Fourier series expansion. One approach is to use:

$$V(t) = \frac{2}{3}D \sin(\omega t) + \frac{1}{3}D \sin(2\omega t - \pi/2)$$

Where  $V(t)$  is the voltage as a function of time,  $D$  is the peak voltage (dispersion voltage, DV),  $\omega$  is the waveform frequency in radians/sec. The first term is a sinusoidal wave at frequency  $\omega$ , and the second is a sine wave at double the frequency ( $2*\omega$ ). The second term could also be represented as a cosine without the phase shift of  $\pi/2$ .

This simple equation is the equivalent of the first two terms of a Fourier series which would describe a square wave with a 2:1 duty cycle.

Therefore, in practice the application of two sinusoidal waves of frequency  $\omega$  and  $2*\omega$  can be used to generate a waveform with the shape shown in Figure 1. The higher

frequency wave is applied with a 90 degree phase shift and amplitude that is 50% of the amplitude of the lower frequency wave. The peak voltage equal to DV (D) is shown in this figure, normalized to one.

A simple circuit that can add the two waves of different frequencies is shown in Figure 2a. Four inductances, IN1, IN2, IN3 and IN4 in a series arrangement are used to drive a capacitive load FAIMS comprised of inner electrode 1 and outer electrode 2. In each case power is supplied to the inductances through a primary coil by a pulsed input. PP1 is a pulse in the positive polarity (plus) applied to IN1 and PM1 is a pulse in the negative polarity (minus) also applied to IN1 but out of phase with PP1. Each of the pulses is applied to a separate primary coil wound onto inductor IN1. Similarly, a series of positive inputs PPn and negative inputs PMn are applied to inductors INn. The inductor is wound with a secondary coil that couples in an LC tuned circuit with an output capacitive load. Since the LC tuned circuit is not a perfect oscillator, the resonance will decay with time. In order to maintain a constant output voltage, the loss rate must be matched by the supply of power introduced through the primary turns on inductors IN1 through IN2.

Inductors IN1 and IN2 are arranged in series with each other, and the input pulses of a first frequency are identical and in exact phase. The combined inductance of IN1 and IN2 must oscillate in tuned resonance with a capacitance of C3 combined in parallel with all of the rest of the circuit attached to the secondary windings of IN3 and IN4, namely C4, C5, C2 plus the FAIMS load and other stray capacitances throughout the circuit. For example, if the combined inductance of IN1 and IN2 is 0.45 mH then the circuit will oscillate at 750 kHz if the capacitance of C3 in parallel with the rest of the circuit is 100 pF.

The secondary windings of IN3 and IN4 are in series, but the center tap between these inductors is attached to the secondary of IN1 and IN2. This means that the combined oscillation of the IN3 and IN4 is around the floating voltage provided from IN1 and IN2. It is therefore possible for IN3 and IN4 to oscillate at a second frequency that is independent of the first frequency of oscillation of IN1 and IN2. The secondary windings of inductors IN3 and IN4 are coupled with three capacitors in a symmetrical arrangement. One capacitor, C5 is parallel to the inductors IN3 and IN4, whereas the other two capacitors C4 and the FAIMS load are each in series with ground (or some other dc potential, for example B1 in Figure 2a). For example, IN3 and IN4 would oscillate at 1500 kHz if the total capacitance (including stray capacitance) is 0.45 mH and the capacitance is 25 pF. Note that the series/parallel arrangements of the FAIMS load, and C5 and C4 in Figure 2 minimize the apparent capacitance. For example, if the FAIMS load (electrodes 1 and 2 in Figure 2) is about 25 pF, and C4 is about 25 pF, with appropriate selection of C5 the net capacitance coupled to the inductors IN3 and IN4 may be as low as 25 pF.

Tuning of IN3 and IN4 in concert with their capacitive load comprised of C5, C4 and the FAIMS load is made possible through adjustment of C5 and C4. Simultaneously, adjustment of C3 is required to ensure that the tuning of IN1 and IN2 with the remaining circuit is retained.

In practice the two frequencies applied to the two tuned circuits may be adjusted independently with the input to the alternative circuit turned off.

Figure 2b illustrates a second electronic circuit for generating an asymmetric waveform to be applied to the FAIMS inner electrode 1. The secondary windings on the inductors IN1b and IN2b are analogous to that shown in Figure 2a, except that the duplicated series inductors have been replaced by a single inductor. The two inductors IN1 and IN2 running at a first frequency in Figure 2a have been replaced by the single inductor IN1b. Similarly the two

inductors IN3 and IN4 operated at a second frequency in Figure 2a have been replaced by a single inductor IN2b shown in Figure 2b. The associated capacitors and the FAIMS load electrodes 1 and 2 are the same in both figures.

Figure 2b also illustrates an optional approach for application of the driving currents to initiate and maintain the oscillation in the tuned LC circuit. In Figure 2b the primary consists of a center-tapped winding. The center tap is connected to a dc power supply (for example +28 volts is shown in Figure 2b). The voltage available at this terminal will affect the amplitude of the wave generated by the particular oscillator. The two halves of the primary winding are alternately connected to ground potential through switches. The primary coil of inductor IN1b is operated at a first frequency by alternately grounding the primary through switches Sa and Sb, only one of which is closed at any time shown in the timing diagram on the bottom right corner of Figure 2b. When Sa is closed current runs through one half of the primary in a first direction. At a later time Sa is opened and Sb is closed to drive current through the other half of the primary but in the second direction. As a result of the changing magnetic fields thus induced in IN1b, an oscillating high voltage appears on the secondary winding (assuming the drive frequency is such that an LC oscillation takes place). The primary of IN2b is operated in a similar manner to that of IN1b except that the frequency is different and a phase difference exists between the oscillations induced in IN1b and IN2b. The switches shown in Figure 2b are electronic.

Figure 3 illustrates the fundamentals of the windings of inductors IN1, IN2, IN3 and IN4 that were discussed in relation to the circuit shown in Figure 2a. A similar approach is taken for IN1b and IN2b in Figure 2b but using one center-tapped winding on the primary rather than two completely independent windings as shown in Figure 2a and Figure 3. Referring to Figure 3, each primary is composed of two inputs 1 and 20, to which are applied a primary positive pulse

(PP1 in Figure 2) and a primary negative pulse (PM1 in Figure 2). The primary positive pulse is composed of a square wave with low side 47 near zero volts and a high side 45 at an adjustable value (shown as +5 V on Figure 3 for example). The primary negative pulse is composed of a square wave with high side 50 near zero volts and negative side 55 at an adjustable voltage (shown as -5 V for example). As shown in the timing diagram on Figure 3, the pulses are applied in an alternating fashion, wherein the voltage 45 is applied on the primary positive pulse while voltage 50 is applied to the primary negative pulse. Similarly, the voltage 47 is applied on the primary positive pulse while voltage 55 is applied to the primary negative pulse. It is the intention of this arrangement to create magnetic fields in the inductive core 10 which alternately change direction during application of pulses in the positive polarity through input 1 and negative polarity through input 2. The pulses are driven through load resistors 15 and 40 on the positive and negative sides respectively. The load resistors 15 and 40 ensure sinusoidal variations in the electrical currents in the primary turns 5 and 25 respectively. The currents in primary coils 5 and 25 create magnetic fields in core 10 that also induce electrical currents in the windings of the secondary coil 35. The voltage induced in the secondary coil is related to the number of times the coil 35 is wrapped around the core 10. As shown in the circuit of Figure 2a, the secondary coils 35 of inductors  $IN_n$  are linked to a capacitive load. The inductance of the coil 35 wrapped around core 10 is suitable for an tuned LC oscillation with the capacitive load.

While Figure 3 illustrates schematically the concepts used in the present invention, a novel approach was necessary to reach the performance required for the FAIMS application. The FAIMS application requires a high voltage (4000 V peak) into an approximately 20 pF load. Minimization of the power consumption also requires an LC oscillator with a high quality factor (Q) of over 200.

Figure 4 illustrates two improvements of the schematic shown in Figure 3. First, the secondary coil 35 is wrapped along a significant portion of the core 10. This permits a maximum number of turns to be placed on the core 10. The primary turns 5 and 25 from the drive circuit are wrapped external to the secondary turns 35 and are spaced away from the core and from the secondary turn by an air gap that prevents electrical discharge between the primary turns (either 5 or 25) and the secondary turns 35. The second improvement is a modification of the core 10. A segment of the core 10 has been removed to leave a gap 100. This gap 100 is required in order to prevent electrical discharge between the two ends of the secondary windings 35 which may have significant voltage differences between them. The core material is chosen not to have a high magnetic permeability. Therefore the gap 100 does not significantly change the inductance of the core 10 and the secondary turns 35.

Figure 5 illustrates yet another necessary and innovative change to improve the performance of this inductor. The system shown in Figure 4 is limited in effectiveness because the ability of the primary turns 5 and 25 to induce magnetic fields in the core 10 is limited by (a) the small number of turns and (b) the limited coverage of the core 10. This deficiency was overcome by running a second, or optionally more, sets of parallel primary turns at different locations around the core 10. In Figure 5 the primary coils are 105, 115, 110 and 120. The primary positive pulse is applied to primary turns at 1 in Figure 5. After load resistance 15, the primary coils 110 and 105 are wound in parallel around the core 10. Similarly, the primary coils for the negative pulse input are wound in parallel at 115 and 120 after load resistance 20 and are powered from the primary negative pulse applied to wire 20. This achieves two necessary improvements. First, the magnetic field induced in the core is higher in part because there are more primary turns around the core 10. Secondly, this improvement in the efficiency of

applying the input pulse is achieved without needing to wrap further turns of the secondary coil 35 around the core 10. In other words, the voltage induced in the secondary coil remains unchanged although the number of primary turns appear to have been significantly increased. Each of the primaries, because they are wound in parallel continues to behave as a small number of turns and the ratio of turns on the primary to the turns on the secondary is unchanged.

Advantageously, a multiplicity of primaries 105, 115 and 110, 120 shown in Figure 5 increases the efficiency of coupling to the core 10. The large diameter turns in the primary minimize the possible discharge from the primary to either the core 10 or to the secondary 35. Further, the large diameter primary turns shown in Figure 5 minimized the capacitance between the primary and secondary turns on the core 10. It would appear that this decreased capacitance would be achieved at the expense of the ability of the primary to induce a magnetic field in the core 10. This expected effect is minimized. Although the primary turns 105, 115, 110 and 120 in Figure 5 are further from the core 10, the wire of the primary is longer and therefore there is a larger magnetic field contribution from the electric current flowing through the wire. A high efficiency of coupling the primary and secondary is made possible by a multitude of parallel primaries, and a low capacitance is maintained by large diameter primaries wound at various locations around the core 10.

Beyond three or four parallel sets of primaries wound around the core 10 shown in Figure 5, it is found that the efficiency of coupling does not further improve significantly since the coupling may be over 90% with three sets of parallel primary windings (for example). Further sets of parallel primary windings will provide minimum improvement in coupling (which may already be very close to 100%) but will have the detrimental effect of increasing the stray capacitance between the primary and secondary windings.



#### **4. Inventions #2 and #3: Algorithms for Automated Optimization of the Asymmetric Waveform Generator LC Tuning Electronics**

Inventors: Roger Guevremont and Lucien Potvin

Operation of FAIMS requires: (a) an asymmetric waveform and (b) strong electric fields (high  $E/N$ ). Separation of ions in FAIMS requires, in addition to the above, another dc electric field applied in superposition to the asymmetric waveform. The electrodes to which the actual voltages are applied is irrelevant, however the fields that exist between the electrodes are essential.

The shape of the waveform and the consequences of application of the asymmetric waveform on the motion of the ions between the FAIMS electrodes have been discussed in several places including:

"Atmospheric pressure ion trapping in a tandem FAIMS-FAIMS coupled to a TOFMS: studies with electrospray generated gramicidin S ions" by Guevremont, R.; Ding, L.; Ells, B.; Barnett, D. A.; Purves, R. W. in the Journal of the American Society for Mass Spectrometry 2001, v12, 1320-1330.

"Calculation of ion mobilities from electrospray ionization high-field asymmetric waveform ion mobility spectrometry mass spectrometry data" by Guevremont, R.; Purves, R. W.; Barnett, D. A.; Viehland, L. A., in the Journal of Chemical Physics, 2001, v114, 10270-7.

Briefly, the waveform must have a difference in the peak voltages in the positive and negative polarity portions of the waveform. In general this is accomplished by changing the relative periods of time of the high and low voltage portions of the waveform. For a square wave

this means that  $V_1 t_1 = -V_2 t_2$  where  $V_1$  is a first voltage applied for a period of time  $t_1$  and  $V_2$  is a second, different, opposite polarity voltage applied for a second period of time  $t_2$ .

In practice this square waveform is difficult to produce and apply to the FAIMS electrodes because of electrical power consumption considerations. Without a tuned circuit the power which would be required to drive a capacitive load of capacitance  $C$ , at frequency  $f$ , with a peak voltage  $V$ , will be  $2(\pi)V^2 fC$ . For example if a square wave at 750 kHz, 4000 V peak voltage is applied to a 20 picofarad load, the power consumption will be 240 Watts. If, on the other hand, a waveform is applied via a tuned circuit, the power consumption will be reduced since the power will be  $P \cos(\theta)$  where  $\theta$  is the angle between the current and the voltage applied to the capacitive load, and  $P$  is  $2(\pi)V^2 fC$ . This power consumption approaches zero if the current and voltage are out of phase by 90 degrees (as they would be in a perfectly tuned LC circuit).

Since a tuned circuit cannot provide a square wave, an approximation of a square wave can be taken as the first terms of a Fourier series expansion. One approach is to use:

$$V(t) = \frac{2}{3} D \sin(\omega t) + \frac{1}{3} D \sin(2\omega t - \pi/2)$$

Where  $V(t)$  is the asymmetric waveform voltage as a function of time,  $D$  is the peak voltage (defined as dispersion voltage DV),  $\omega$  is the waveform frequency in radians/sec. The first term is a sinusoidal wave at frequency  $\omega$ , and the second is a sinusoidal wave at double the frequency ( $2 \times \omega$ ). The second term could also be represented as a cosine (without the phase shift of  $\pi/2$ ).

In practice, both the optimization of the LC tuning and maintenance of the exact amplitude of the first and second applied sinusoidal waves and the phase angle between the two waves is required for the long term, stable operation of a FAIMS system powered by this asymmetric waveform generator. The waveform generator must include a method for self-control through feedback to ensure that the output signal is stable and maintains the correct waveform shape.

Two approaches for retaining the optimum shape of the applied asymmetric waveform are discussed.

#### **4.1 Algorithm for Control of the Asymmetric Waveform: INVENTION #2**

Inventors: Roger Guevremont and Lucien Potvin

As noted above the waveform applied in FAIMS is a combination of two sinusoidal waves of frequency  $\omega$  and  $2\omega$ . The two waves are of amplitudes that differ by a factor of two. The two waves are also offset by a phase angle ( $\Theta$ ).

$$V(t) = A\sin(\omega t) + B\sin(2\omega t - \Theta)$$

Where  $V(t)$  is the asymmetric waveform voltage as a function of time,  $A$  is the amplitude of the first sine wave at frequency  $\omega$ , where  $\omega$  is the waveform frequency in radians/sec, and

B is the amplitude of the second sine wave at a frequency two times omega. This second sinusoidal wave is offset from the first by a phase angle theta (which should be equal to  $\pi/2$ ).

In the waveform with optimum shape,  $A = 2B$ , and theta is equal to  $\pi/2$ . The electronic circuit must maintain these two parameters in order to achieve the waveform with the correct asymmetric waveform shape for stable performance of the FAIMS system attached thereto. In a related function, the peak voltage on the highest voltage side of the asymmetric waveform (defined as DV above) must be constant, and equal to  $A+B$ . The electronic circuit must therefore track, modify and control three parameters, namely A, B and theta while simultaneously ensuring that  $A=2B$  and that  $A+B$  equals the dispersion voltage (DV).

The correct asymmetric waveform shape shown in Figure 6 can be established by collecting sample data points from the waveform (for example by analog-to-digital, A/D, sampling), in order to get a representative set of points from all portions of the waveform. In other words, the A/D points can be taken randomly, at frequencies that are higher or lower than the waveform itself, however it is necessary that this array of data points of the signal intensity of the asymmetric waveform correctly represent all time periods within the waveform. For example, the samples should include points near the peak voltage 1 in the polarity of maximum voltage applied, as well as points near the two peaks 10 of maximum voltage at the other polarity and in the dip 5 between those two peaks. If the waveform is sampled across all times, the series of points thus acquired can be subjected to simple tests to determine if the waveform shape is optimum.

As an example, if a perfect sinusoidal wave is sampled, the number of data points with positive measured signal equals the number of data points with negative measurements.

Similarly the number of points at any given measurement value (signal voltage) in the positive

polarity equals those of the same absolute negative voltage. These results are predicted because of the symmetry of the original sinusoidal wave. A similar analysis is possible for the asymmetric waveform used in FAIMS. For example, the maximum signal voltage on one polarity must not equal the maximum measured signal of the opposite polarity. The maximum measurement should correspond to  $A+B$  described above and the opposite polarity maximum should be  $(A+B)/2$ . Moreover, since there is one peak 1 in the first, maximum polarity side of the waveform, and two peaks 10 in the opposite polarity, the number of points at each of these two values of signal measurement differ, while remaining higher in number than most other measurement values. Because of the shape of the waveform, another measurement value will be significant however, and this is the value of the dip 5 between the two peaks on the lower voltage side of the waveform. Since the voltage temporarily doesn't vary in this valley, the number of data points with this measurement value will appear anomalously high (when compared to a sinusoidal waveform which will lack any significant numbers of data points other than at the maxima). From the definition of the asymmetric waveform function, the measured signal in the dip should be  $A-B$ .

Figure 6 illustrates several cycles of an asymmetric waveform that is formed according to the equation above. The values of  $A$  and  $B$  are taken so that  $A+B=1$ , and  $A/B=2$ . The peak values 1 of the waveform are therefore equal to  $A+B$ . The opposite polarity part of the waveform is characterized by a dip 5 and two peak values 10 (negative polarity in this example). As noted above, the peak 1 in one polarity is  $A+B$ . The value at dip 5 is  $A-B$  (in this case  $A-B=1/3$ ), and the peaks 10 in the opposite polarity are each  $(A+B)/2$  (in this case  $(A+B)/2 = 1/2$ ).

Figure 7 illustrates the distribution of data points from one cycle of the waveform shown in Figure 6. Data points have been obtained by sampling the voltage randomly in time. The data

points are then sorted from lowest to highest voltage value and are plotted sequentially as individual points along the horizontal axis. This provides a curve that is characteristic of the shape of the waveform. For simplicity the total number of data points has been normalized to 100 (percent). In other words the horizontal axis in Figure 7 is percent of the data points. If 1000 points were collected and arranged in order of size, the smallest point (number 1) would be 0.1%, the 500th point would be 50% and point 1000 (largest) would be at 100% on the horizontal axis of Figure 7. The data points are sorted from smallest to largest, shown from left to right in Figure 7. Referring to Figure 7, about 62% of the data points are of negative polarity and the remainder are positive. The polarity cross over point is labeled 25 in the figure. The maximum voltage of points in the positive polarity are labeled at 15 and have a normalized magnitude near 1. The most negative voltage data points are indicated by 30 on the figure, and have a normalized voltage near -0.5. At point labeled 20 on the figure, it is clear that a number of data points correspond to amplitude near 0.33, at about 50% of the data points as indicated by the labels on the x-axis. These are the data points from the dip 5 in Figure 6.

The curves shown in Figure 6 and Figure 7 illustrate ideal waveform results. Deviation of several types are possible. The electronics of the asymmetric waveform generator must be able to identify changes from the ideal waveform shape and make adjustments to the drive electronics accordingly.

If the two sinusoidal waves that are added together to create the asymmetric waveform shown in Figure 6 are shifted in phase angle the two minima labeled as 10 in Figure 6 will not have the identical values. In other words one of the minima becomes more negative and the other becomes more positive. If a 5% error is imposed on the phase angle (5% of 90 degrees), the two minima 10 differ significantly in values. If the data points of the waveform are analyzed

using the method used to produce the curve on Figure 7, the effect of this change becomes apparent. Under these experimental conditions of distorted waveform, the data points of the most negative values were found to become more negative than expected by about 4%. In other words, looking at Figure 7, the data points labeled 30 on the figure moved from about -0.5 to about -0.52 (data points from about 0% to 3% on the x-axis) when the 5% error on phase angle was imposed.

In a second type of error, the ratio of  $A/B$  can be altered while retaining normalized relationship  $A+B=1$ . This causes an error in the value of the dip 5 located on Figure 6. When the data points from this distorted version of the asymmetric waveform are arranged in order of ascending values from negative to positive as shown in Figure 7, the points that appear near  $x=50\%$  (near labeled point 20), are found to become more positive (than those of the perfect waveform) by about 6%.

In a third type of error the ratio  $A/B=2$  is retained but the sum  $A+B$  deviates from 1. A deviation of 5% in  $A+B$  (so that  $A+B=1.05$  for example) will result in a 5% error in all of the points plotted using the method shown in Figure 7, when compared to the ideal waveform. For example, it is clear that the points found near 15 in Figure 7 will be 5% too large (i.e., 1.05) compared to the 1.0 shown in Figure 7 in region 15.

Figure 8 illustrates an analysis of the magnitudes of changes and where deviations appear in Figure 7 when the waveform is distorted by the three methods described above. The data on Figure 8 was generated by a comparison of ideal asymmetric waveforms with waveforms that had specific distortions. The first step in the procedure is to collect a series of data points, i.e., signal voltage magnitudes during the waveform, that represent all parts of the waveform. For example, if 100 points were collected rapidly in succession during one cycle of the waveform,

this sampling of 100 points would represent all times during the waveform. If the data collection was uniform in time, then these 100 points are equally spaced over the duration of the waveform. In a second step of processing the data, these 100 points are arranged in order from smallest to largest, which will produce a plot shown in Figure 7. Next, each of the 100 points which was arranged from smallest to largest is compared with the points from an ideal waveform, and a plot of the difference (normalized to the magnitude at that point) is prepared. This approach will give a plot shown in Figure 8. If the new data set represents a perfectly formed waveform, all data points appear very near zero, as each point from smallest to largest in turn is compared to the ideal expected value and the plot on Figure 8 is a straight line near zero.

If the waveform is generated with some error, for example a 5% shift in the phase shift of the higher frequency sinusoidal wave, then the resulting asymmetric waveform is not perfectly shaped. Although a plot of all of the data points may look very much like Figure 7 when arranged from smallest to largest in magnitude, there are some significant differences from the same array of points from the perfect waveform. These differences are more apparent in Figure 8, where the difference between this distorted waveform is shown more clearly. For example, the 5% shift in phase angle will result in a error plot on Figure 8 shown as a solid line. An expanded view in Figure 9 shows this solid line more clearly, labeled as 41. From Figure 9, the data points of most negative polarity (in this example), appear near the label 41 and are about 4% lower than equivalent points in the case of the ideal asymmetric waveform.

Figure 8 and 9 show traces of three types of error: First, a phase shift error; second an error in the ratio of  $A/B$  (keeping  $A+B=1$ ); and third, an error in the sum of  $A+B$  (keeping the ratio  $A/B = 2$ ). The easiest type of error to observe is the third, in which the sum  $A+B$  is wrong



by about 2.4%. The net result of this distortion is errors of 2.4% at every point throughout the cycle of the waveform. This is shown as a dashed line indicated by label 56.

A second type of error, a phase shift is shown in Figure 9 as a solid line. The data points of lowest magnitude (left side of the figure labeled 41), are clearly too negative. Although elsewhere on the plot, especially in the region shown by label 51, the errors can be very large, this large error is not as useful because the absolute values of the amplitudes of the data points are close to zero. Recall that the magnitude of the data points change from negative to positive near 62 (horizontal x-axis), therefore the data in this vicinity is near zero.

The third type of error is shown as a dash-dot line in Figure 8 and Figure 9. In the region labeled 46 in Figure 9 it can be seen that the error in the magnitude of the points from the distorted waveform differ from those of the ideal waveform by over 3%. Note that in this region, shown as 20 in Figure 7, the data points are expected to be approximately constant and about 1/3 of the amplitude of the maximum in the opposite polarity. This is the dip region shown as 5 in Figure 6. This dip is found in Figure 7 as midway among the data points (i.e., if 100 points were collected, then the dip is near 50 when the points are arranged from smallest to largest). This region is labeled as 20 on Figure 7.

From the above discussion the three types of errors in A, B and phase angle can be independently distinguished.

#### **4.1.1 Waveform Feedback and Control Algorithm**

The application of the above information permits a simple algorithm for feedback and control of the asymmetric waveform in FAIMS. The waveform parameters are:

(a) dispersion voltage =  $A+B$

(b)  $A = 2B$

(c) phase angle,  $\theta = \pi/2$

The electronics of the waveform generator will maintain these three relationships.

First, a sampling of the waveform is needed. This can be a fast A/D that collects (for example) 100 points that covers one cycle of the waveform. The plot of the magnitude (A/D values) of these points as a function of time of collection will yield a trace that resembles an oscilloscope trace of the original asymmetric waveform. Alternatively this data can more easily be obtained as a slow, random, sampling version of A/D which eventually collects samples from every portion of the waveform. This is easy to visualize. Consider the A/D collection of 100 points randomly, one new point each millisecond, and the 100 points finally collected in about 100 milliseconds. Since the asymmetric waveform is repeating rapidly (perhaps in the megahertz range), no two of these A/D points could come from the same cycle of the waveform. However, the point does come from somewhere during the cycle of the waveform. Similarly, each of the following 99 collections come from random points during widely separated (in time) cycles of the waveform. If the points are actually random, then every region (given the finite number of points collected) of the waveform has been sampled although one does not know from which time slot in the waveform each sample has been acquired. One cannot reconstruct the equivalent of an oscilloscope trace of the original waveform shape because the "time" values of the points relative to the original waveform is unknown. Clearly this is the unique advantage of forming a plot like Figure 7. The data points, collected randomly, are arranged by order of magnitude from smallest to largest as shown in Figure 7. If the points were collected randomly

from all parts of the waveform, then the distribution will resemble that in Figure 7. The larger the number of collected points, the closer the distribution will resemble that shown in Figure 7.

In a second step of the processing of the data, three comparisons are taken. First question: do the data differ from expected in the high end of the scale (see label 56 in Figure 9)? Deviation in this range is suggestive that the amplitude of the waveform must be corrected upwards, because the sum of  $A+B$  is too large (negative error, i.e.  $([\text{ideal}-\text{actual}]/\text{ideal})$  is the formula for calculating the error relative to the ideal waveform, ideal is the magnitude from the perfect waveform and actual from the waveform under test).

In a second comparison, using Figure 9, the magnitude of difference between ideal and actual is compared at the most negative points shown in the area of label 41 in Figure 9. If the error in region 56 was small, and the error in region 41 is finite and observable, then the waveform suffers not from distortion in the magnitude of  $A+B$ , but rather from a phase shift error. A correction of the phase angle is therefore warranted until the deviation near the region 41 of Figure 9 is reduced to zero. Clearly, since the  $A+B$  function can cause deviation in the same region of the array of points, the  $A+B$  must be correct prior to adjustment of the phase angle (and revised repeatedly during this adjustment).

In a final evaluation of error of the waveform, if the region labeled 56 seems correct, and the region labeled by 41 seems correct, both matching well with ideal waveform, a final distortion may arise from an error in the magnitude of  $A/B$ . This error is indicated by non-zero errors in the middle points of the arrangement from smallest to largest values of the data. These middle points, near the region labeled 46 in Figure 9 (and 20 in Figure 7) deviate from zero error (compared to ideal) when the ratio of  $A/B$  deviates from 2 and  $A+B$  is still 1.

Correction of the phase angle or the correction of the ratio  $A/B$  can be performed in either order, but the  $A+B$  must be set first. From Figure 9, a small error in the phase angle has minimum contribution to the error at the 50% region of Figure 9. Similarly, small shifts of  $A/B$  contribute small errors in the 0-5% region of Figure 9.

These calculations are readily implemented in control software of the waveform generator. The type of error can be found and corrections taken as appropriate.

For example, if  $A+B$  is too large, the amplitudes of both sinusoidal waves that are used to form the waveform are decreased. This returns the  $A+B$  to a correct value.

Secondly, if an error is detected in phase relationship, then one sinusoidal wave must be shifted relative to the other. The direction that is necessary can be ascertained from the polarity of the error (such as shown near 41 in Figure 9). The shifts are applied until the error at 41 in Figure 9 decreases to zero.

Finally, if an error is detected in the ratio of  $A/B$  then one amplitude is increased while the second is decreased. A check of the value of  $A+B$  immediately follows to restore the sum to its correct value. This process is iterated until both  $A/B$  and  $A+B$  are correct.

The waveform is optimized and maintained in its ideal form by a cyclic process of repeating these tests and adjusting the amplitudes and phases of the sinusoidal waves used to produce the asymmetric waveform.

## 4.2 *Algorithm for Control of the Asymmetric Waveform: INVENTION*

### #3

Inventors: Roger Guevremont and Lucien Potvin

As noted above the asymmetric waveform applied in FAIMS is a combination of two sinusoidal waves of frequency  $\omega$  and  $2\omega$ . The two waves are of amplitudes that differ by a factor of two (as well as frequencies that differ by two). The two waves are also offset by a phase angle ( $\theta$ ). The equation of the asymmetric waveform is:

$$V(t) = A \sin(\omega t) + B \sin(2\omega t - \theta)$$

Where  $V(t)$  is the voltage of the asymmetric waveform taken as a function of time,  $A$  is the amplitude of the first wave at frequency  $\omega$ , where  $\omega$  is the waveform frequency in radians/sec, and  $B$  is the amplitude of the second wave at double the frequency  $\omega$ . This second wave is offset from the first by a phase angle  $\theta$  (which should be equal to  $\pi/2$ ). As noted above, in comparison to the maximum point of the waveform previously defined as the dispersion voltage  $DV$ , the  $DV$  is  $A+B$ . Also noted above, the dip in the waveform on the opposite polarity from  $DV$ , is equal to  $A-B$ .

In the previous section we described a method for analyzing the data points acquired from an A/D conversion applied to the waveform, either rapidly to sample one or more cycles of the waveform perfectly (as would appear on an oscilloscope), or slowly wherein the array of amplitudes would eventually match that of the waveform even though the points were not collected in rapid succession on the same cycle of the waveform. Using a slow, random

acquisition provides data amplitude values (A/D values) but the time of each of the points relative to the original waveform cannot be ascertained.

In this section we describe a related, but uniquely different, approach. As before, the waveform must be sampled using an A/D conversion at a high or low data acquisition rate. As before, it is only essential that the waveform be sampled to provide values of the signal (for example A/D values) that represent points distributed (systematically or randomly distributed) throughout the cycle. Reconstruction of the waveform shape as a function of time, as shown by an oscilloscope, is not necessary. Unlike the previous method, arranging the data points from smallest to largest is also not necessary.

In the first step of this new algorithm, the points are normalized so that the largest value (positive or negative) is one. It is assumed from this process that the peak voltage of the waveform,  $A+B$  is already fixed to the expected value. The following steps therefore are taken independently of the value of  $A+B$ . The value of  $A+B$  is available by searching for the largest (or most negative) point in the data set. After this point is obtained, all of the points are divided by this maximum value, so that all data points fall between -1 and +1. The data points originally collected by the A/D process are therefore normalized to 1.

In the second step of this new algorithm the "cube" of each data point is calculated. For example, if the A/D normalized result is 0.4, then 0.4 cubed is 0.4 times 0.4 times 0.4 equals 0.064. In this example -1 cubed is of course equal to -1, and -0.2 cubed is equal to -0.008. These examples are given to avoid misunderstanding of this extremely simple algorithm. In addition, the sign of the result is important. Use of other functions, including squares, will be discussed below.

In the second step to this algorithm, the average (or sum) is taken of the cubes of these normalized data points. For this discussion we will consider the average, but the sum could be used as an alternative. Use of the sum gives a value of the sum that depends on the number of points collected, whereas for this discussion the average is not dependent number of points collected (unless the number of points is too small).

This averaged result of the cubes of all the data points reaches a maximum value when the asymmetric waveform is optimized. When DV is positive, then the average of the cubed points is positive (about +0.113), and maximum. When the DV is negative then the average of the cubed points is negative (about -0.113) and is at its most negative value. In each case, if the phase angle offset between the two sinusoidal waves is changed from the optimum of  $\pi/2$ , then the average of the cubes will begin to deviate towards zero. If the relative ratio of A/B deviates from the optimum value of 2, the average of the cubes also deviates towards zero.

In the algorithm using the average of the cubes, the objective of the electronic control circuit is therefore to adjust the values of A, B and the phase angle to maximize (in appropriate polarity) the value of the average of the cubes. At the maximum of this "average of the cubes", the asymmetric waveform is shaped in the way shown in Figure 6.

This algorithm works because the absolute value of the voltage of the waveform is significantly different in the positive and negative polarity. As shown in Figure 6, the maxima 1 in the positive polarity are about equal to one, whereas the most negative points near 10 are about negative one-half. The cube function, applied to all of the data points, covering all parts of the waveform, will result in larger "cubes" for the points on the higher voltage polarity side of the waveform than the points in the opposite polarity. This tends to push the average of the cubes in the direction of the polarity of DV. It should be noted that application of this algorithm

to symmetrical waveforms (such as a sinusoidal wave) will result in a zero average of cubes. This is because all points in the positive polarity are matched by a point of equal magnitude in the opposite polarity. The cubes of these two points are equal but opposite polarity, and therefore the average of these two points is zero. This applies to all the points of the waveform, and the net average of the cubes of a sinusoidal wave is zero.

Will other functions provide the same benefit as the cube? The cube function was chosen as an illustration because it automatically maintains the sign of the data points. A negative value cubed remains negative. However, the cube function does have all the prerequisites for application of this algorithm.

In order to apply the algorithm, the selected function must have several characteristics. The function should be monotonic increasing or decreasing, have a monotonic increasing (or decreasing in the case of decreasing functions) first derivative, retain the sign (or consistently applies the opposite sign to the data points) of the data points and, finally, the function should result in magnitudes of calculated points that are the same irregardless of the sign of the data. For example, the square function can be used as long as the calculation enforces the rule that the square of the negative data points results in a negative "square". In this case the "modified square" function would square the absolute value of the data point, and apply the sign of the original data point back to this squared value. Other even polynomial and power functions might have to be adjusted in like manner to maintain the sign of the original data. In other words, the function applied must produce outputs which distinguish between input points of opposite polarity (in sign, but not in magnitude). The square function has a monotonic increasing first derivative ( $2x$ ) and a positive second derivative at all positive  $x$ . In this modified square function the correction for signs results in the correct derivatives for negative values of  $x$ .



The cube root function cannot be used, because, although it is monotonic increasing (and decreasing in the negative values) and it retains the signs of the data, this function does not give a useful average value. In this case the function (applied to positive values) does not have a monotonic increasing first derivative (i.e, it has a negative second derivative). In this case the derivative of  $X^{1/3}$  is  $(1/3)X^{-2/3}$ , thus the derivative is not increasing as the input values are increased. In this case the second derivative is negative.

The logarithm function cannot be used because the magnitudes of the results from calculation for the positive and negative points would be different, i.e.,  $\log(x)$  is not equal to  $\log(-x)$  (which doesn't exist). Even if this problem is corrected using the "modified log function" where  $\log(-x)$  is defined to be  $\log(x)$ , the second derivative of the logarithm function is negative. On the other hand the exponential function can be used if the effect of the sign of the data point is eliminated. For example, a "modified exponential" function can be defined, in which we first take absolute values of the data points, followed by an application of the sign of the original data point. In other words, if we define  $\text{sng}(x)$  to give +1 for positive, and -1 for negative values of  $x$ , we can define a modified exponential to be  $\text{sng}(x)\exp(\text{abs}(x))$  where  $\text{abs}(x)$  is the absolute value of  $x$ . The second derivative of this modified exponential is positive for positive values of  $x$  and negative for negative values of  $x$ .

The algorithms to be used in this optimization process therefore are not limited to cube, modified square, modified exponential functions, but rather all functions with the appropriate properties including derivatives.

#### 4.2.1 Waveform Feedback and Control Algorithm

The application of the above information of applying a function to further analyze data points permits a simple algorithm for feedback and control of the asymmetric waveform in FAIMS.

In practice, the asymmetric waveform is therefore monitored and optimized using an algorithm with an appropriate function. For further discussion the example will assume that the function will be the "average of the cubes". Other functions are easily substituted. The electronics of the waveform generator will include a microprocessor which processes the output of a fast or slow A/D programmed to collect sufficient points to monitor the waveform. Since the points may be taken randomly, a random distribution may take a larger number of points than a systematic, high frequency A/D with evenly spaced (in time) points. The points are processed by the average of the cubes method. If the value of this average of the cubes data processing is lower than the predicted +0.113 for a positive polarity (DV) waveform then corrective action is taken.

The order of corrective action must be considered. For example, if the output of the waveform generator is sinusoidal (one of the two necessary input sinusoidal waves is zero), then modification of the phase angle cannot change the average of the cubes to a non-zero value. If the average of the cubes is zero, both input sinusoidal waves must be set to a predefined value, without concern about the particular ratio of A/B. If the average of the cubes remains at zero, a failure of one of the input waves is possible. If under these conditions the phase angle is changed and the average of the cubes continues to be fixed at zero, failure of one of the input waves is certain.

After setting the amplitudes of the two sinusoidal waveforms to non-zero values, the adjustment of phase angle will readily provide non-zero values of the average of the cubes.

Clearly, if the amplitudes of the waves are comparable (for example about 2:1), the average of the cubes will deviate from zero very readily.

After ensuring significant amplitudes of the two sinusoidal waves, the average of the cubes is maximized using the phase angle. Following the maximizing of the average of the cubes using the phase angle, the relative amplitudes of the waves must be again modified. The amplitude of each wave is increased and decreased to ascertain the direction of change necessary to maximize the average of the cubes. After the maximum is reached, the phase angle is again changed until the average of the cubes maximizes. This cyclic process need not continue indefinitely if the average of the cubes has reached 0.113. Re-optimization can be carried out at times dependent on the expected possible drift rates in the amplitudes of the sinusoidal waves and expected drifts in phase angles that may be related to operating temperature (for a possible example).

## **5. Inventions #4 and #5: New Versions of the FAIMS Electrodes: Stacked Plates.**

Inventor: Roger Guevremont

A number of variations of the electrodes for use with FAIMS have been described by the present inventor. Some of these appear in previous patent submissions that describe:

- (a) cylindrical FAIMS electrode terminating in a dome shape (see Figure INTRO4b).
- (b) trapping versions of FAIMS (see Figure INTRO6).
- (c) side-to-side geometry in which ions travel around the circumference of cylinders or spheres (see Figure INTRO5).
- (d) flat plates, usually three or more, permitting trapping at ends of powered electrodes.
- (e) parallel plates that are curved in one or more dimensions.

A second development evolved from this work. The FAIMS technology was further modified for the purpose of enabling the user to introduce samples from several sources into a single mass spectrometer. This would in some cases improve the efficiency of use of the instrument and may permit the user to improve sample analysis throughput without investing in a separate new mass spectrometer. A number of techniques that permit multiple sample introductions were described in a provisional patent filed in February 8, 2002 (US 60/354,711). The FAIMS technology, permitting trapping of ions at atmospheric pressure, should lead to a system which could trap ions from several sources and feed them consecutively into the inlet of a mass spectrometer without significant loss of ions from any of the sources. To do so the FAIMS must trap and coordinate delivery of ions to the mass spectrometer. The provisional patent filed in February 8, 2002 (US 60/354,711) described approaches to accomplish this goal.

In this report the same inventor will discuss three types of new electrode assemblies for FAIMS.

### ***5.1 New FAIMS Electrode Assembly based on Stacked Parallel Plates, INVENTION #4***

Several versions of parallel plate and multiple plate FAIMS have been considered previously. In each of these cases the ions entered a FAIMS system through an orifice, and the ions passed between plates (flat or curved or parallel) while being carried by a flow of gas. In every case the ions were transported in a direction approximately along (parallel to) the surfaces of the electrodes. In each case the electric fields were oriented to be perpendicular to the direction of the travel of the ions (keeping in mind that the ions are also oscillating in the fields created by the asymmetric waveform) as they are carried along the space between the electrodes by the flow of gas. For example, in a two parallel plate device, one plate is at a fixed dc voltage and the other has an asymmetric waveform applied, plus a dc offset voltage (compensation voltage, CV). The ions are transported between a first inlet edge of the plates to an opposite outlet edge of the plates by a gas flow. During the transport through the space between this pair of electrodes the ions are separated. Those ions whose high field mobility to low field mobility ratio is appropriate for the combination of waveform peak voltage (DV) and dc differences (CV) between the two plates are able to pass between the plates. Some of these ions are lost through collisions with the plates, since the ions are free to diffuse in any of 3 dimensions, including in the direction towards the plates. In conclusion therefore, this device separated ions as they were carried by a gas along the space between two parallel conductive electrodes to which were

In this first new version of the FAIMS electrodes the ions pass through an electrode system composed of parallel plates, however the ions do not travel in the space between the facing surfaces of the parallel plates. The ions travel in the space between the edges of two sets of plates that are displaced apart by a short space. Moreover, the asymmetric waveform is applied to specific plates, with a design in which the powered plates are surrounded by plates to which only a dc voltage is applied.

Figure 10 shows the electrode set of the new FAIMS. The ion inlet and ion outlet ends of the device are defined by two plates, ion entrance plate 10 with ion entrance orifice 20, and ion exit plate 60 with ion exit orifice 70. The plates are arranged parallel to each other with a gap 50 between two additional sets of electrodes 55 and 56 on the left and right side of the gap 50. The sets of plates 55 and 56 are composed of two types of plates identified by the electric voltages applied to them. The plates 30 all have the asymmetric waveform applied to them, and the plates 40 have a dc voltage (or ground potential) applied to them. The arrangement of the plates is important. Each plate 30 is surrounded above and below by a plate that does not carry the asymmetric waveform (i.e. either a plate 10, 60 or 40). The arrangement of the plates 30 and 40 are not identical on the two stacks 55 and 56 found on opposite sides of the gap 50. Each of the plates 30 on the stack 55 on the left side of gap 50 are aligned (i.e., located at the same distance

from plate 10) with a plate 40 on the stack 56 found on the right side of the gap 50. Similarly, each of the plates 30 on the right side are aligned with plates 40 on the left side.

The arrangement of the electrodes in Figure 10 is selected so that each electrode 30 to which the waveform is applied is surrounded by electrodes 40, 10 or 60 to which only the dc voltage is applied. In other words, relative to a given electrode 30, the electrodes that are above and below, and on the opposite side of the gap 50, are electrodes 40, 10 or 60 to which the dc voltage is applied. Electrodes 40, 10 and 60 need not have the same dc potential applied.

Figure 10, which shows the electrodes in 2d view, has an appearance similar to that of the electrode set (series of plates) used in drift tube ion mobility spectrometry (DTIMS). This is an illusion because the plates in DTIMS are usually circular plates with a hole in each plate, the series of holes through the stack of plates defining a drift region through which the ions move under influence of an electric field. The ions drift along this drift region because each of the electrodes is biased to a different dc voltage, thus creating an electric field along the drift region. In other words, the electrode on the left side of the drift region is at the same potential as its corresponding section on the right side. The electrode set shown in Figure 10 does not resemble a series of plates with holes drilled into each of the plates. The electrodes in Figure 10 are square plates. A series of plates 30 and 40 are stacked together separated by insulation (not shown) to form stacks 55 and 56. Electric connections to each plate permit connection to an electronic controller capable of applying the waveform to plates 30 and dc voltages to plates 40. In other words, the electrode on the left side of the gap 50 is at a different potential than its facing electrode on the right side.

Two such stacks 55 and 56 composed of alternating electrodes 30 and 40 are prepared, a set 55 that starts with plate 30 and the second set 56 starting with plate 40. The two sets of

stacked electrodes 55 and 56 are then located next to each other with the small gap 50 between them. For further clarification, if a series of cross sections are taken through the electrode set above and below the plane of the paper in Figure 10, the cross sections will continue to resemble Figure 10 (perhaps lacking orifice 20 and 70). A series of similar cross sections taken through the DTIMS will give variable gaps between the electrodes, and if cross sections are taken at extremes, no gap will be seen (because the DTIMS electrodes are circular in geometry).

Figure 11 is the same electrode geometry as Figure 10, with a first optional pattern of flow of gas shown. In this case a gas flow 80 is provided from between a pair of electrodes (or optionally from between all of the pairs in the stacks of electrodes). This gas converges in region 90 and flows out of the orifice 70. In this way the ions are carried predominantly along the channel 50 between the stacks 55 and 56. Ions are channeled into the orifice 70 because of the convergence of gas flows 90 to this location.

Figure 12 illustrates the ions 100 entering through orifice 20 in ion entrance plate 10. The ions follow various trajectories, one (hand-drawn) trajectory 110 shown for an example. Since the device operates on the FAIMS principle, where the ions whose trajectory through the electrodes is stable is based upon the DV and CV applied, the ions 120 represent a sub-set of all of the types of ions 100 entering the device, namely those ions with the appropriate behavior of the ratio of high field mobility to low field mobility. Some finite portion of the ions 120 constituting this sub-set of the original mixture get through the exit orifice 70. Those ions passing through 70 may be detected by a means including electrometers or may be passed for further analysis in a mobility or mass analyzer (mass spectrometer) system. A number of hybrid analyzers have been described by the present inventor, including FAIMS-TOFMS, FAIMS-ion trap MS, FAIMS-DTIMS, DTIMS-FAIMS, and FAIMS-ion trapping FAIMS, for examples.



## ***5.2 New FAIMS Electrode Assembly based on Stacked Parallel Plates facing a Flat Surface, INVENTION #5***

A second new version of the FAIMS electrodes is illustrated in Figure 13. A series of flat electrodes 330 and 340 are stacked in alternation sequence with a space between each electrode (and supported by an insulator, not shown) to produce a stack 352. The asymmetric waveform and dc compensation voltage (for example) are applied to electrodes 330 and a dc voltage or ground potential applied to electrodes 340. One of the flat sides of the stack 352 is located adjacent and spaced apart from a flat plate 410, defining a small space 350 between the stack 352 and the plate 410. The ions 380 enter this FAIMS through orifice 320 in the flat ion entrance plate 310. The ions pass along the channel 350 between the stack 352 composed of electrodes 330 and 340, and the flat plate electrode 410. Electrodes 410, 310 and 360 may be at a dc voltage or ground potential (for this example). Since this device transports and separates ions based on the FAIMS principles, only a sub-set of the original mixture of ions 380 will be transported to the exit orifice 370. Some of these selected ions 390 pass through the orifice, and may be transported to an ion detection system, another ion mobility spectrometer, or alternatively to a mass spectrometer for further analysis.

As discussed in relation to previous FAIMS devices, the voltages are applied to the plates to establish appropriate fields between the conductive plates. Many other possible combinations of dc and waveforms that achieve this result will be apparent to those knowledgeable in the field.

### ***5.3 Ion Motions in the FAIMS Electrode Assemblies Based on Layered Plates.***

In this section we consider the motion of ions in devices with configurations shown in Figure 10 and Figure 13.

Figure 14 illustrates ion motions in the electrode geometry shown in Figure 13. The asymmetric waveform and compensation voltage is applied to electrodes 530, and a dc voltage (or optionally ground potential) is applied to electrodes 540 and 550. The electric fields between the electrodes 530 and 540 has been discussed in relation to flat plate versions of FAIMS. The fields are composed of a variable and a constant (in time) component. The application of the asymmetric waveform results in an electric field that is stronger in one polarity than in the other. Since the mobility of the ion may be higher or lower in the stronger field than in the lower field of opposite polarity, the oscillation of the ion may carry it towards one of the electrodes. The second, dc component of the field is applied to counteract, or compensate, for this drift. Under the correct combination of asymmetric waveform (peak voltage defined as DV) and applied dc voltage difference between the plates (compensation voltage defined as CV), ions with the appropriate ratio of mobility at high field to mobility at low field will be in a balanced condition. In other words, the field arising from the applied CV just matches the drift effect caused by application of the waveform with peak voltage DV.

Although the fields between the electrodes 540 and 550 in Figure 14 may optionally be selected to achieve a balanced condition without migration towards either plate (for example, the same applied dc voltage applied to 540 and 550) for a particular type of ion, the electric fields that exist around the ends of the electrodes 530 are not identical to the fields between the

electrodes 530 and 540. However, beneficially, the fields create the effect of an ion trapping region in the vicinity of the edges of the electrodes 530. In brief, the electric field around the edges of plates 530 is not constant with distance from the end of the electrode. This contrasts to the conditions between the electrodes (away from the edges) in which the fields are constant (in space). The so-called balanced condition that exists for a given ion, while located between the plates 530 and 540, fortuitously, continues to extend around the end of the electrode in region 570 on Figure 14. For the appropriate types of ions, because the regions closer to the end of electrode 530 give rise to stronger electric fields, the ion migrates away from the end of the electrode. At further distances the ions are attracted towards the end of the electrode because of the dc voltage differences that comprise the application of the CV. For further clarification an example is necessary. Assume that an ion is in a balanced condition between the plates 530 and 540 with  $DV=+4000$  volts and  $CV=-10$  volts. In one method of application, the asymmetric waveform and the CV are both applied to plates 530, and the other plates (including 540 and 550) are held at a dc voltage of 0 V. Without consideration of the waveform, this means that the dc level of the plates 530 is -10 volts and the plates 540 and 550 are at 0 volts. In general a positively charged ion located between plates 530 and 540, or at the ends of the plates 530 adjacent to plate 550 is always attracted towards plates 530. The application of the waveform tends to reverse this motion if the electric fields created by the waveform are high enough to create an increase in the ion mobility (used in this example as one possible change in ion mobility with field strength). In this example, the ion realizes a net displacement away from electrode 530 in the time of one cycle of the waveform (ignoring effect of dc fields). If we assume that the pull of the dc fields between plates 530 and 540 is just strong enough to balance the effect caused by the asymmetric waveform, it can be assumed (for this example) that if the

fields originating from the waveform are increased the ions located between the plates will move away from plates 530, and if the fields of the waveform are decreased, then the ions located between the plates will tend to move towards the plates 530. Around the edges of the plates 530 shown in Figure 14 a modified version of this effect also takes place, but changes in voltages are not necessary to change ion drift speed and direction. Since the fields change strength as a function of distance relative to the ends of the electrodes 530, the direction and velocity of motion automatically also becomes a function of distance. Near the ends of the electrodes 530 the fields caused by the waveform are strong (stronger than in the region between electrodes 530 and 540) and the ions will move away from the electrode towards the balance region indicated as 570. At greater distances from the end of the electrodes 530, the electric fields generated from application of the waveform are weaker and the original effect of the dc voltages, namely to attract the ions towards the plates 530 again predominates.

The ion trajectory shown in Figure 14 is therefore a result of selecting the appropriate combination of voltages to apply to the electrodes 530, 540 and 550. The waveform is applied (in this example) to electrodes 530. The dc voltages which constitute CV can be applied to 530 or to 530, 540 and 550 to achieve the required dc differences that produce the fields necessary to compensate for the effect of the waveform. For example, above we assumed that electrode 530 was biased -10 volts relative to electrodes 540 and 550. The same electric fields between electrodes 530 and 540 can be achieved by putting -5 volts on electrodes 530 and +5 volts on electrodes 540. The balancing condition for the ion simply requires the 10 volt difference between the electrodes (with correct polarization). The voltage difference between electrodes 530 and 550 and between 540 and 550 can also be selected. As noted above electrode 530 can be held at -5 volts, electrode 540 at +5 volts. This suggests that the dc voltage applied to

electrode 550 might be selected to push the ions closer to electrodes 530 and pull the ions away from electrodes 540. A voltage of 0 volts would have this effect. The voltage applied to electrode 550 must be established empirically by measurement of the efficiency of transport of ions carried by gas flow 580 through the channel. At appropriate voltages applied to electrodes 530, 540 and 550, combined with the waveform applied to electrodes 530, the ion will approximately follow trajectory 500 through the space between the electrode stack and electrode 550. A flow of gas 580 will carry the ions along the space. The trajectory 500 is hand-drawn and is only an approximation for purposes of illustration. A computer simulation shows similar results. Computer simulation of the flows of gas is problematic, and therefore trajectories are approximate. Imperfectly simulated computer generated trajectories do not limit the advantages and applicability of the present invention.

As shown in Figure 14, the ions will tend to move to the focusing regions marked at 570, because of the attractive dc fields caused by application of CV. The ion will be carried out of the focus region by the gas flow, and with appropriate voltages will move away from electrode 540, shown in the trajectory as region 505. Once past electrode 540, the ion will begin to move towards the next electrode 530 in the stack. This undulating motion will continue as the ions traverse the channel between the stack and electrode 550. Ions with other than the correct ratio of high field mobility to low field mobility will collide with an electrode prior to being carried to the exit orifice. Although this discussion assumed a positive ion, with mobility that increased with electric field strength (recalling that field strength is being used to represent  $E/N$ ) this discussion is only used for example, and this electrode arrangement can be used with negative ions and ions of either polarity whose mobility increases or decreases with  $E/N$ .

Figure 15 illustrates ion motions in the electrode geometry shown in Figure 10. The asymmetric waveform is applied to electrodes 730 and a dc voltage (or optionally ground potential) is applied to electrodes 740. The electric fields between the electrodes 730 and 740 has been discussed in relation to flat plate versions of FAIMS. The fields are composed of a variable (asymmetric waveform) and a constant dc (in time) component. The application of the asymmetric waveform results in an electric field that is stronger in one polarity than in the other. Since the mobility of the ion may be higher or lower in the stronger field, in the absence of other electric fields, the oscillation of the ion will carry it towards one of the electrodes. The second, dc version of the field is applied to counteract, or compensate for this drift. Under the correct combination of asymmetric waveform (peak voltage defined as DV) and applied dc voltage difference between the plates (compensation voltage defined as CV), ions with the appropriate ratio of mobility at high field to mobility at low field will be in a balanced condition. The field arising from the applied CV just matches the drift effect caused by application of the waveform with peak voltage DV.

As previously considered with regard to Figure 14, we begin by assuming that the ions located between the plates are in a balanced condition as result of appropriate DV and CV. As before, the balanced condition is found to continue around the terminus at the edges of the electrodes 730 to form a focusing region 770 for ions with appropriate ion mobility characteristics as a function of  $E/N$ . Every one of the electrodes 730 has such a focus region in the electrode arrangement shown in Figure 15. As noted above, from the point of view of the dc voltages, if CV is applied to the same electrodes as the asymmetric waveform, the ions are attracted to these electrodes 730, rather than to the other electrodes. In the case described above, for a particular kind of ion, the CV of -10 volts was applied to each electrode 730 (in addition to

the waveform) and other electrodes were held at 0 volts. This means that positive ions are attracted to the electrode 730 and away from electrode 740.

During application of the asymmetric waveform to electrode 730, the ion is attracted towards the end of the electrode when it is at some distance away from the electrode where the fields have decreased in strength. However, the ion cannot collide with the electrode because the field strength increases as the ion approaches the electrode and acts to push the ion away from the surface of the electrode to the focusing region indicated by 770.

The ions travel with trajectories shown as 700 in Figure 15. When the ion is between electrodes 740 and 730, the ion will prefer to be located at the focus area 770. If the ion is carried from between one pair of 730 and 740 to the next adjacent pair by the flow of gas 780, the electrodes have effectively switched sides and the new optimum focus region is now on the other side of the channel between the stacks of electrodes. The ion therefore undulates from one side to the other as it is carried by gas flow 780.

The ion motion shown in Figure 15 suggests that alternative methods for applying the dc voltages to the electrodes can be visualized. For example, the CV voltage which creates the dc fields between electrodes 730 and 740 can be distributed between electrodes 730 and 740. In the example above, all of the CV of -10 volts was applied superimposed on the waveform onto electrode 730. Alternatively electrode 730 may have -5 volts superimposed on the waveform, and electrode 740 be biased to +5 volts. The net difference of 10 volts between electrodes is maintained.

In yet another variation, a dc voltage gradient can be created along the length of the electrode set shown in Figure 15. In this case, a first voltage gradient along the length of the electrodes must be introduced by an offset in dc voltage from layer to layer along the stack. For

example at the first layer, both electrodes 740 and 730 are held at +10 volts. At the next layer, both electrodes 730 and 740 (in opposite order than in the previous level) are held at +9 volts. This imposes a 1 volt difference between layers, and therefore a field along the length of the electrode stack. Each subsequent layer is also biased 1 volt lower than the layer above.

The application of dc offset voltages from layer to layer does not create a FAIMS system, hence further voltages must be superimposed on these dc voltages. It is relatively easy to visualize the superposition of the waveforms onto each of electrodes 730 in the stack in Figure 15. Unfortunately a selected ion cannot be transmitted under these conditions because we have not provided a compensating field to balance the effect of the waveform (and the effect of the alternating strong and weak fields thereby created). How does the CV get applied when we have already defined the dc voltages on all of the electrodes? The CV is not defined by an absolute voltage, but rather as a difference in voltages between the electrodes. For example we hope to ensure that each electrode 730 is 10 volts more negative than each electrode 740 or alternately stated that a dc potential difference of 10 volts in the right polarity exist between each electrode 730 and 740. In order to apply both a voltage gradient along the length of the assembly as well as the compensation voltage a compromise condition must be selected. The dc compensation field cannot be identical on both sides of each plate since a fixed voltage difference (to create the gradient) is superimposed on the requirement for a compensation voltage.



## **6. Invention #6: New Version of the FAIMS Electrodes: Parallel Rods**

**Inventor: Roger Guevremont**

A number of variations of the electrodes for use with FAIMS have been described by the present inventor. Some of these appear in previous patent submissions that describe:

- (a) cylindrical FAIMS electrode terminating in a dome shape.
- (b) trapping versions of FAIMS.
- (c) side-to-side geometry in which ions travel around the circumference of cylinders or spheres.
- (d) flat plates, usually three or more, permitting trapping at ends of powered electrodes.
- (e) parallel plates that are curved in one or more dimensions.

Two new versions of the FAIMS electrodes were described in an earlier section of this report, based on stacks of parallel plates facing each other edgewise, and alternatively with the side face of the stack (edges of the electrodes) facing a flat plate. Both of these approaches took advantage of the formation of a focusing region around the ends of the parallel plates. The focus region formed because, unlike the region between the parallel plates, the end regions are characterized by electric fields that vary in strength with distance from the edges of the electrodes. This focus region was described above, in this report, but also was considered in some detail in previous reports filed by this inventor describing parallel plate versions of FAIMS in which the focus region at the edges of the plates were used to help direct and confine ions in such a way to maximize the number of ions successfully exiting the device through an exit orifice (without collision with electrodes or the ion exit plate). In these previous parallel plate

systems the ions were carried along between parallel plates by a flow of ion carrier gas. Those ions for which the combination of DV and CV were appropriate to create a balanced condition for the ion between the plates, flowed along in a direction approximately parallel to the plates, and upon exiting from between the plates were confined preferentially in the focus region at the terminus of the plate. This confinement in the focus region ensured that a maximum number of ions were collected from the regions between the plates, and were directed towards the exit orifice.

### **6.1 A FAIMS Electrode Based upon an Array of Parallel Rods.**

Figure 16 illustrates a new FAIMS based on an array of parallel rods (wires if the diameter is small). Ions enter this FAIMS through an ion entrance orifice 4 in the ion entrance plate 2. The ions that successfully are transported through the FAIMS electrodes will exit through the ion exit orifice 8 in the ion exit plate 6.

The array of FAIMS electrodes are composed of two types of rods (optionally wires) arranged in alternation (cubic array in the example shown here). Rods 12 have electrical connectors through which the asymmetric waveform is applied (and optionally the dc compensation voltage). The other rods 14, the ion entrance plate 2 and the ion exit plate 6 have electrical connectors to which a dc voltage is applied. The dc voltages are not necessarily identical, since the ion entrance plate 2 will be biased to tend to push the ions towards the parallel rod assembly, whereas the ion exit plate 6 will be biased to pull the ions away from the electrode assembly towards the ion exit orifice 8. If a flow of gas is traveling from the region near the ion entrance orifice 4 and through the electrode assembly, and out of the device through

ion exit orifice 8, the ions that are pulled toward the plate 6 will tend to be carried by the gas flow towards the orifice 8.

Figure 17 shows the same parallel rod electrode assembly as shown in Figure 16, but with additional detail. The ions are carried into the region of the parallel rods by gas flow 18, and the ions which have passed through the array are carried away by gas flow 22. The electrodes to which the asymmetric waveform is applied are labeled 12, and shown in dark on Figure 17. The other electrodes 14 are held at a fixed dc voltage (or ground potential). For an ion with appropriate field-dependence of the ratio of mobility at high field to mobility at low field, the application of the DV and CV to the rods 12 (with other rods at ground potential) will result in a focusing region surrounding each of the rods 12. For example for a low mass positive charged ion such as  $\text{Cs}^+$ , the DV and CV might be about +4000 and -30 volts respectively (with both applied to the same electrode, other rods at 0 volts). Although both CV and DV are applied to the same rods 12, it is possible to apply the waveform to the rods 12 without offset from ground potential, and to bias the rods 14 with the compensation voltage. Under this case the waveform  $\text{DV}=+4000$  would be applied to the rods 12, and +30 volts applied to the rods 14 (recalling that the compensation voltage is applied to create an electric field that pulls the ion towards the electrode 12). In either case, for the ion under discussion, the focus regions will form as shown by the region 16 around each of the rods 12.

The focus region 16 around each rod 12 is characterized by the motion of the ions in the vicinity of this region 16. If the ion under discussion is closer to the rod 12 than the region 16, the effect of the asymmetric waveform pushes the ion away from the rod 12. If the ion is located beyond the region 16, the ion moves towards the rod 12. The region 16 is the distance from the rod 12 at which the effect of the waveform that pushes the ions away from the rod 12 is exactly

balanced by the attractive force towards rod 12 caused by the compensation voltage. Although this balance point might be considered an infinitely thin 2 dimensional surface, the regions 16 around electrodes 12 have been drawn with thickness in recognition that the ion oscillates in the field and can be found over some range of distances from the rod 12. In addition, the ions are also under the influence of diffusion, fluctuations in the motion of the gas, ion-ion repulsion, that cause the ions to be located over some finite range of distances rather than compressed to one thin 2 dimensional surface.

In the absence of a flow of gas among the rods shown in Figure 17, ions that were originally located at random points in the spaces among the array of rods 12 and 14 will eventually be found within, or in the vicinity of focus regions 16.

## ***6.2 Ion Motions in the FAIMS Electrode Assemblies Based on Parallel Rods.***

The motion of the ions through the array of parallel rod electrodes will be considered. As shown in Figure 17 it will be assumed that a flow of gas 18 is used to carry the ions from some inlet through the electrode array. As discussed with respect to Figure 17, in the absence of a gas flow the ions will migrate to and collect in the focus regions around the rods 12 to which DV and CV is applied. Moreover, the ions will be located at all locations equally around the circumference of the focus region 16.

The introduction of a flow of gas will result in two possible changes to the distribution just described. First, at low flows, the ions will move around the circumference of the rods 12 following the curvature of the focus region 16. There will be more ions located on the side of rods 12 that is downstream from the flow of gas. This is because there are no barriers to motion of the ions around the focus region 16. Second, at higher gas flows, the ions will not be held permanently in the focus regions but will be pulled out of the focus region by the movement of the gas flow.

Figure 18 illustrates approximately the motion of the ions among the rods of the same electrode assembly as shown in Figure 16. A mixture 32 of ions of different types originate from some ion source, possibly one of electrospray, corona discharge, radioactive Ni foil, MALDI, and flow into the array of rods 12 and 14. For this example the DV and CV are applied to rods 12 and the others are at ground potential. Ions with the correct behavior at high electric fields relative to low fields, will be transported through the array whereas other types of ions will collide with the rods. The ions of the appropriate type, shown as 34 in Figure 18, are carried out of the array and optionally to a detection system or a mass spectrometer. Two trajectories are shown in Figure 18 for illustration. In this case the flow of gas 18 into the array and gas flow 22 out of the array is sufficiently rapid to pull the ions away from the focus regions. In general, positive ions 32 approaching the array will be pulled in the direction of the rods 12 because of the CV (negative polarity in this case) applied to the rods 12. Trajectory 24 therefore carries the ion to the focus region of the first electrode 12, and around the electrode following the focus region 29. The ion is pulled away from the first electrode by the gas and moves to the focus region 29 of the next electrode 12. The second trajectory also travels from one focus region 28 to the following region 28 as the ion winds a path through the array.

In Figure 18 it is important to note that at the region 26 shown near the end of trajectory 24, the two trajectories have passed through the focus region of the same rod 12 and appear to be much closer to each other than when they entered the array. The array of parallel rods can be used to funnel the ions formed from over a wide range of locations, to exit from the array over much smaller physical distance. The flow of gas can be used to assist in this funnel effect if the gas flows through the array towards a single exit orifice 8 shown in Figure 16.

Figure 19 shows the funnel effect that will result if the gas flows 48 converge from various locations in the array towards one ion exit orifice 8. Optionally the gas is introduced with ions through a multitude of apertures 4 in the ion inlet plate 2. Three possible ion trajectories are shown. The first trajectory 42 begins at one of the entrances 4 and is directed immediately towards a rod 12 to which CV and DV are applied (in manner described above). Because the gas flow is directed towards the exit orifice 8, the ions move from focus region to focus region in the general direction of the orifice 8. Similarly trajectories 44 and 46 also carry ions towards the exit orifice 8. By rotating Figure 19 it becomes clear that the placement of the rods is not important to the overall motion of the ions, rather it is the fact that the array is symmetrical around each rod 12. The ions may travel preferentially in any direction that the gas may flow and experience the same conditions. To show this, the rods in Figure 20 are arranged in a second optional pattern, different from the cubic array shown in Figure 19. Figure 20 shows this alternative arrangement. From study of crystal structure (which is an array of spheres) various optional arrangements of two type of rods (or in crystals, two types of spheres such as Cl and Na in salt) can be visualized. The trajectory 15 in Figure 20 illustrates the advantage of this particular arrangement of rods. The ion will travel from one focus region to another in a well defined pathway. The ion moves from the focus region around a rod to which is applied the

waveform, and moves to the next rod to which is applied the waveform. If the ion inlet 4 is aligned with one of the electrodes 12 to which the waveform and compensation voltages are applied, the ion can easily follow a trajectory 15 to the exit orifice 8. Similarly, the ion with trajectory 42 on Figure 19 travels from a rod with applied waveform, to the next rod with applied waveform. This undulation motion follows a series of focus regions and the ion transmission efficiency is very high, since no part of the trajectory permits the ion freedom to diffuse to collide with an electrode. Trajectory calculations show that the fields are always moving the ions away from colliding with the rods.

Figures 16 and 20 illustrate two arrangements of the array of rods embodied in this type of FAIMS electrodes.

## **7. Invention #7: Operation of FAIMS Electrodes in Quadrupole Configuration.**

Inventor: Roger Guevremont

A number of variations of the electrodes for use with FAIMS have been described by the present inventor. Some of these appear in previous patent submissions that describe:

- (a) cylindrical FAIMS electrode terminating in a dome shape.
- (b) trapping versions of FAIMS.
- (c) side-to-side geometry in which ions travel around the circumference of cylinders or spheres.
- (d) flat plates, usually three or more, permitting trapping at ends of powered electrodes.
- (e) parallel plates that are curved in one or more dimensions.

In a previous disclosure by the same inventor it was shown that four parallel rods of the same configuration as used in quadrupole mass analyzers (quadrupole mass spectrometers) could be adapted for use in a FAIMS mode of operation. (PCT/CA01/00314 TANDEM High Field Asymmetric Waveform Ion Mobility Spectrometry (FAIMS)/Tandem Mass Spectrometry, Published as: WO 01/69647 A2 (20.09.2001). In this disclosure an asymmetric waveform may be applied to one or more of the parallel rods of a quadrupole assembly. Ions passing through this assembly would be lost to the walls if the ratio of ion mobility at low field and ion mobility at high field were not appropriate for the applied field strengths (asymmetric waveform and constant compensation field). As in previous versions of FAIMS, for simplicity, the amplitude of the applied waveform is described by the peak maximum in the higher voltage polarity of the



waveform (DV) and the dc fields are defined by the application of a compensation voltage (CV). It is understood that the voltages are converted to fields that occupy the space among the electrodes and the ions are in motion because of these applied fields. It is also understood that the strength of the field is actually  $E/N$  where  $E$  is the field in volts/cm and  $N$  is the number density of the gas. Clearly, the application of lower voltages is appropriate under conditions of lower gas pressure while higher voltages are required at higher gas pressure, each arriving at the same  $E/N$ . The behavior of ions in the FAIMS technology is based on changes in the mobility of the ion under conditions of changing  $E/N$  (which is often simplified to "conditions of changing electric field strength").

To better define the use of quadrupole assemblies that exist inside of commercial mass spectrometers for the purposes of ion separation based on the FAIMS principles, this disclosure describes optional methods to overcome problems of residence times of ions in electrodes operated at pressures significantly below atmospheric pressure. For example, ions that are passed through a quadrupole collision cell in a triple quadrupole instrument may have several eV of translational energy and be transmitted through the collision cell in a very short time. If the pressure is sufficiently high, the ions could in principle be separated by the FAIMS approach. However, the residence time within the quadrupole collision cell may be short and the separation period may be insufficient to achieve a good separation.

The quadrupole collision cell can theoretically be used to act as an ion trap by application of appropriate stopping voltages at the ends of the quadrupole rods. Ions inside the rod assembly may be held temporarily within the assembly by the trapping fields. During this storage period, the application of an asymmetric waveform will achieve an ion separation using the FAIMS

approach. This disclosure discusses the apparatus and methods used to realize a multiple use of quadrupole rods for both storage of ions and for separation based on FAIMS.

Quadrupole rods in a triple quadrupole mass spectrometer are used in two ways. If only rf sinusoidal waveform alone is applied to the rods, the rods are said to be operating in rf-only mode. In this mode a wide range of ions of differing mass may be simultaneously transmitted (or stored in linear quadrupole traps). In a second mode, the mass analyzer mode, a dc voltage is superimposed on the rf on the rods and the mass range of ions whose trajectories remain stable is significantly reduced. With the appropriate rf and dc voltages, ions within a mass ranges of one  $m/z$  can be stable and all others collide with the walls of the quadrupole rods.

In general, quadrupole rods assemblies that are used for collisional dissociation experiments are used in rf-only mode in order to retain both the parent ion, and as many of the newly formed daughter ions as possible.

The sets of quadrupole rods that will be used in FAIMS mode will likely be those used in rf-only mode in the presence of a bath gas. Under these conditions, irrespective of the geometry of the remaining components of the mass spectrometer, the set of quadrupole rods under consideration can be used alternatively in rf-only and FAIMS modes. Moreover, the quadrupole rods can be used in ion trapping or ion storage mode simultaneously (and preferentially) in order that the ions remain in the rod assembly for periods of time sufficiently long for the FAIMS separation to be effective. The operations of the quadrupole rods can be intermittently changed from rf-only mode (with bath gas) to FAIMS separation mode (with bath gas). In the first step, the rf-only mode the ions will tend to collect at the center axis of the quadrupole assembly because the trajectories of the ions are degraded by collisions with the bath gas and the motion of the ions gradually decreases in physical dimensions as the ions, on average, are found for longer

periods near the center axis of the rods. In the second step, the voltages applied to the quadrupoles are modified temporarily to achieve FAIMS separations.

In a possible experiment, a quadrupole assembly, in a housing suitable for adjusting the pressure of a bath gas, is operated in ion trapping mode. The ions are permitted to enter the quadrupole assembly and prevented from leaving by the application of retaining voltages at the ends of the assembly. In rf-only mode the ions will lose translational energy to collisions with the bath gas and gradually move preferentially to the center axis of the rods. Due to the retaining voltages at the ends, the ions cannot leak out of the ends of the rods. After this decrease of translational energy (e.g., cooling of the ions), the voltages applied to the rods are modified so that the ions are subjected to the changing electric field strengths caused by an asymmetric waveform (i.e., peak maximum fields in one polarity differ from those in the opposite polarity) for a period of time. During this time the ions whose ratio of mobility at high  $E/N$  to mobility at lower  $E/N$  are appropriate for the applied waveform and dc compensation fields remain within the electrode assembly whereas the other ions whose mobility behavior is other than appropriate begin to drift away from the center axis of the rods and collide with the walls of the quadrupole rods. The waveform and compensation voltage are stopped after a period of time and the quadrupoles returned to rf-only operation causing the remaining ions return to the center axis of the rods. Ions which collided with the walls are no longer present and the ion mixture has been separated to leave only those types of ions with certain selected mobility properties. Finally, the retaining voltage on the exit end of the quadrupole assembly is dropped and the ions allowed to be transmitted to other parts of the instrument. In this case the next step of ion processing is probably a time-of-flight mass analysis since the ions escape from the quadrupole trapping assembly intermittently, rather than as a continuous stream.

Since the translational motion of the ions have been significantly cooled by collisions with the bath gas during storage in such a quadrupole ion trap, it is preferential that the quadrupole assembly be segmented so that the application of a voltage gradient along the length of the quadrupoles can be used to eject the ions after the storage and FAIMS separation steps outlined above.

Figure 21 illustrates the experimental apparatus and methods described in the preceding paragraphs. A quadrupole assembly can be formed using four solid rods (wires) or by assembly of a number of short segments to form rods, which are subsequently arranged as shown at the top of Figure 21. In one example of a segmented quadrupole assembly a different dc potential can be applied to each segment, superimposed upon the sinusoidal waves that are normally applied to the rods. The dc voltage can be used to extract the ions out of the assembly by applying a series of voltages to the rods that differ by some fixed voltage, thereby creating a potential gradient (electric field) that has a component directed along the length of the rods. In this example the ions inside the rod assembly then move towards the end of the rod and out of the rods to another element of the instrument.

Figure 21 also shows a series of cross sections taken across the rods as shown in the dashed line at the end of the solid rods. Since such a section misses two of the rods, the cross section appears to be identical to that of two parallel plates. It is important to note that in regards to the behavior of ions there is little similarity between the quadrupole rods, and flat plates.

Ions are shown in the cross sections at times A, B, C, and D during an experiment involving the application of sinusoidal waveforms and asymmetric waveforms to effect both rf-only and FAIMS modes of operation. At time A, the ions flow into the quadrupole assembly. If a gas is present and the rods are operated in rf-only mode, the ions which were distributed in

various locations between the rods will cool by collisions with the gas and move to the center axis as shown at time B. In this example the ions are assumed to lack significant translational energy along the length of the rods. At time C, the voltages applied to the four rods are changed to affect a FAIMS mode separation.

For the FAIMS mode of operation, many optional methods of application of the asymmetric waveform are available. For example, three rods can be operated with a dc voltage and the asymmetric waveform and compensation voltage applied to the fourth rod. In another example the dc voltage can be applied to a pair of opposite rods and the asymmetric waveform and compensation voltage applied to the remaining two rods. In yet another example the dc voltage can be applied to a pair of adjacent rods and the asymmetric waveform and compensation voltage applied to the remaining two adjacent rods. Irregardless of the details of which rods carry the asymmetric waveform and compensation voltage, the method described here requires that the separation of ions takes place because of the difference in mobility of various ions in fields ( $E/N$ ) that are strong and fields that are weak. The FAIMS method requires that the fields ( $E/N$ ) that the ions experience are strong in a first direction and subsequently weak in the opposite direction with the durations of time selected so that if the ion mobility was independent of the field strength the ion would arrive back at the same location at the end of one complete cycle of the waveform. If  $E/N$  is high enough that the mobility does not remain constant, the ion will drift because of the net difference in distance traveled during the forward and reversed directions of travel.

Referring back to Figure 21, at time C the ions drift away from the center axis at rates of motion that are dependent on the relative mobility of the ion in high and low fields. The application of a compensation field tends to create a balanced condition for some ions so that

they do not collide with the rods. This compensation field is used to separate the ions at time C of Figure 21, so that after a time the remaining ions are a subset of the mixture of ions originally in the rods at time A and time B.

At time D of Figure 21, the voltages applied to the quadrupole rods are returned to their original rf-only operating state (i.e., at time A and B). The ions which were drifting as a result of the asymmetric waveform and compensation voltage return to the center axis of the quadrupole. This minimizes further loss of the ions by returning them to a virtual potential well in the middle of the quadrupole assembly. The process of applying rf-only followed by the FAIMS voltages can be repeated, especially if the ions are trapped in the quadrupole rods by voltages applied to plates at the ends. Repetitive application has the benefit of maintaining the benefit of the potential well caused by the rf-only mode of operation. The FAIMS fields may have virtual minima but these may not be located at the center of the assembly. The ions may alternatively be moved from the virtual well caused by the rf-only mode of operation and the potential well caused by the FAIMS focusing effect. This will be considered further in the discussion below.

Figure 22 illustrates an embodiment which includes an entrance lens and an exit lens (together comprising the end lenses) used to confine and hold the ions in a quadrupole rod assembly containing a low pressure of bath gas. The rods are segmented to permit control (for example extraction, storage) of ions within the assembly. At time A the ions enter through the entrance lens, which is optionally biased at the same (or higher voltage) than the quadrupole rods. If this lens is biased higher than the rods, the ions (having lost energy in collisions) cannot pass out of this lens. At time B in Figure 22 the end lenses are both biased higher than the quadrupole rods and the ions (having lost energy in collisions) cannot exit through either

aperture. At time C, the cooling effect continues, the ions fall to the center axis, and cannot exit through either end lens.

At time D, in Figure 22, the asymmetric waveform and dc compensation voltages are applied to one (or more) rods of the quadrupole assembly and the ions begin to drift. If the balanced condition is not reached for a given ion, the drift is likely to result in collision with one of the rods. Those ions for which the waveform amplitude and the compensation fields are appropriate will not collide with one of the rods. After a separation time, the waveform is again replaced by the sinusoidal wave to operate the rods in rf-only mode, as shown at time E in Figure 22. The ions which were displaced from the center location of the rods will return to the center axis. At time F in Figure 22 the ions are subjected to an electric field by application of dc voltages to the segments of the quadrupole assembly and the ions drift from the assembly through the exit lens.

For brevity in this description, it will be assumed that the reader is familiar with the operation of quadrupole mass spectrometers and the use of quadrupoles in rf-only and in mass analysis modes. It will also be assumed that the reader understands the concepts of ion focusing in FAIMS. This report will extend these understandings to illustrate the use of quadrupole rods for ion storage in rf-only mode and ion separation by FAIMS. Figure 23 is used to assist in the description of the novel application of these technologies for significant improvement in the performance of mass spectrometers.

Figure 23 illustrates an end-on view of quadrupole rods. The diameters of the rods may vary among instruments and the ratio of rod diameter to the spacing between the rods may vary from that illustrated in this figure. The figure is a schematic to help illustrate the fundamentals of the present inventions.

Section A of Figure 23 illustrates several ions 53 that are located among four quadrupole rods (wires), two opposite rods 51 which are connected electrically and the pair of opposite rods 52 also connected electrically (conventional operation in rf-only mode). The pairs 51 and 52 are at the same dc voltage in rf-only mode. If the quadrupole is in a low pressure bath gas, the ions will begin to converge to the center axis due to loss of energy by collisions with the bath gas. After a cooling period, the ions whose trajectories are stable under the conditions of rf voltage and frequency will tend to be found near the central axis of the rods as shown in Figure 23 section B.

Section C of Figure 23 illustrates the conditions during application of the asymmetric waveform to rods 51, and a dc voltage to rods 52. As is practice in any FAIMS system, the voltage of the waveform and the dc voltages are set to select conditions of E/N and compensation fields for establishing a balanced condition for an ion with appropriate mobility behavior as a function of field strength. Around electrodes 51 a balanced condition is established, shown by dotted lines 57, at which the selected ion will neither migrate towards the rod or away from the rod. This region 57 is the focusing region previously discussed in regard to behavior of ions in a FAIMS system.

It is important to note that one might consider the Section C. of Figure 23 to be similar to a group of 4 parallel rods shown in the electrode assembly of Figure 17. The focusing region is shown to be circular and surrounding the electrodes, which will be a good approximation when the four parallel rods shown in Figure 23 Section C are in turn surrounded by a conductive container that provides the same effective conditions as the surrounding (dc voltage) electrodes in Figure 17. For clarity, each of the powered electrodes 12 in Figure 17 are surrounded on all sides by the electrodes 14 held at a dc potential. The four parallel electrodes 51 and 52 in Figure



23 are certainly held within a conductive enclosure held at a dc voltage (or ground potential). With the appropriate dc voltages and distances to the container walls (not shown) a focusing region 57 will surround each rod 51 as shown in Figure 23 Section C. This focusing region will take on different shapes and distances from the electrodes, as a function of the dc voltages and distances to the walls of the container. Nevertheless, the portions of the focusing regions that are inside the space confined by the four rods will be approximately independent of these outside conditions.

Figure 23 Section D, shows that the ions 54 which were located near the center axis of the electrodes in Section B in rf-only mode, will drift in a change to FAIMS modes as they oscillate under the influence of the asymmetric waveform due to the differences in their ion mobility under conditions of low and high  $E/N$ . Some ions 61 will fall into the potential well defined by the FAIMS focus region 57. Other ions for which the waveform voltage and compensation fields are other than appropriate will move to other locations. For example some ions 63 will drift and collide with the rods. Other ions 62 and 64 will drift slowly or find balanced conditions that differ from those of ions 61.

After the conditions shown in Figure 23 Section D have been applied for a period of time, the sinusoidal wave used for rf-only operation of the quadrupoles is restored, and the ions will again move to the center axis shown in Figure 23 Section B. It may be advantageous to alternate between these conditions for a number of times. Recall that some ions collide with the electrodes and these ions are lost. The FAIMS separation therefore leaves a sub-set of the original ions within the electrodes. Also note that this sub-set of ions may not be defined as the same sub-set of ions that might be found after operation of FAIMS of other electrode geometries. For example, parallel plate FAIMS electrodes operated under similar conditions of  $E/N$ ,

waveform voltages, compensation fields, waveform frequency, temperature and gas pressure, may not result in the same sub-set of ions. This will be due to two factors which are dependent on electrode geometry: the resolution of the separation of the ions, and the focusing ability of the electrode assembly. Note that the electrode geometry of Figure 23 may retain ions whose motion (low mobility) is very slow even though the conditions may not favor focusing or a balanced condition for these particular type of the ions. This will be a function of the periods of time during which the quadrupole rod set is operated in rf-only mode and in FAIMS separation mode. These relative periods of time were not present or were not applicable to flat plate FAIMS (or many other FAIMS geometries) previously considered.

The details of the electronic methods for application of the sinusoidal waves or the asymmetric waveform have not been considered. Many possible approaches will be applicable. It is worthy of note however, that the time required for transition between these modes of operation is in practice other than zero. However it is important that the electronic transitions be controlled in a manner to avoid loss of ions to the walls of the electrodes. For example, removal of the waves and waveforms with remaining dc voltages in place will result in loss of the ions. The waveform transitions must be synchronized with changes in dc voltages. Note also that at lower gas pressures, the ion mobility is very high and the ions may respond to the fields quite rapidly. Therefore the transitions between modes of operation must be controlled carefully.

In one possible approach to managing the waveforms, the sinusoidal waves of the two frequencies used to form the FAIMS asymmetric waveform can be applied to the rods in an independent fashion. In other words, one of the sinusoidal waves may already be on a given rod (e.g., for purposes of operation in rf-only mode), and the second (higher or lower) frequency added by ramping the amplitude of this second wave from zero to the target amplitude. After the

selected period of time the amplitude of this second wave is ramped back to zero leaving the original sinusoidal wave (which then forms part of the voltages applied during rf-only mode of operation). During the slew up and slew down of the second wave, the applied dc voltages are also slewed in a manner to maintain conditions (e.g. focus region) for the ion of interest.

In a second suggested manner for control of the transitions between rf-only and FAIMS modes of operation, the component sinusoidal waves could always be present on the rods, but in phase relationships that will not give the FAIMS separation. For example certain values of the phase shift (for example zero radians) may result in a waveform that is symmetric (rather than asymmetric). A controlled change of the phase angle could then be used to convert to FAIMS operation. The gradual change in phase angle between the two sinusoidal waves allows the applied waveform to be converted smoothly to the desired asymmetric shape. The appropriate dc levels would be applied in synchronization with the phase shifts in order to maintain balanced conditions (FAIMS operation), or at low levels of asymmetry, to maintain rf-only operation.

For clarity, in operation in rf-only mode, the sinusoidal waves applied to the opposite pairs of electrodes are 180 degrees out of phase as shown in the upper right corner of Figure 24. This means the maximum positive voltage is applied by rf power supply 3 to one pair 1 of (diagonally opposite) rods at the same time as the maximum negative polarity voltage is applied to the other pair of electrodes 2. Put in another way, the center axis of the four rods is at a fixed dc value and the pairs of rods are alternately held above and below this dc value. In mass separation mode another dc difference between the rods is also imposed.

It is possible for the quadrupole assembly to operate in rf-only mode with asymmetric waveforms applied to the rods. Consider the application of square waves with a short time of higher voltage and a longer time of opposite polarity lower voltage as shown on the lower right

corner of Figure 24. In a type of rf-only operation this waveform can be applied so that one pair of rods is at the high voltage 5 in positive polarity while the opposite rods are at the same voltage 8 of opposite polarity. The two pairs of rods switch simultaneously to the opposite polarity and one pair is held at the lower voltage 6 and the other pair is at the same voltage 9 of opposite polarity. This establishes the same condition of the center axis remaining at a constant fixed dc potential. In rf-only mode of operation  $V_1$  and  $V_2$  will be equal. If  $V_1$  and  $V_2$  are not equal the rods operate in mass analysis mode. Difference in  $V_1$  and  $V_2$  establishes a compensation voltage in FAIMS mode of operation.

Will application of asymmetric waveforms as shown in Figure 24 create a FAIMS type of separation? The answer lies in asking the same question for voltages applied to parallel plates. It is clear that there are many ways to achieve the introduction of the fields between parallel plates, including the method of holding one plate at a fixed dc voltage while applying the waveform to the other plate. This means that the middle point between the two plates does not stay at the same apparent dc level. If a constant dc level at the middle point between the plates was required, one plate would be positive and the other plate negative relative to this middle dc voltage. Two asymmetric waveforms would be applied to the opposite parallel plates using the traces shown in the lower right corner of Figure 24. Taking the square waveform example, the electric field in a first direction would be established by a positive voltage 5 on one plate and a negative voltage 8 on the second plate. Simultaneously both plates would change voltage to the opposite polarity, both voltages being of equal magnitude (absolute value), for example 6 and 9 in Figure 24. In other words both plates would carry an asymmetric waveform of opposite polarity. Together, the appropriate fields are established between the plates. A compensating dc

field must also be applied through, for example, the dc offset voltage via a difference of values of  $V_1$  and  $V_2$  in Figure 24.

Hence the quadrupole rods can be operated in rf-only mode by application of the asymmetric waveform and the conditions for the FAIMS separation can simultaneously be applied. The transition between purely rf-only mode and FAIMS separation mode is created by phase shifts in the two sinusoidal waves that comprise the asymmetric waveform. For example, Figure 25 illustrates waveforms with phase shifts ranging from the usual  $\pi/2$  to zero radians, where the maximum asymmetry is affected with a phase shift of  $\pi/2$  and no asymmetry results with a phase shift of zero radians. In a FAIMS system consisting of parallel flat plates, an ion separation takes place during application of compensation voltage and a waveform generated with phase shift of  $\pi/2$ , while at the other extreme, no ion separation can be achieved if the waveform is generated with a phase shift of zero radians. On the other hand, when applied to quadrupole rods, the phase shift of zero radians will result in conventional rf-only mode of operation (with mass range and low mass cutoff as appropriate to voltages and frequencies of the sine waves).

Note that the dc voltages appropriate to the FAIMS separation must accompany application of the asymmetric waveform because the application of fields that are asymmetric in time will establish an ion drift towards one of the electrodes. Collision with a wall will occur unless some balancing force is established. In the quadrupole electrode geometry the virtual potential well of the rf-only mode of operation can be used to effect this balancing action. For example if the potential well developed in rf-only mode (with bath gas) causes the ions to drift at a finite rate towards the center axis of the quadrupole assembly, and the drift caused by application of an asymmetric waveform causes a given type of ion to drift towards the rod, the



Behavior of ions in each of these cases can be readily deduced with understanding of the mechanism of FAIMS focusing and ion separation.

## Figure Captions (incomplete descriptions)

- Figure INTRO1** Three possible examples of changes in ion mobility as a function of the electric field strength.
- Figure INTRO2** Illustration of the trajectory of an ion between two parallel plate electrodes under the influence of the electrical potential  $V(t)$ .
- Figure INTRO3** A "domed" FAIMS device described in filings by the same inventor.
- Figure INTRO4** A "domed" FAIMS device as previously described
- Figure INTRO5** A "side-to-side" FAIMS device as previously described.
- Figure INTRO6** Tandem FAIMS device consisting of two side-to-side FAIMS and one dome FAIMS device.
- Figure 1** The asymmetric waveform used for FAIMS, shown as a function of time (x-axis is time).
- Figure 2** Electronic circuit (simplified) for generating the asymmetric waveform for application to the FAIMS electrodes.
- Figure 3** Simplified schematic of the inductance used in the tuned LC circuit for FAIMS.
- Figure 4** The inductance shown in Figure 3, with refinements including split core.
- Figure 5** The inductance shown in Figure 4, with improvements including the parallel application of primary turns.
- Figure 6** The asymmetric waveform used for FAIMS.
- Figure 7** The data points of the waveform shown in Figure 6, but arranged from smallest to largest (x-axis is percent of the number of points available).



- Figure 8** Error analysis of the three types of distortion of the asymmetric waveform, with data arranged in the same manner as shown in Figure 7, the original points were sorted from smallest (most negative) to largest (most positive).
- Figure 9** Error analysis of Figure 8, with expanded y scale to show about 5% errors in both positive and negative sense.
- Figure 10** The electrodes of a new geometry FAIMS, asymmetric waveform power on 30 and dc voltage on 40. Ions enter at 20 and leave at 70.
- Figure 11** The electrodes of the new geometry FAIMS as shown in Figure 10, with gas flows indicated.
- Figure 12** The electrodes of the new geometry FAIMS as shown in Figure 10, with ion flows into orifice 20 and out of 70 indicated. The ion trajectory 110 is hand-drawn and does not reflect a computer generated oscillation.
- Figure 13** A new geometry FAIMS, in which one of the sets of plates shown in Figures 11 and 12 are replaced by a single plate held at a dc voltage. An asymmetric waveform on this plate makes the geometry similar to the previous 3 parallel plate electrode version of FAIMS.
- Figure 14** The new geometry FAIMS shown in Figure 13, with indication of gas flow and the ion motion. Although the curve is hand drawn for simplicity (to remove the many repeat oscillations caused by the waveform) the ion trajectory represents the results from computer simulation of the directions that the ions will take while traveling through an electrode assembly of this type. Regions labeled 570 are focusing regions around the ends of the electrodes to which the asymmetric waveform is applied.

- Figure 15** The new geometry of FAIMS shown in Figure 10, with the indications of the focusing regions at the ends of the powered electrodes, and the approximate trajectory the ion will take while passing through this electrode arrangement. Although the curve is hand drawn for simplicity (to remove the many repeat oscillations caused by the waveform) the ion trajectory represents the results from computer simulation of the directions that the ions will take. Regions labeled 770 are focusing regions around the ends of the electrodes to which the asymmetric waveform is applied.
- Figure 16** A geometry of FAIMS based on an array of parallel rods.
- Figure 17** The geometry of parallel rods FAIMS, showing gas flows and regions of ion focusing around electrodes to which the asymmetric waveform (DV) and the dc compensation voltage (CV) are applied, other rods and electrodes are at a dc potential (ground potential for example).
- Figure 18** Ion trajectories as they pass through the parallel rod geometry FAIMS. The ions jump from focus region to focus region as the gas carries the ions through the electrode array, assuming that the ion focuses around electrodes to which the asymmetric waveform (DV) and the dc compensation voltage (CV) are applied. The other rods and electrodes are at a dc potential (ground potential for example).
- Figure 19** Ion trajectories as they pass through the parallel rod geometry FAIMS. The ions jump from focus region to focus region as the gas carries the ions through the electrode array, assuming that the ion focuses around electrodes to which the asymmetric waveform (DV) and the dc compensation voltage (CV) are applied.

The gas flow tends to pull the ions from a multitude of spaced inlets to a single outlet in a ion funneling fashion.

- Figure 20** Alternative arrangement of the parallel rods in a new geometry of FAIMS electrodes.
- Figure 21** Storage and separation of ions in quadrupole rod assembly operated in rf-only mode and in FAIMS separation mode.
- Figure 22** Storage and separation of ions in a segmented quadrupole rod assembly with entrance and exit lenses, operated in rf-only mode and in FAIMS separation mode.
- Figure 23** End view of ions motions, for storage and separation of ions in a segmented quadrupole rod assembly with entrance and exit lenses, operated in rf-only mode and in FAIMS separation mode.
- Figure 24** Application of sinusoidal and asymmetric square waves to quadrupole rods.
- Figure 25** Phase shifts between the two sinusoidal waves comprising the asymmetric waveform modify the asymmetry of the waveform for use in a multi-use quadrupole rod assembly.

Figure INTRO1

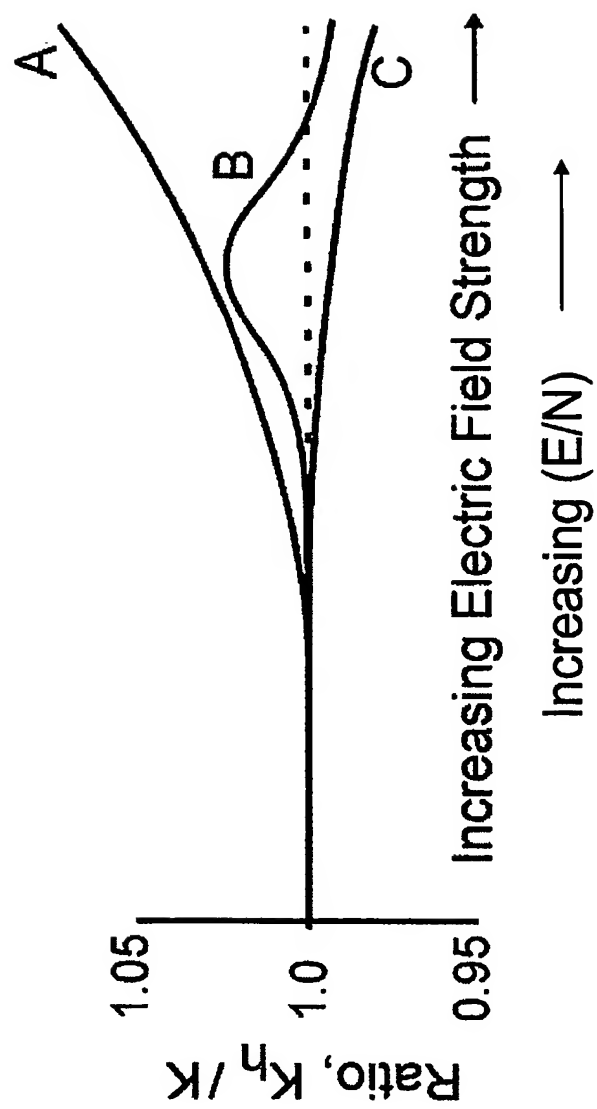


Figure INTRO2

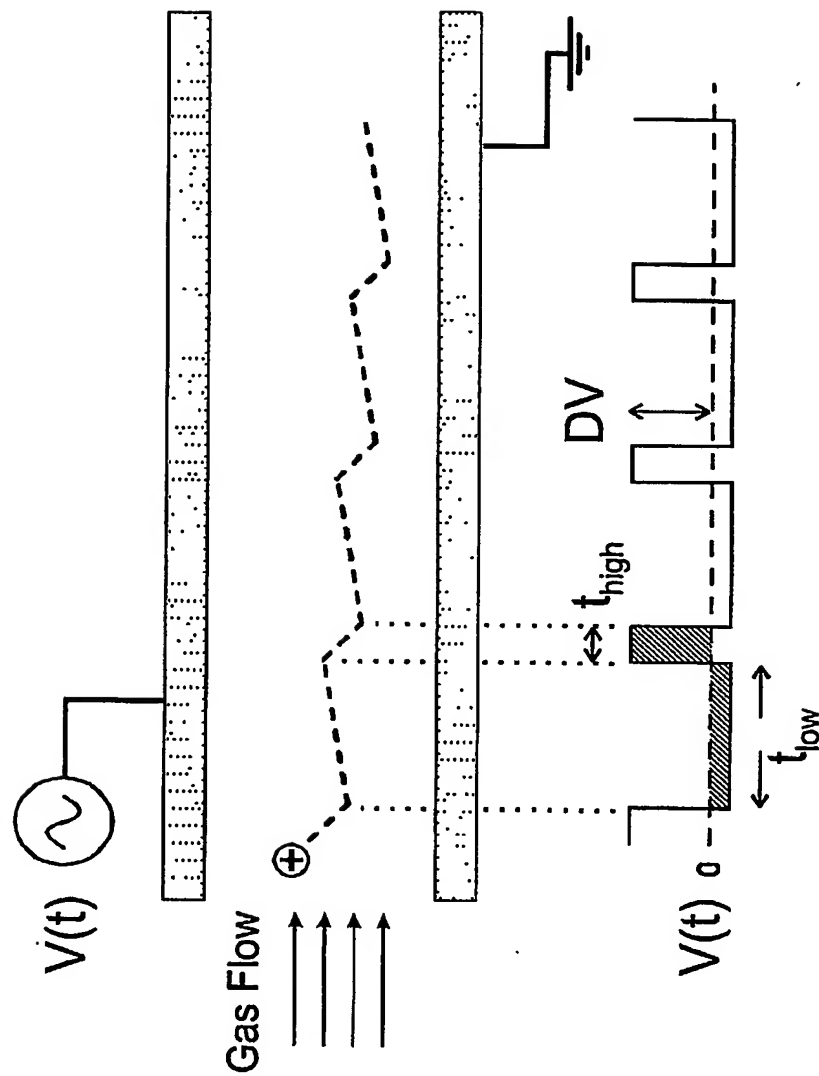
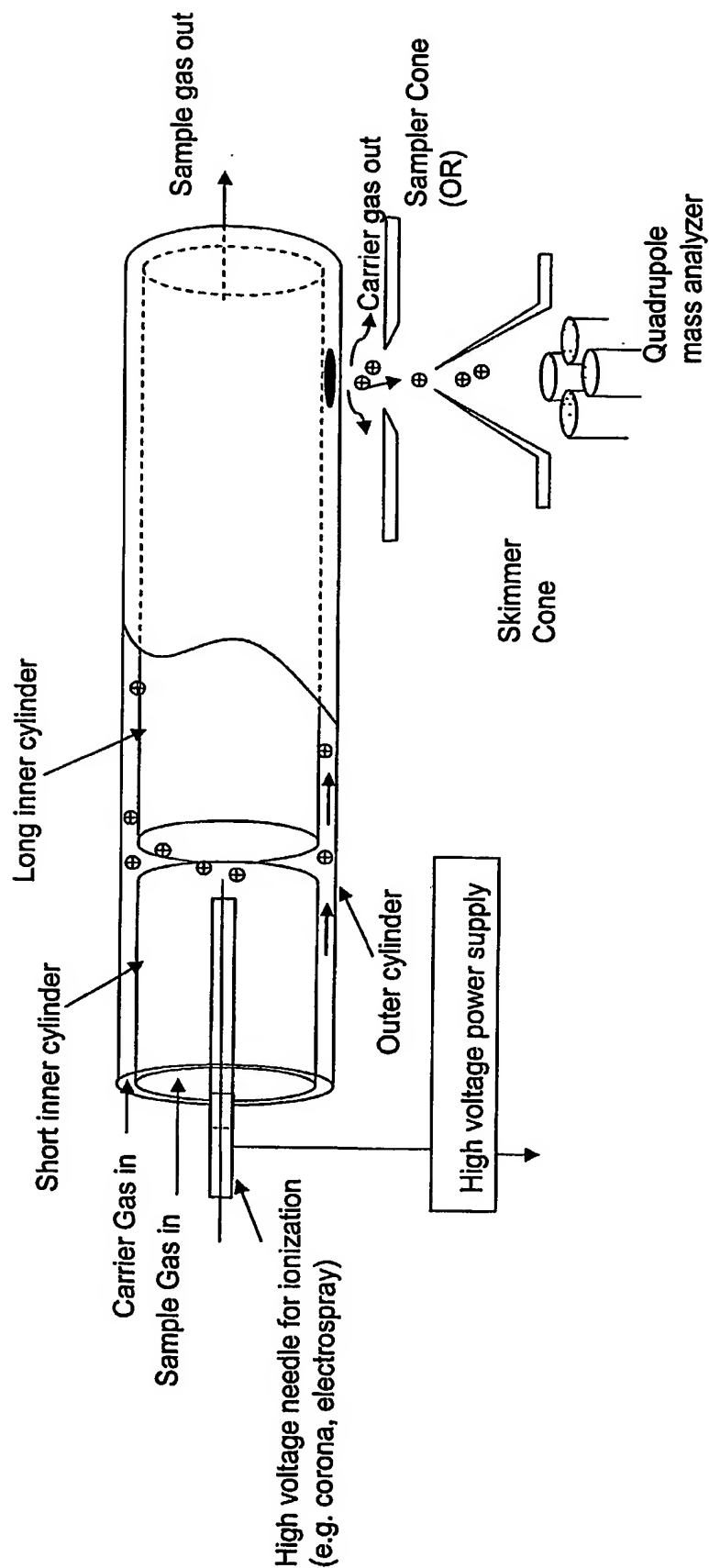


Figure INTRO3



60413162, 092502

Figure INTRO4a

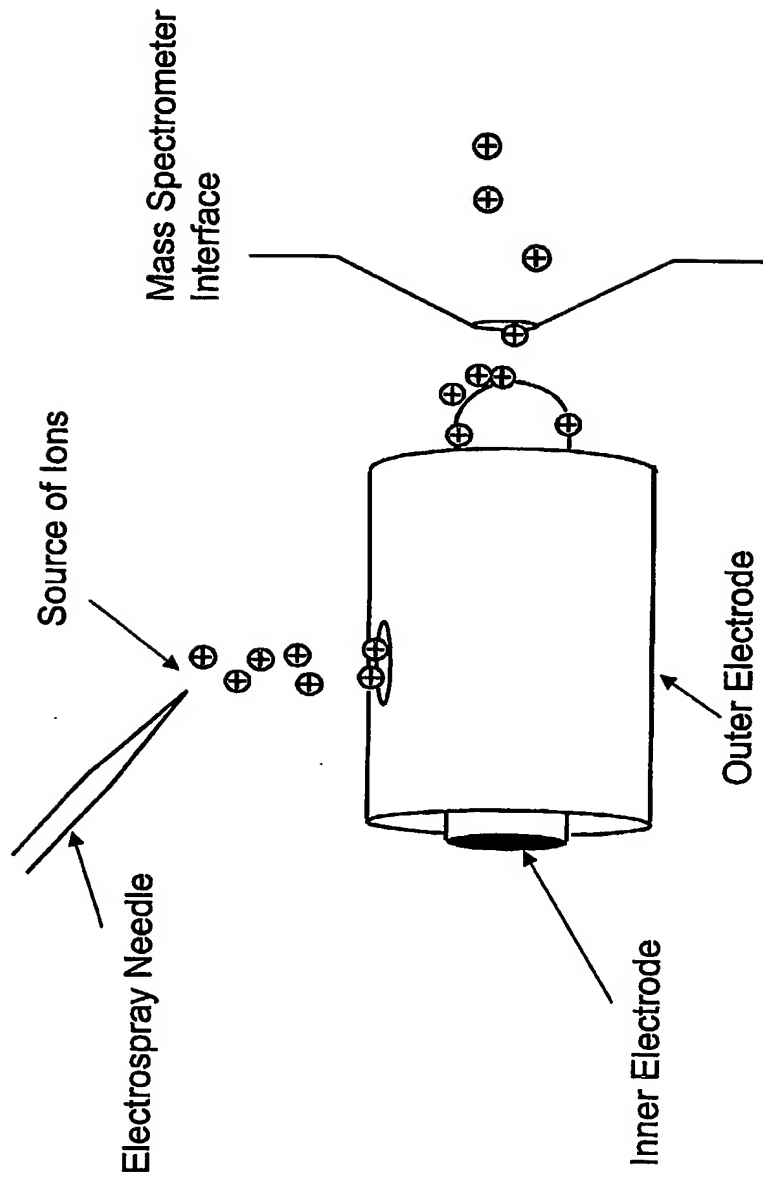
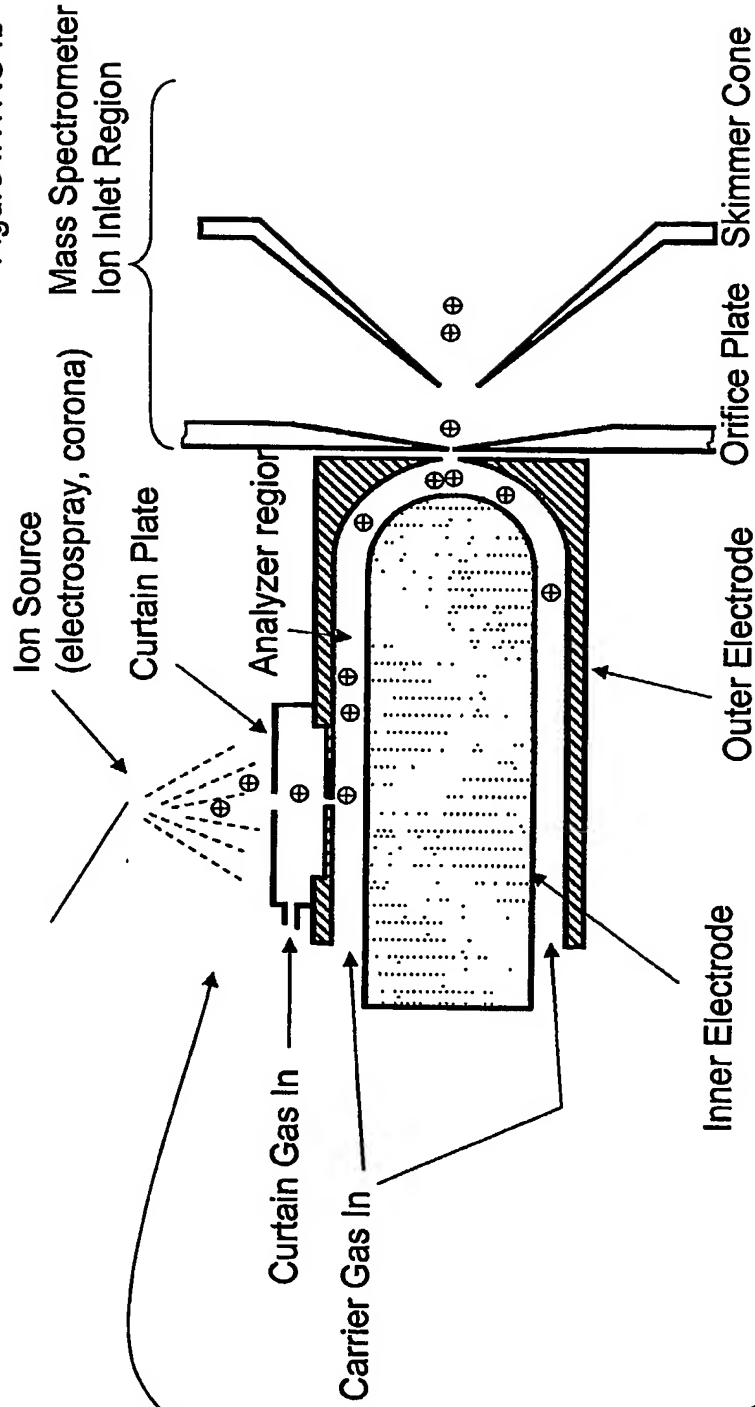


Figure INTRO4b



Expanded view of curtain plate region

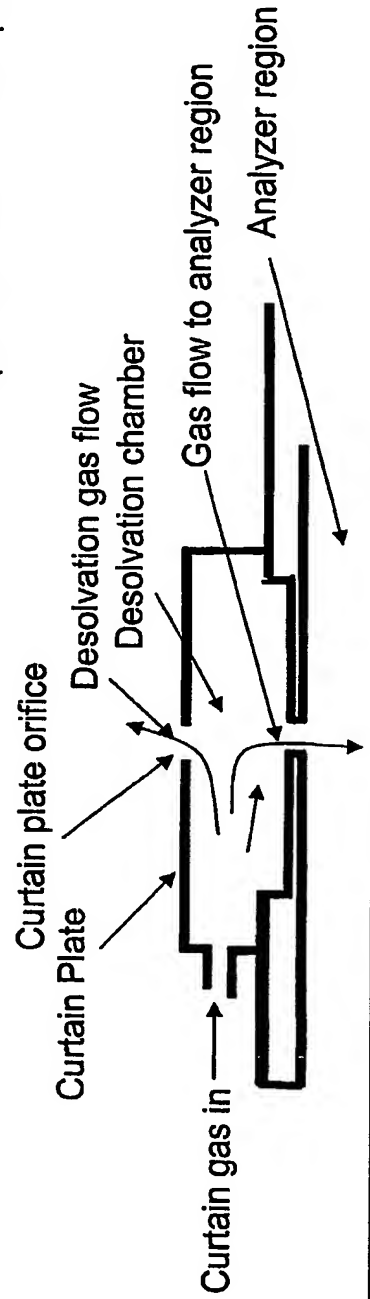




Figure INTRO5

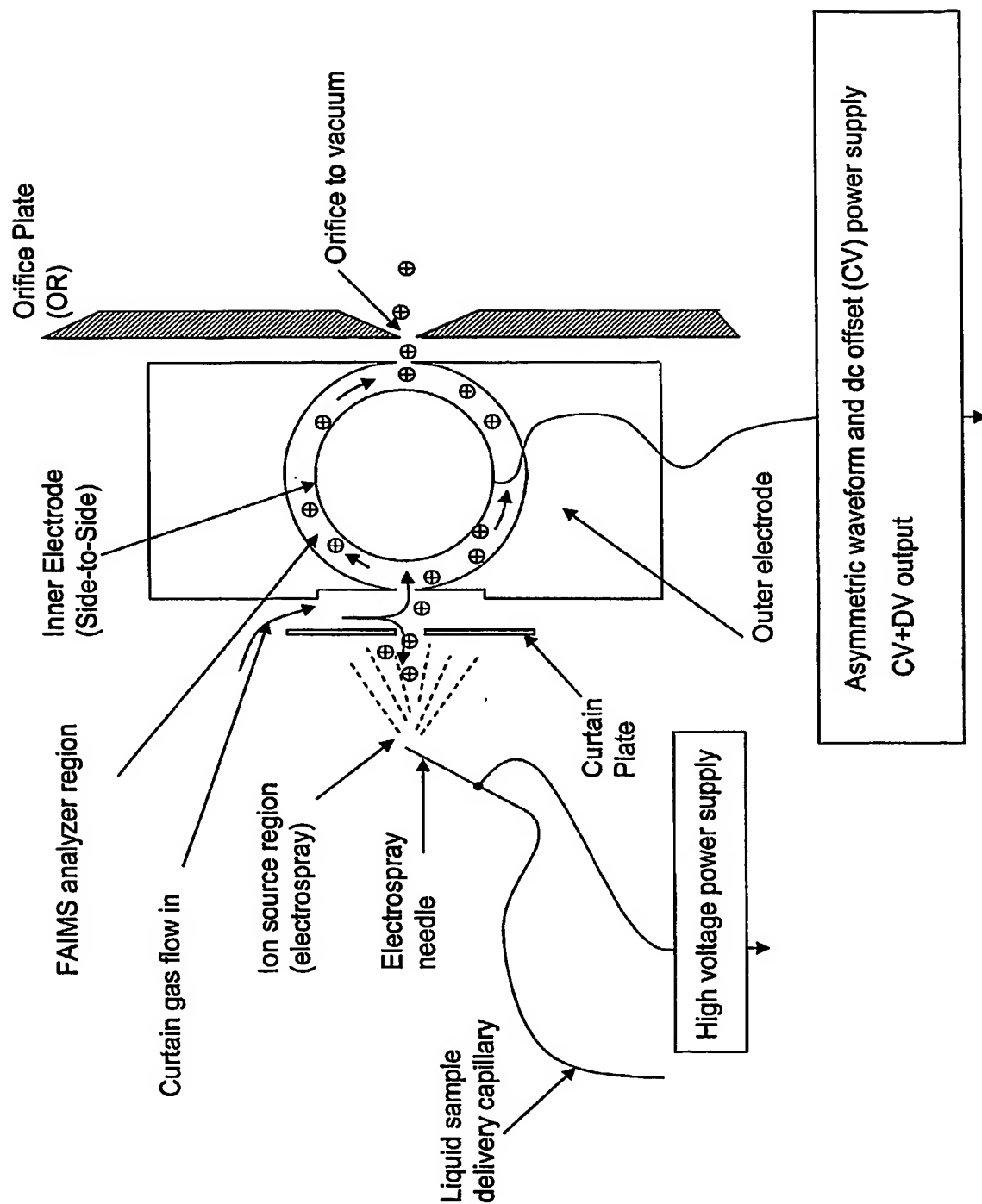
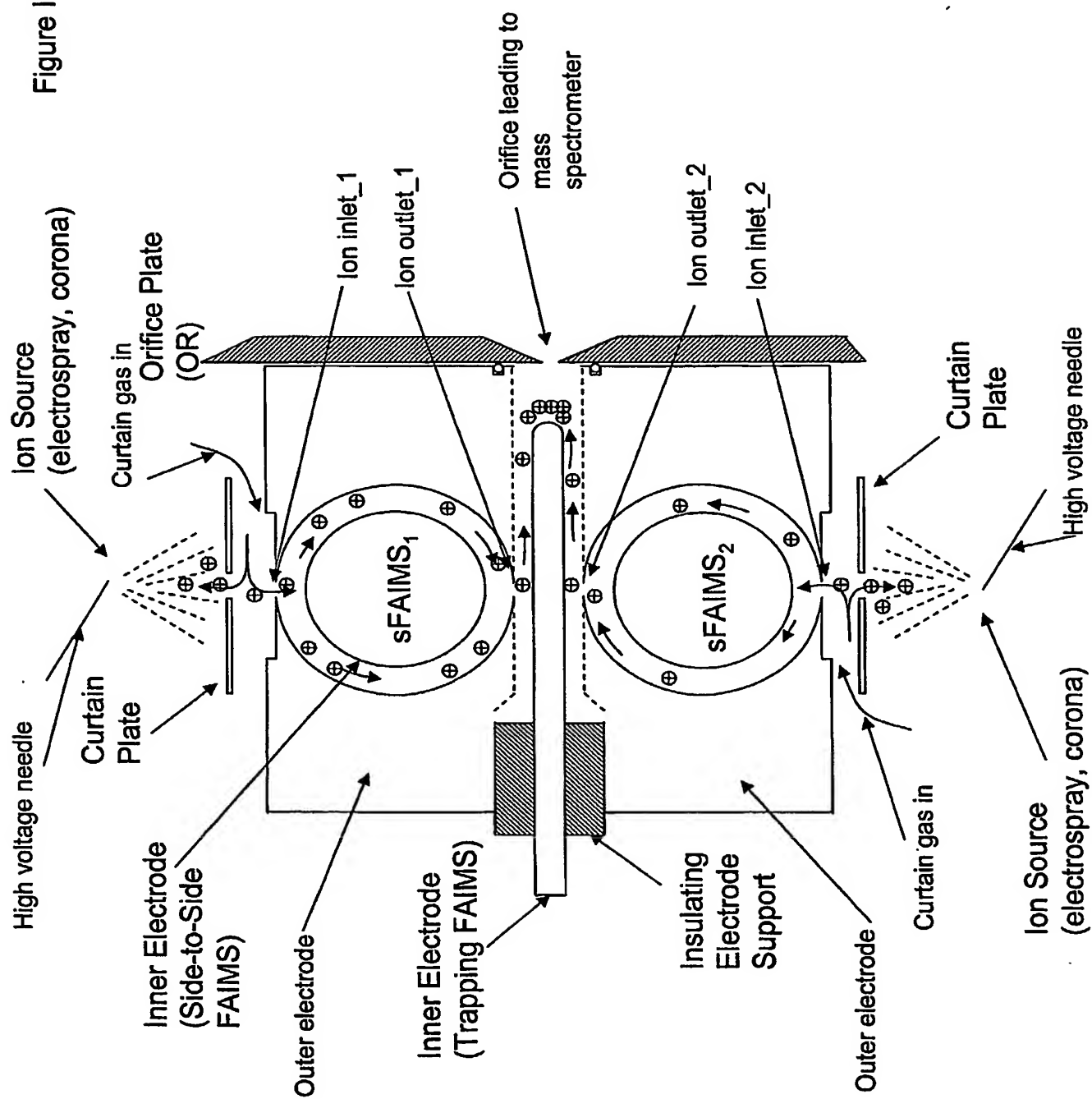


Figure INTRO6



Asymmetric Waveform used in FAIMS. This waveform has the maximum voltage in the positive polarity (positive polarity DV). The waveform is normalized to give  $DV=1$ . In operation DV is usually about 4000 volts with a 2mm space between FAIMS electrodes.

Figure 1

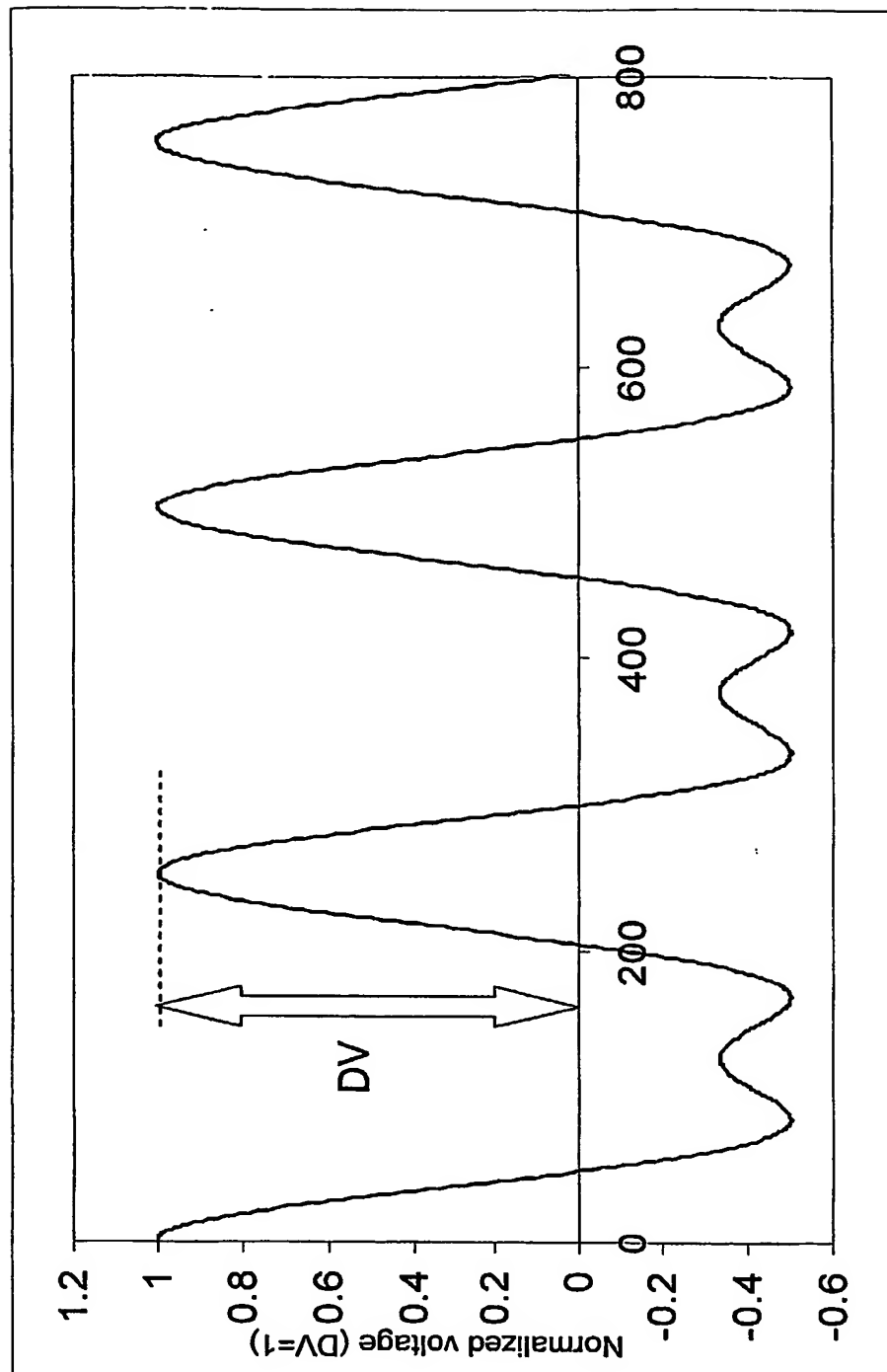
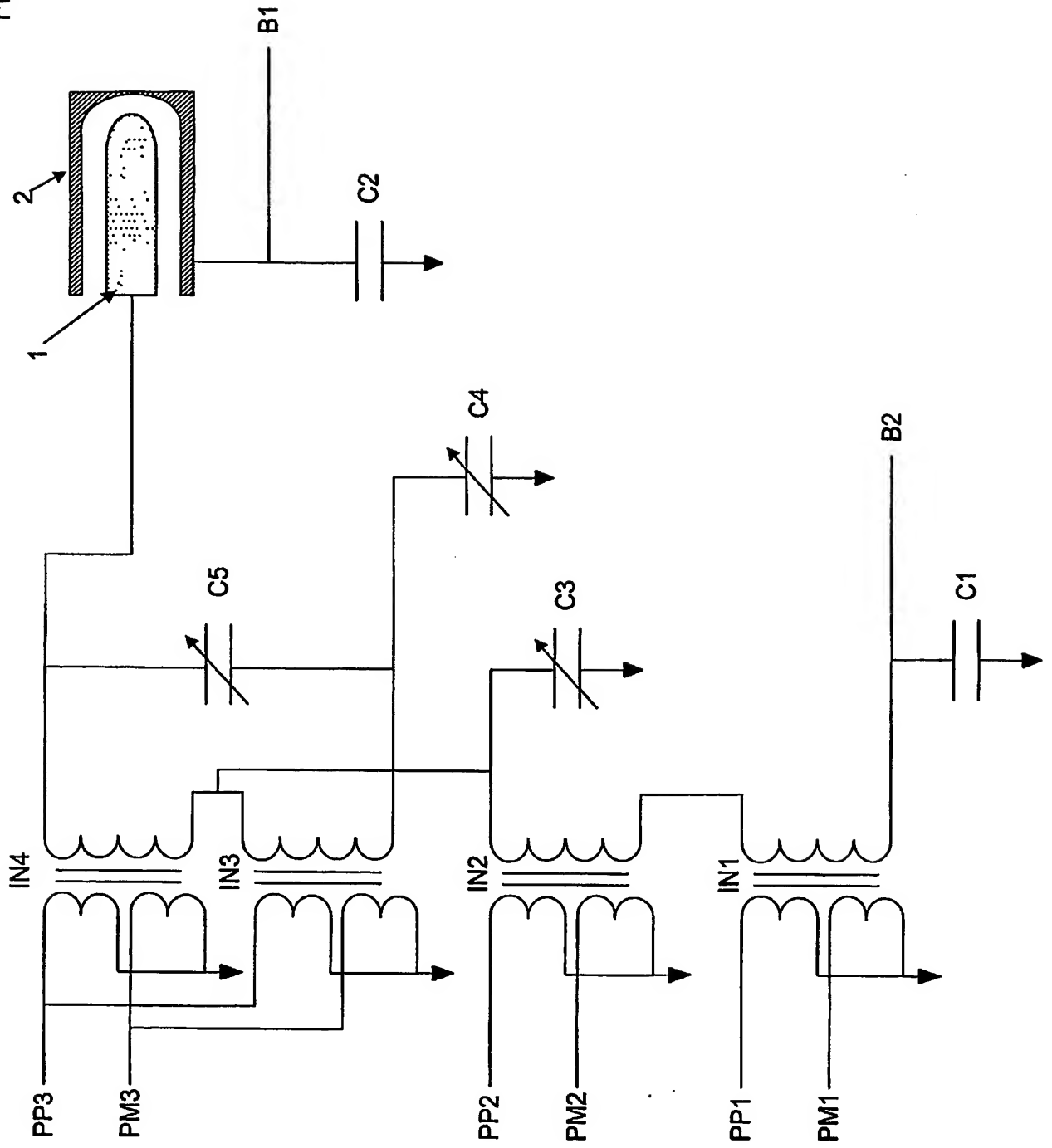


Figure 2a

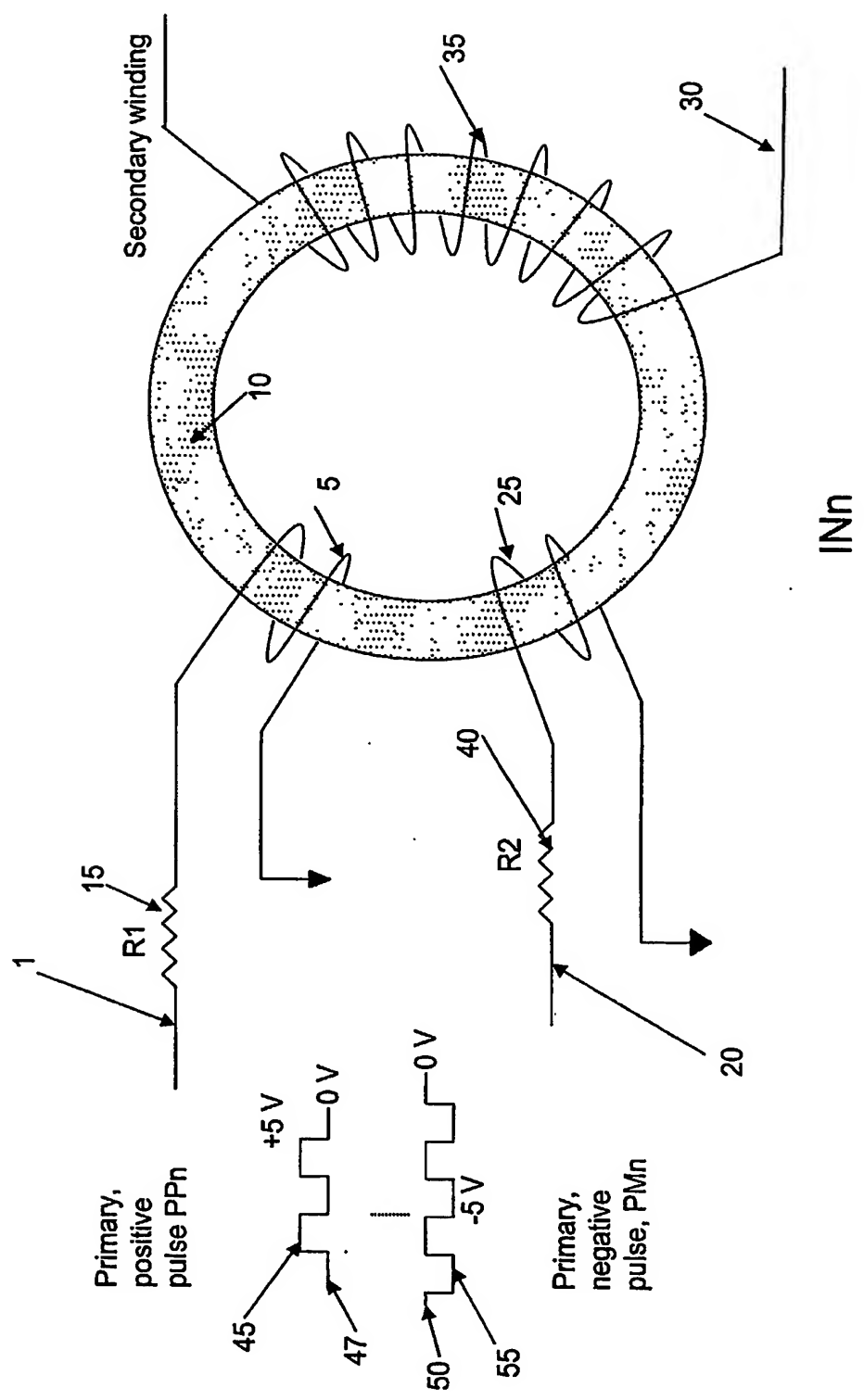


[illegible]

**Note: Switches C,D operate similarly but different frequency, and with a phase offset from A, B**

The diagram shows two digital signals, Switch A, Sa and Switch B, Sb, over time. Switch A starts in the 'open' state, transitions to 'closed', and then back to 'open'. Switch B starts in the 'closed' state, transitions to 'open', and then back to 'closed'. The transitions for both switches occur at the same time points, indicated by vertical dashed lines. The labels 'open' and 'closed' are placed above the signal lines with arrows pointing to the corresponding state.

Figure 3





The diagram illustrates a multi-layer printed circuit board (PCB) structure. It consists of a top layer (1) and a bottom layer (20), separated by a core (15). The top layer (1) contains a resistor (R1) and is connected to a terminal (15). The bottom layer (20) contains a resistor (R2) and is connected to a terminal (40). The core (15) is shown as a central rectangular block between the two layers.

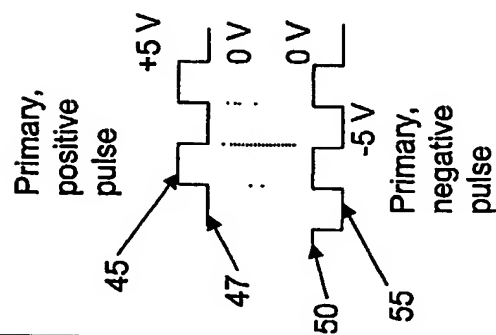




Figure 6

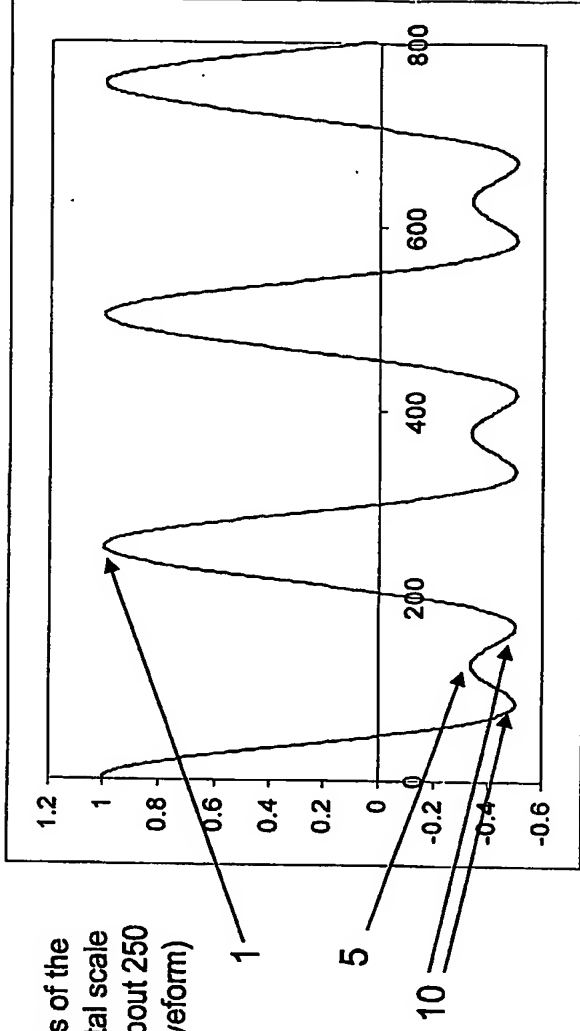


Figure illustrating several cycles of the asymmetric waveform, horizontal scale is arbitrary number of points (about 250 data points per cycle of the waveform)

Figure 7

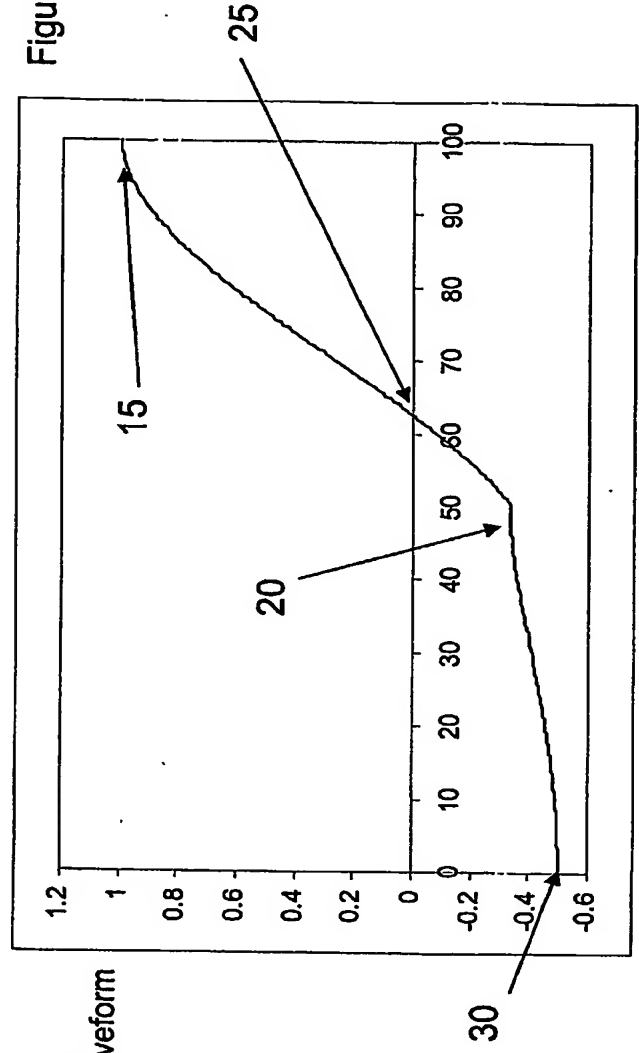
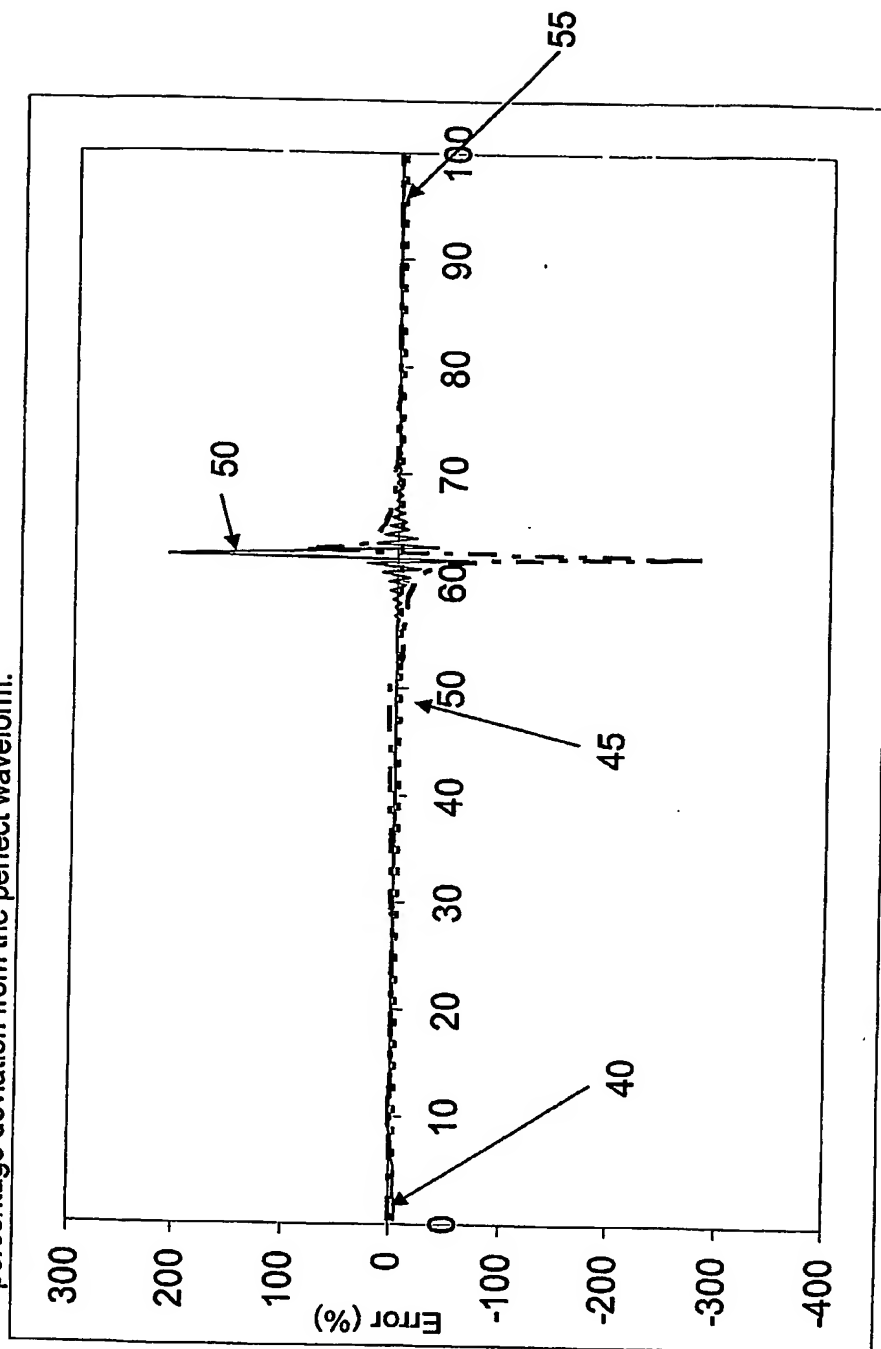


Figure illustrating the distribution(%) of data points in one cycle of the waveform Illustrated in the figure above.

Figure illustrating the percentage deviation from the ideal distribution of magnitude data points from an ideal waveform. The horizontal axis is percentage of one cycle of the waveform, and the vertical axis is percentage deviation from the perfect waveform.



Three types of errors are represented

- (a) Solid line: 5% error in phase
  - (b) Dot-Dash line: 5% error in ratio  $A/B$ , but  $A+B=1$
  - (c) Dash line: 2.4% error in  $A+B$ , but  $A/B=2$
- $\%Error = 100 \cdot (p-d)/p$  where  $p$  are points on the ideal curve, and  $d$  are points on the curve under test.

Figure illustrating the percentage deviation from the ideal distribution of magnitude data points from an ideal waveform. The horizontal axis is percentage of one cycle of the waveform, and the vertical axis is percentage deviation from the perfect waveform. The vertical axis has been expanded to permit viewing of details of the order of 5% error from the expected waveform shape.

Figure 9

Three types of errors are represented  
 (a) Solid line: 5% error in phase  
 (b) Dot-Dash line: 5% error in ratio  $A/B$ , but  $A+B=1$   
 (c) Dash line: +2.4% error in  $A+B$ , but  $A/B=2$   
 $\%Error = 100 \cdot (p-d)/p$  where  $p$  are points on the ideal curve, and  $d$  are points on the curve under test.

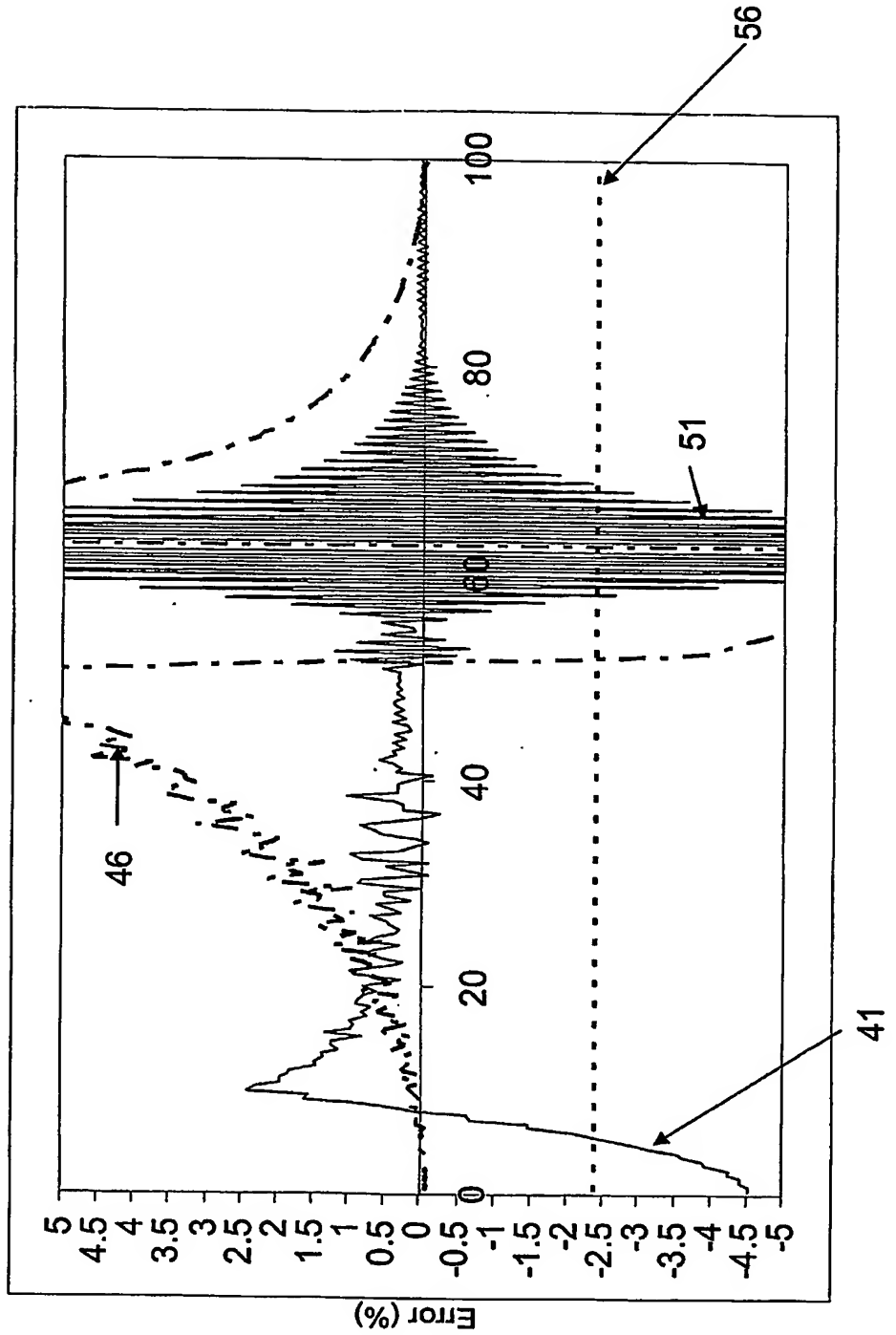


Figure 10

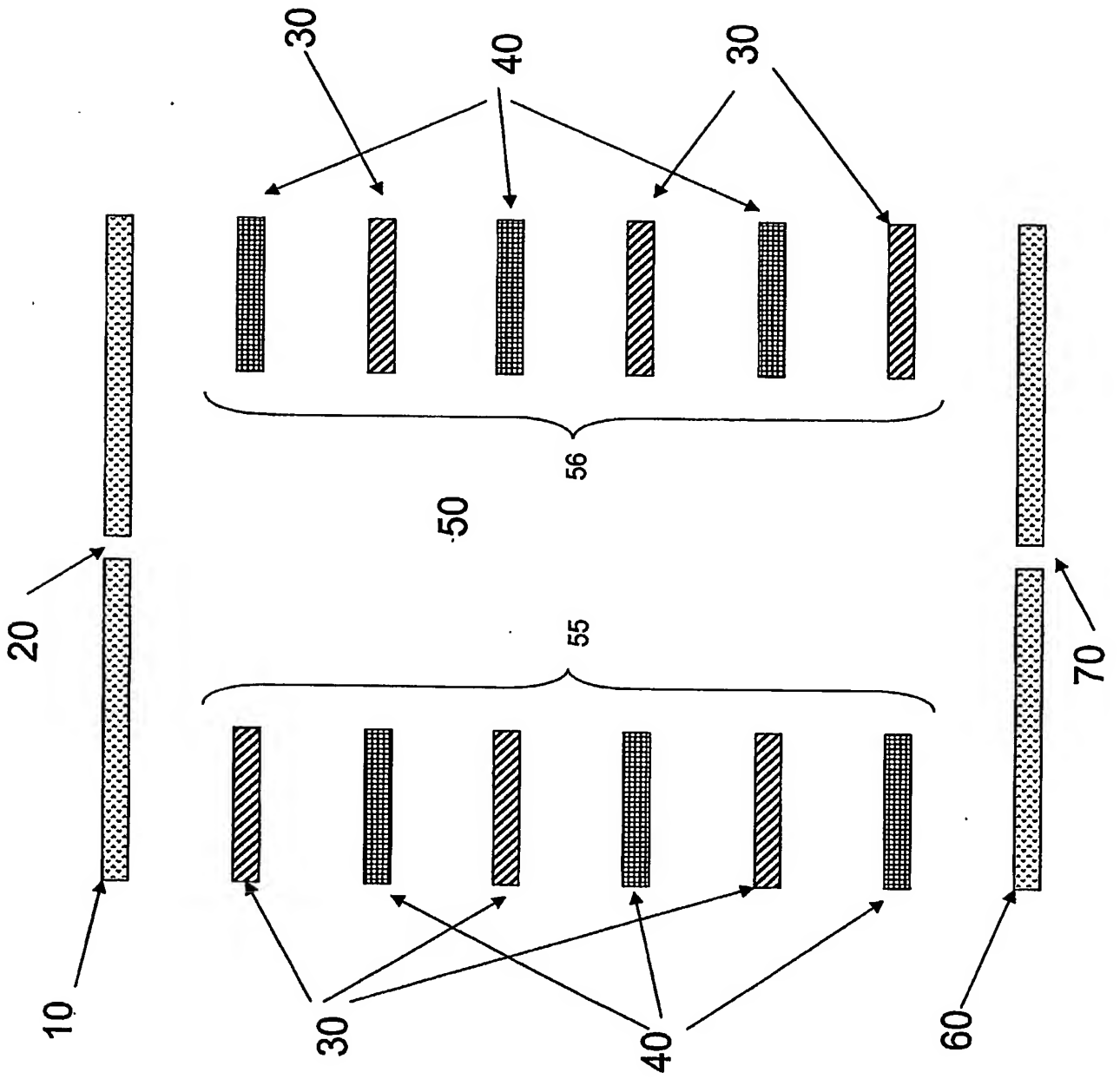


Figure 11

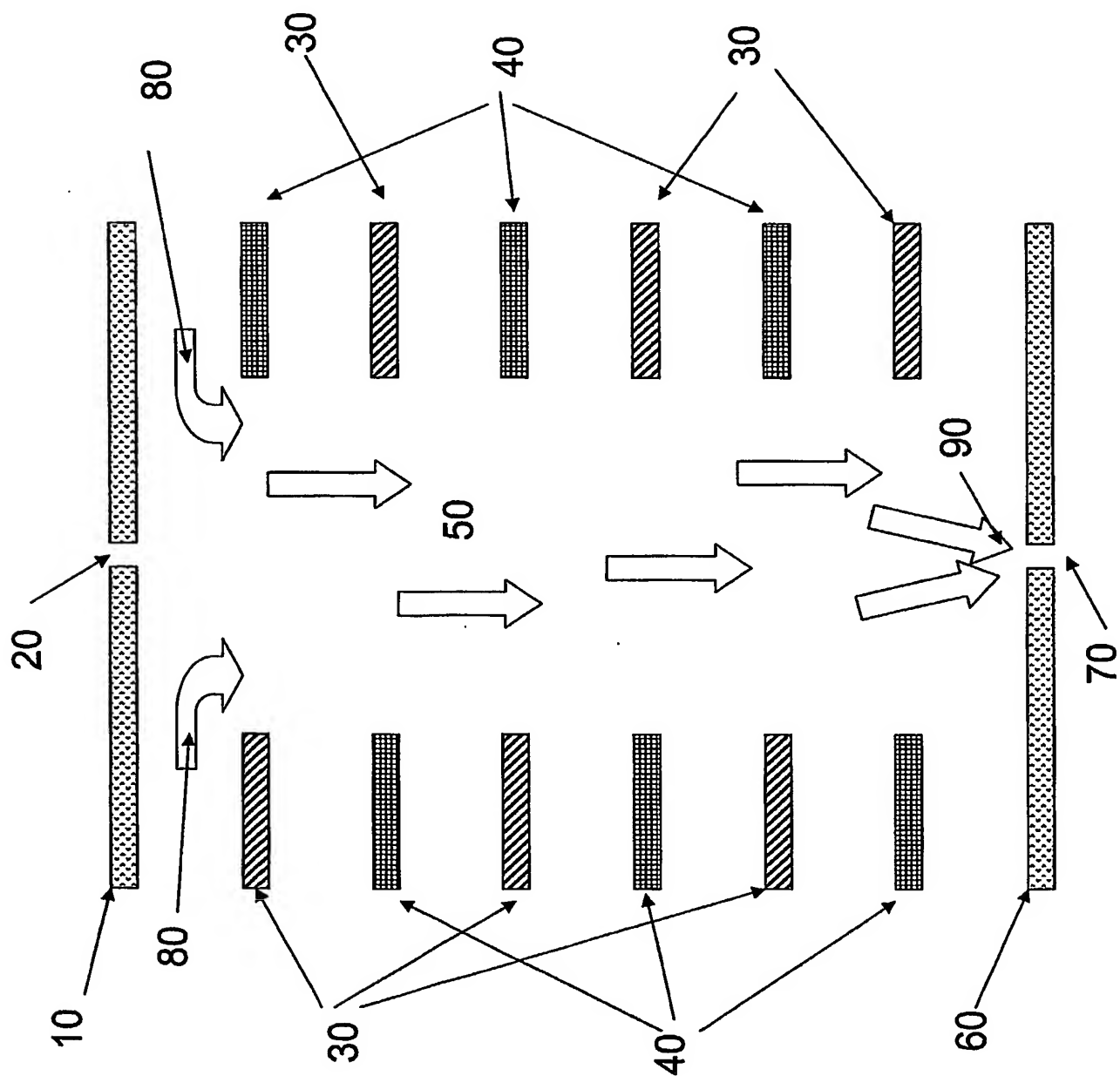


Figure 12

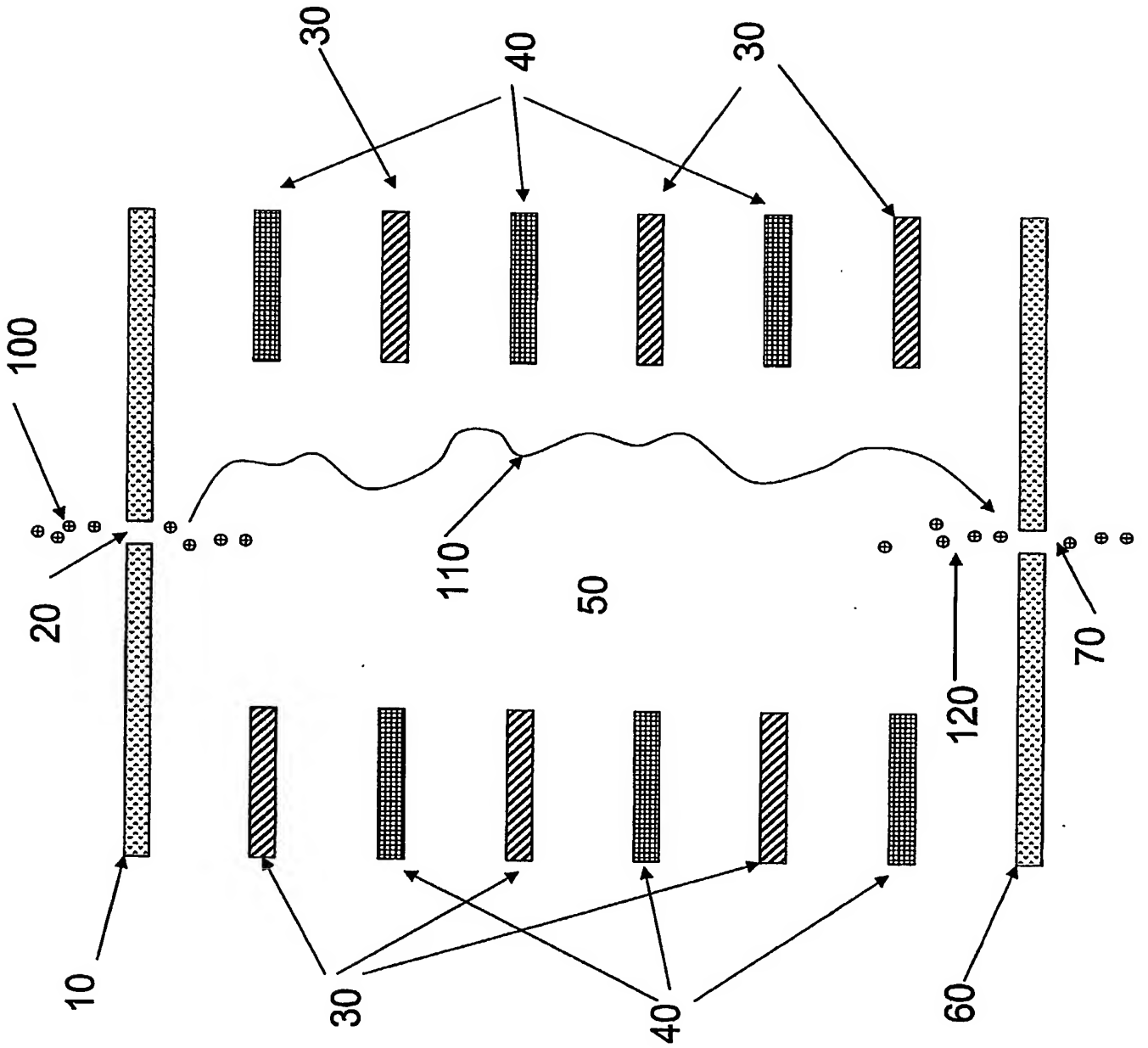


Figure 13

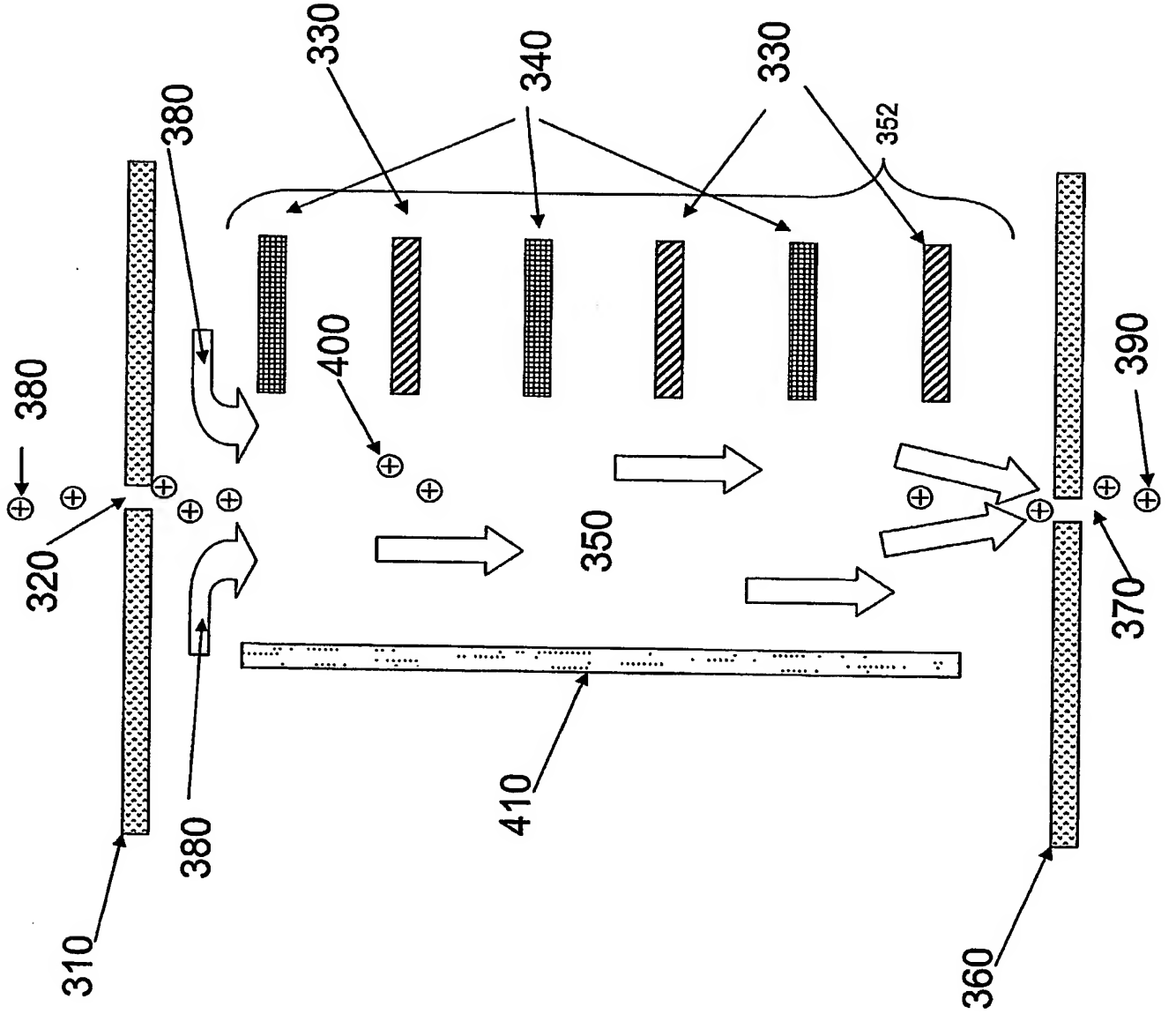


Figure 14

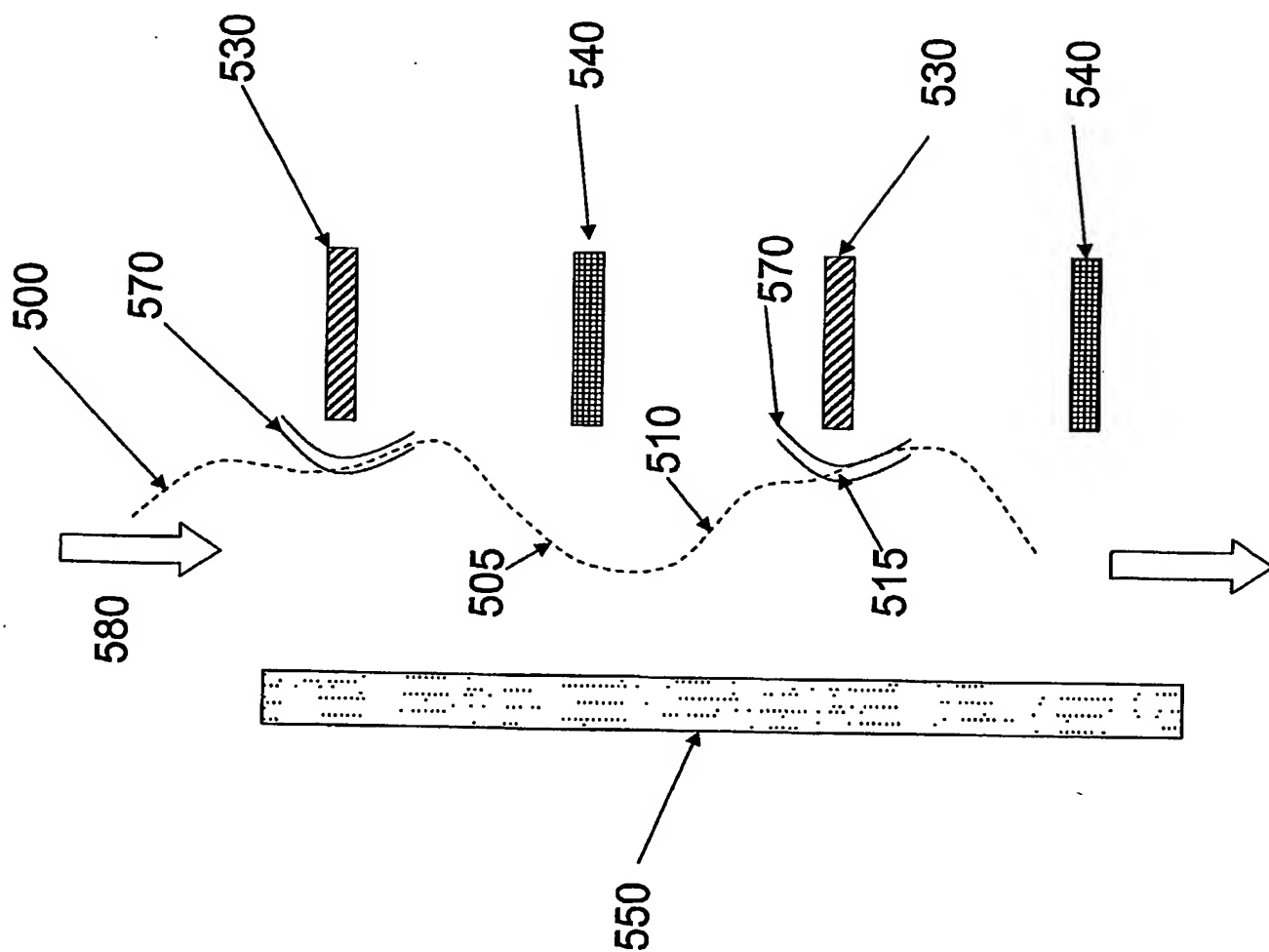




Figure 15

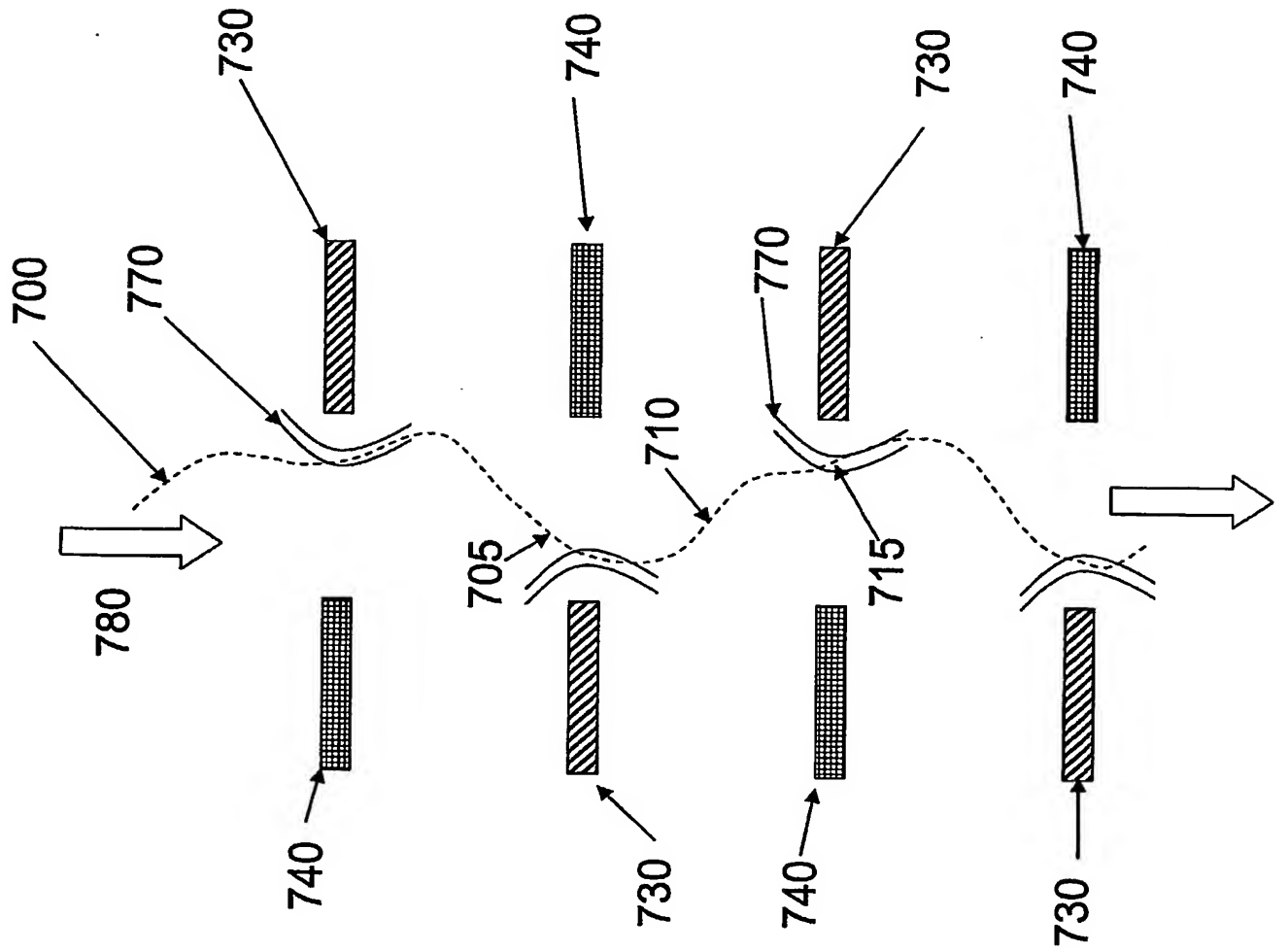


Figure 16

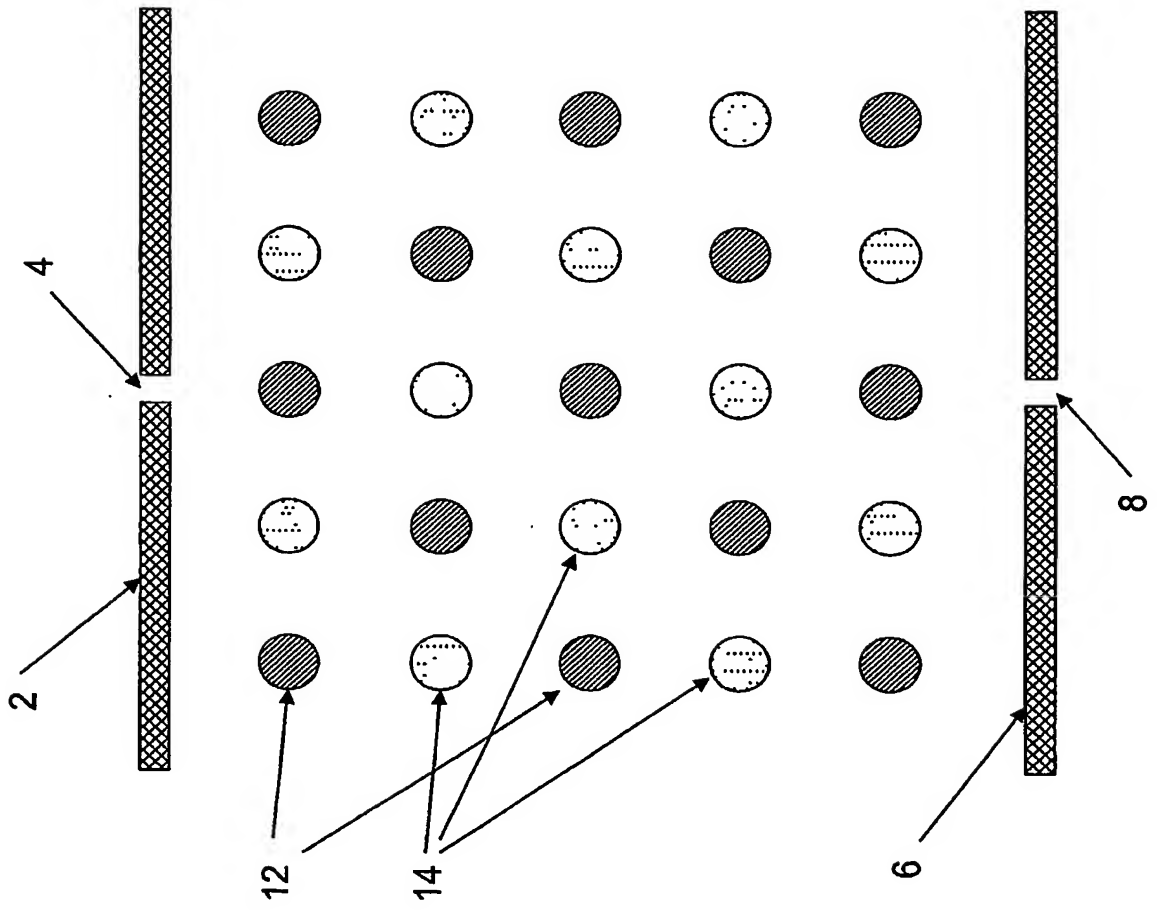


Figure 17

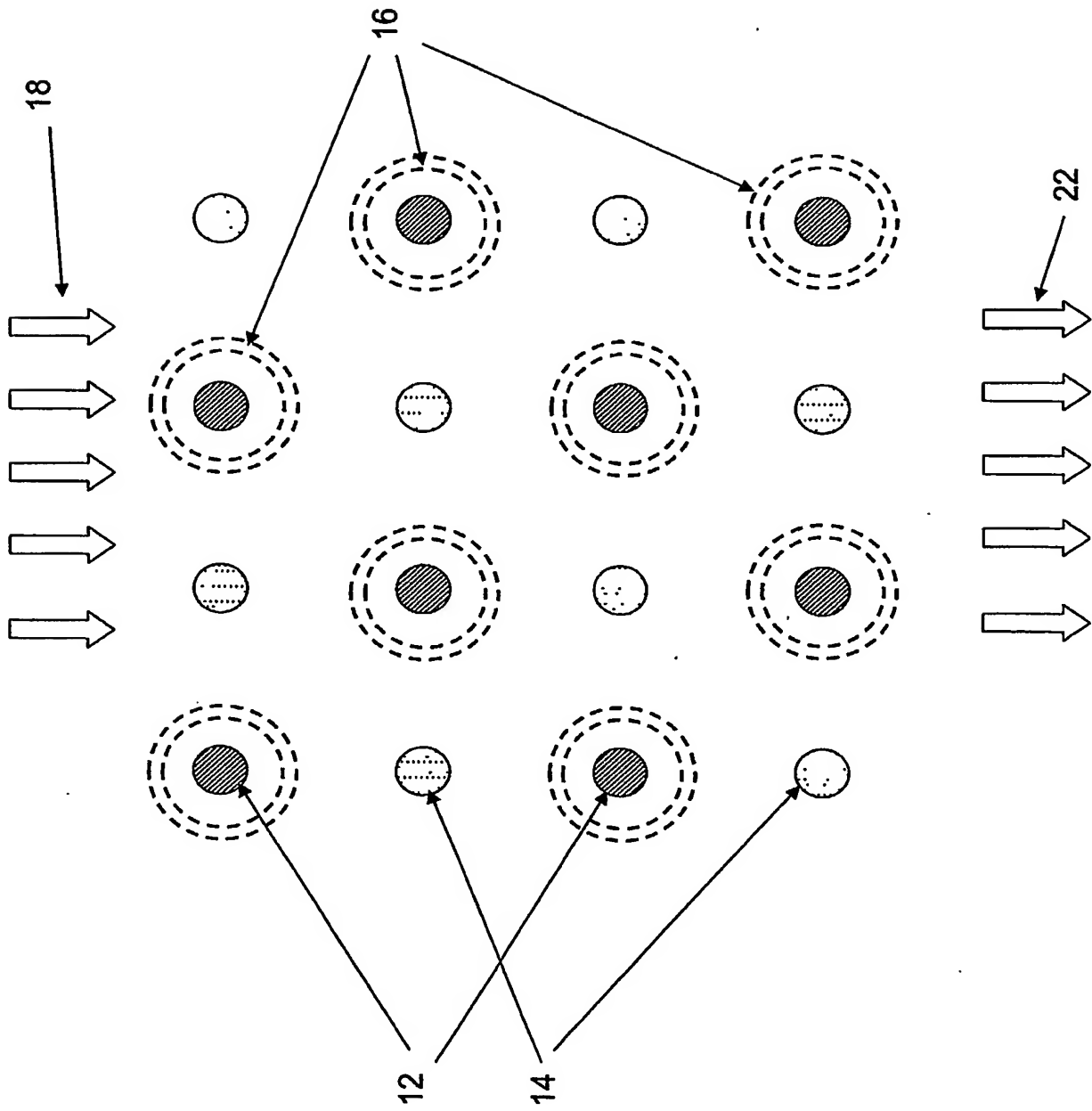
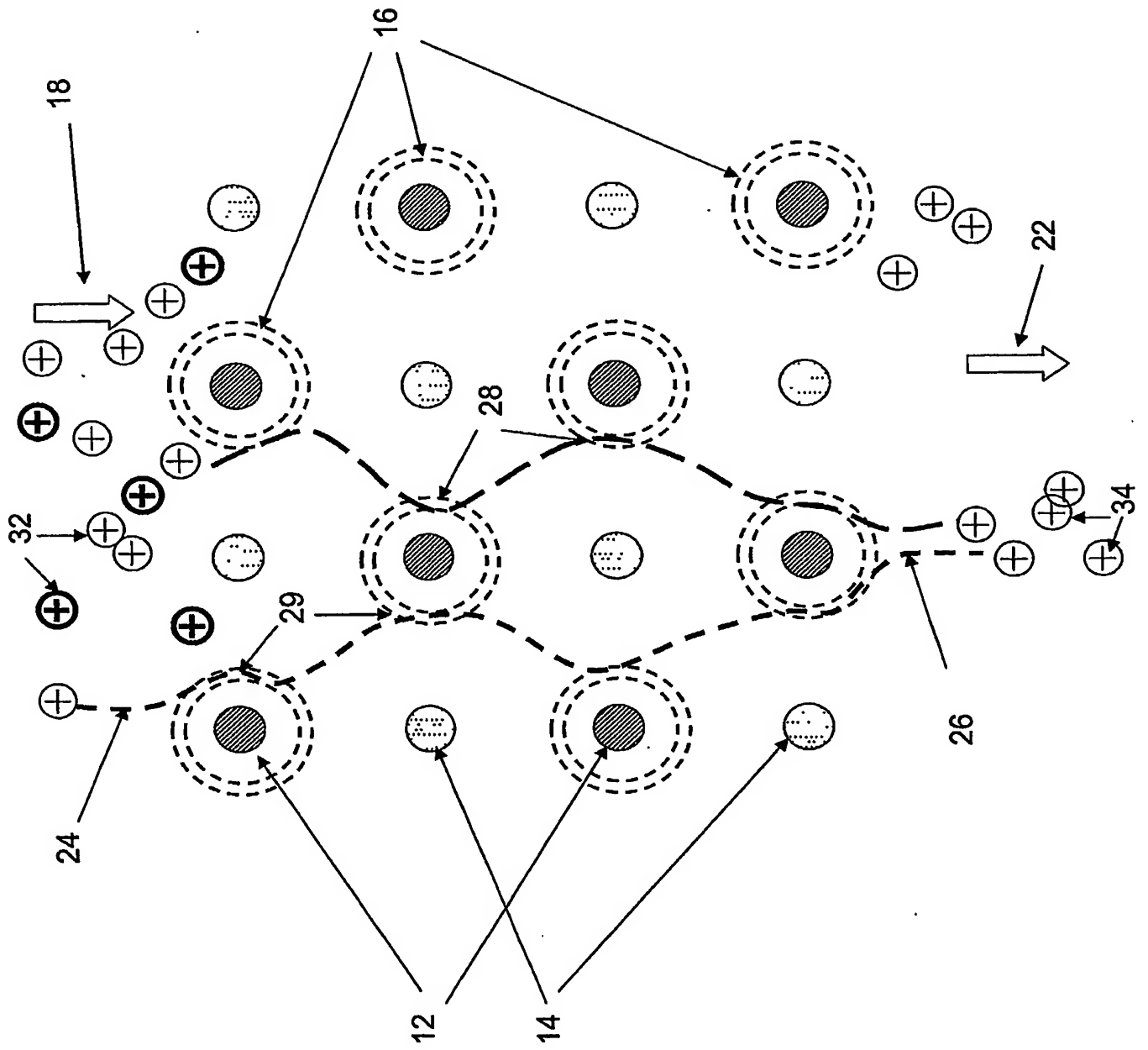


Figure 18



[illegible]

Figure 20

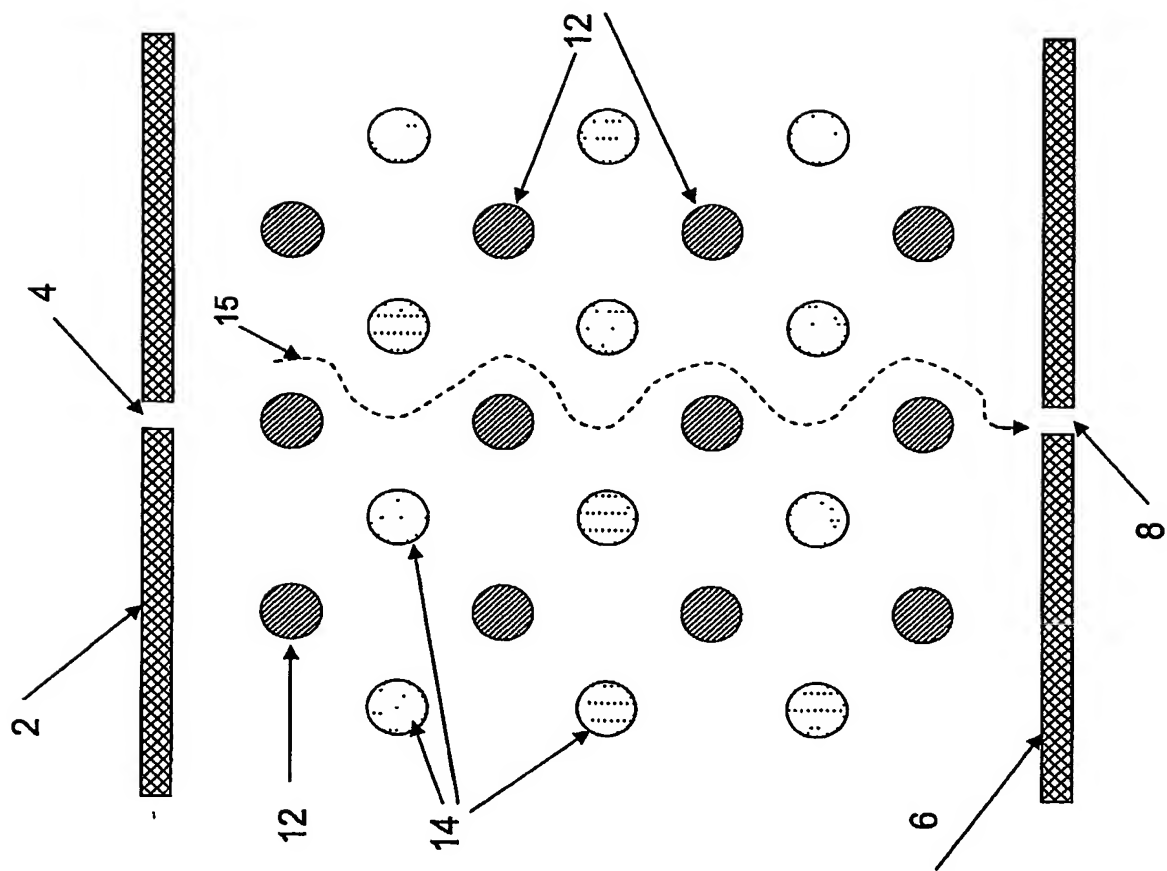


Figure 21

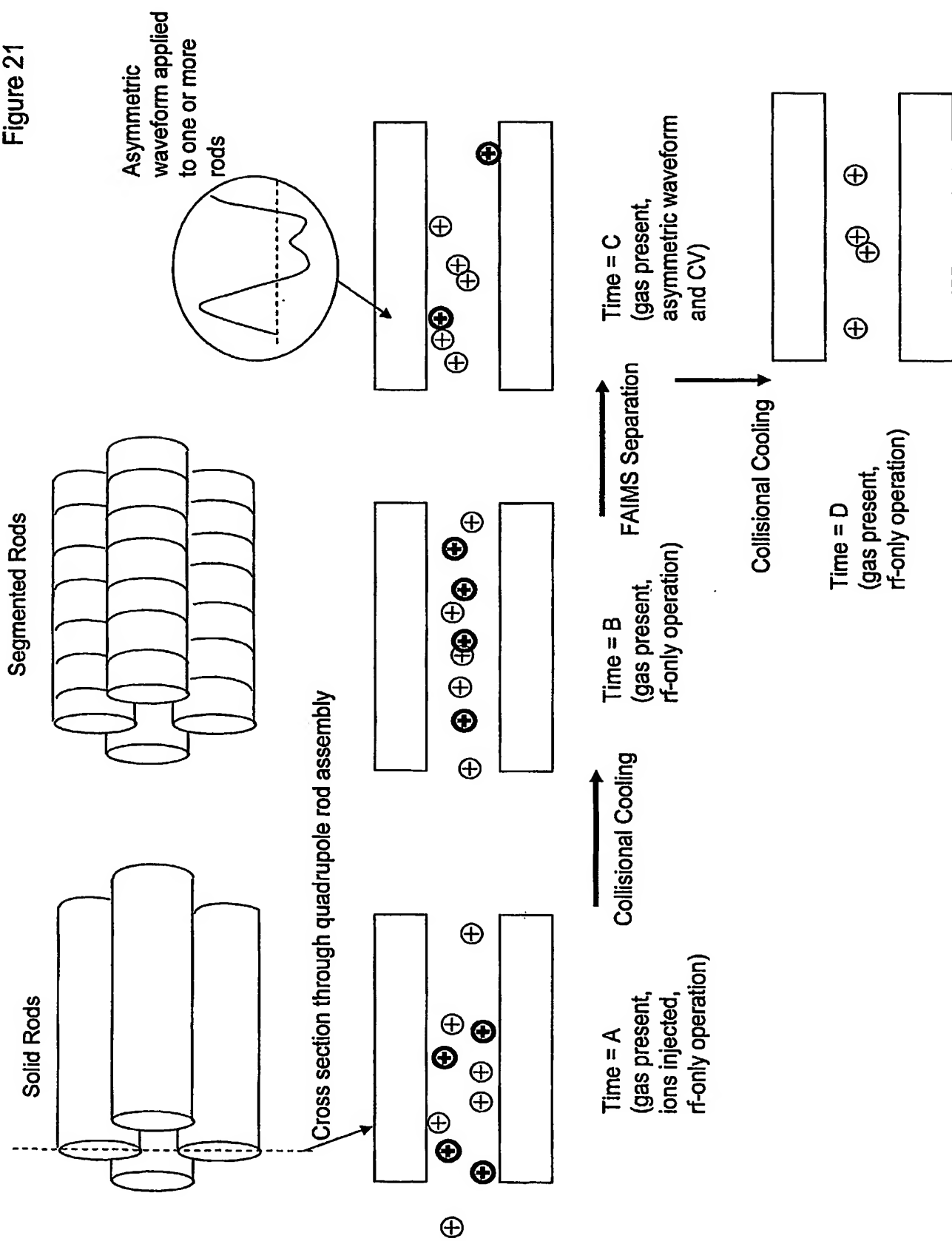


Figure 22

Cross section through segmented quadrupole rod assembly

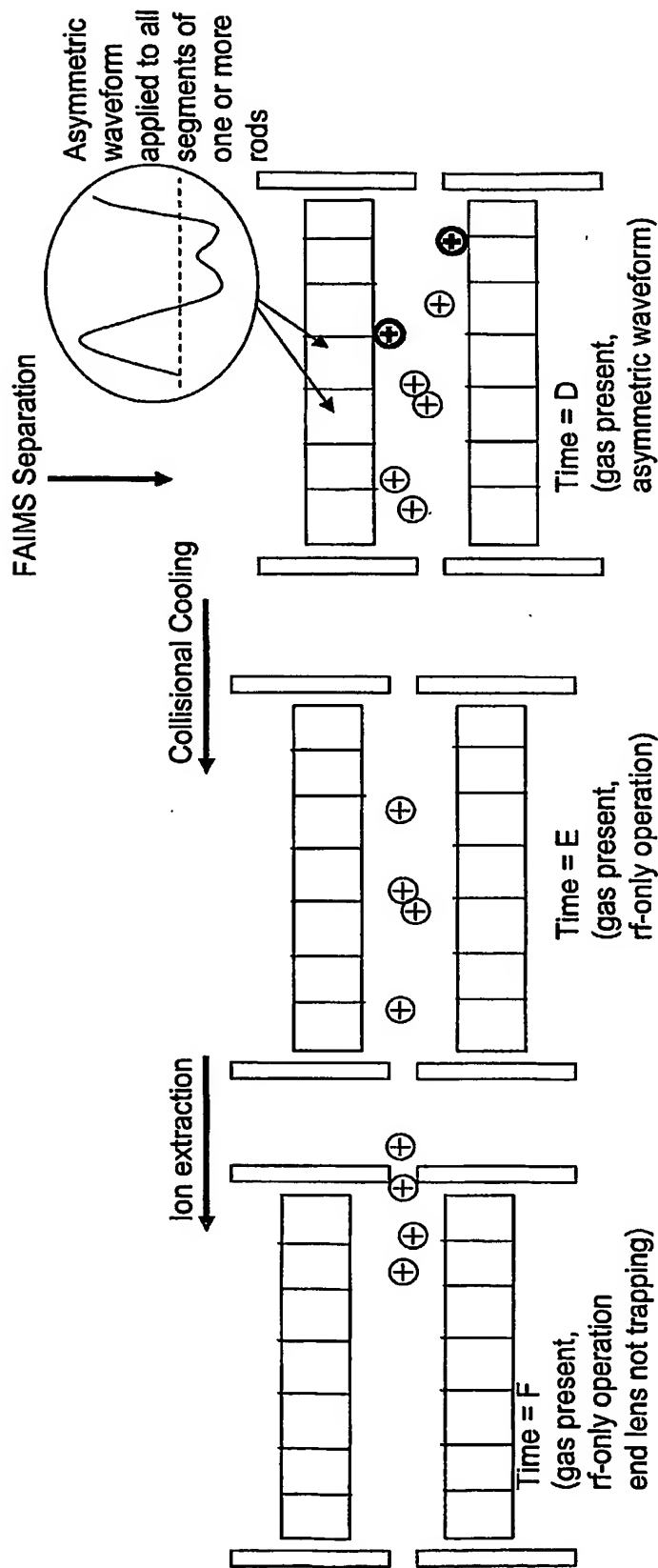
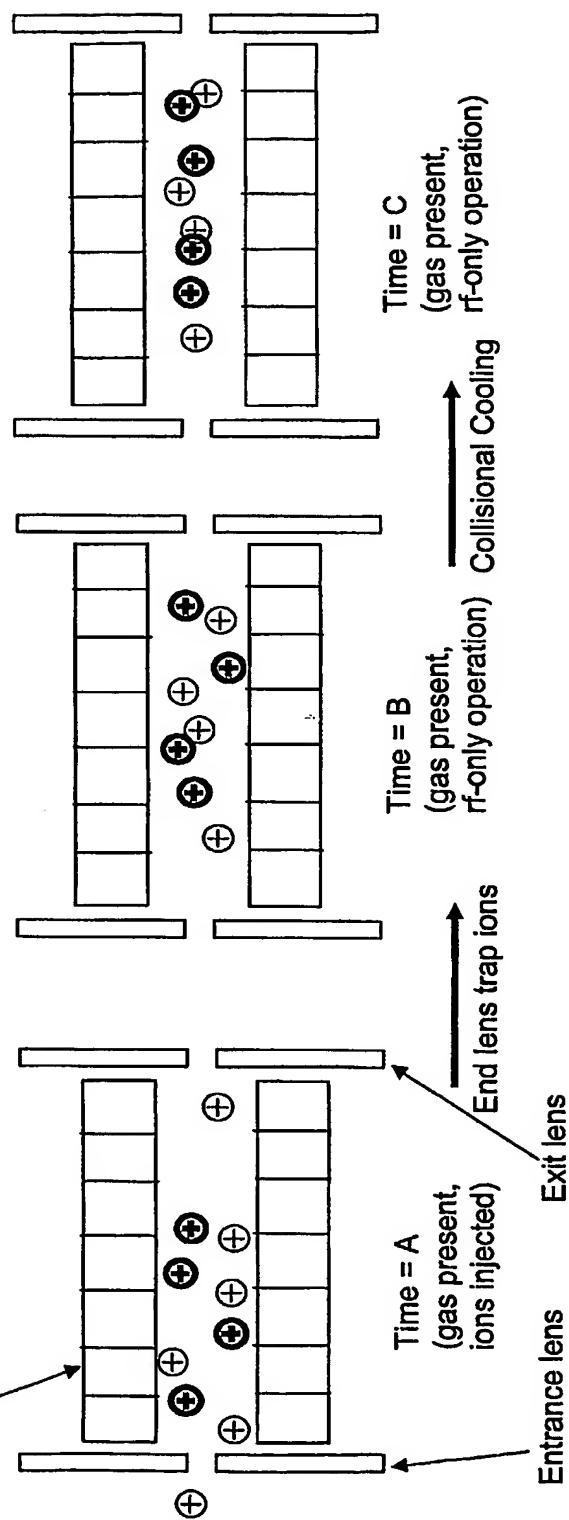




Figure 23

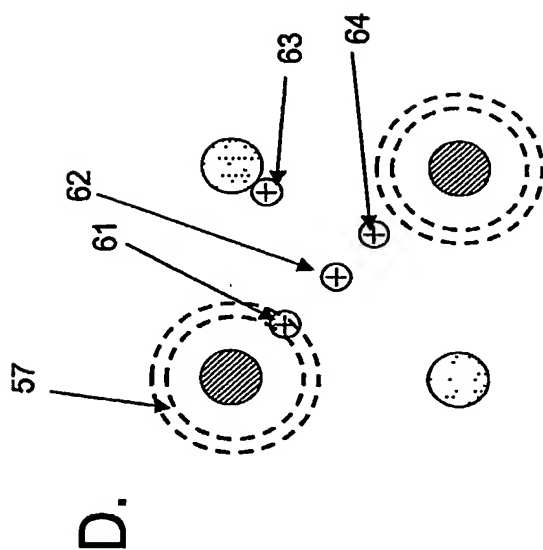
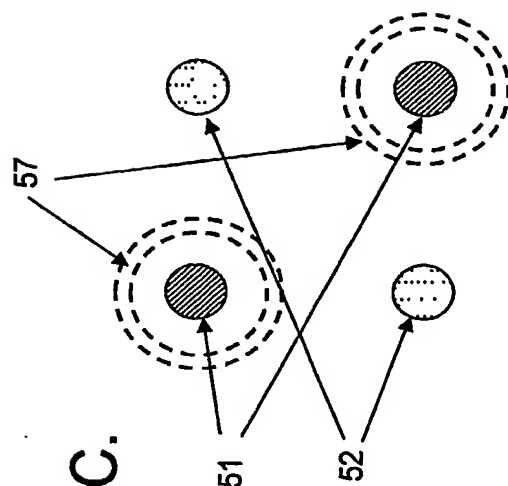
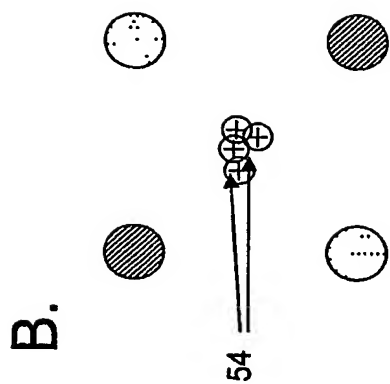
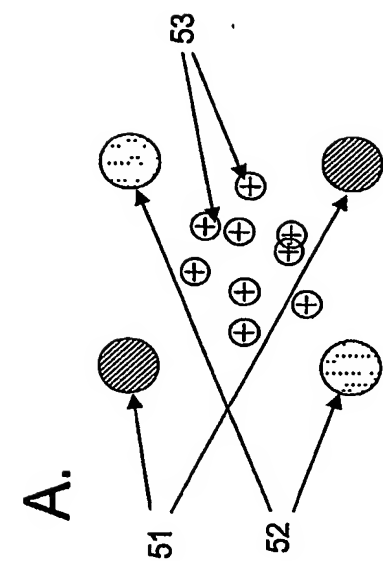
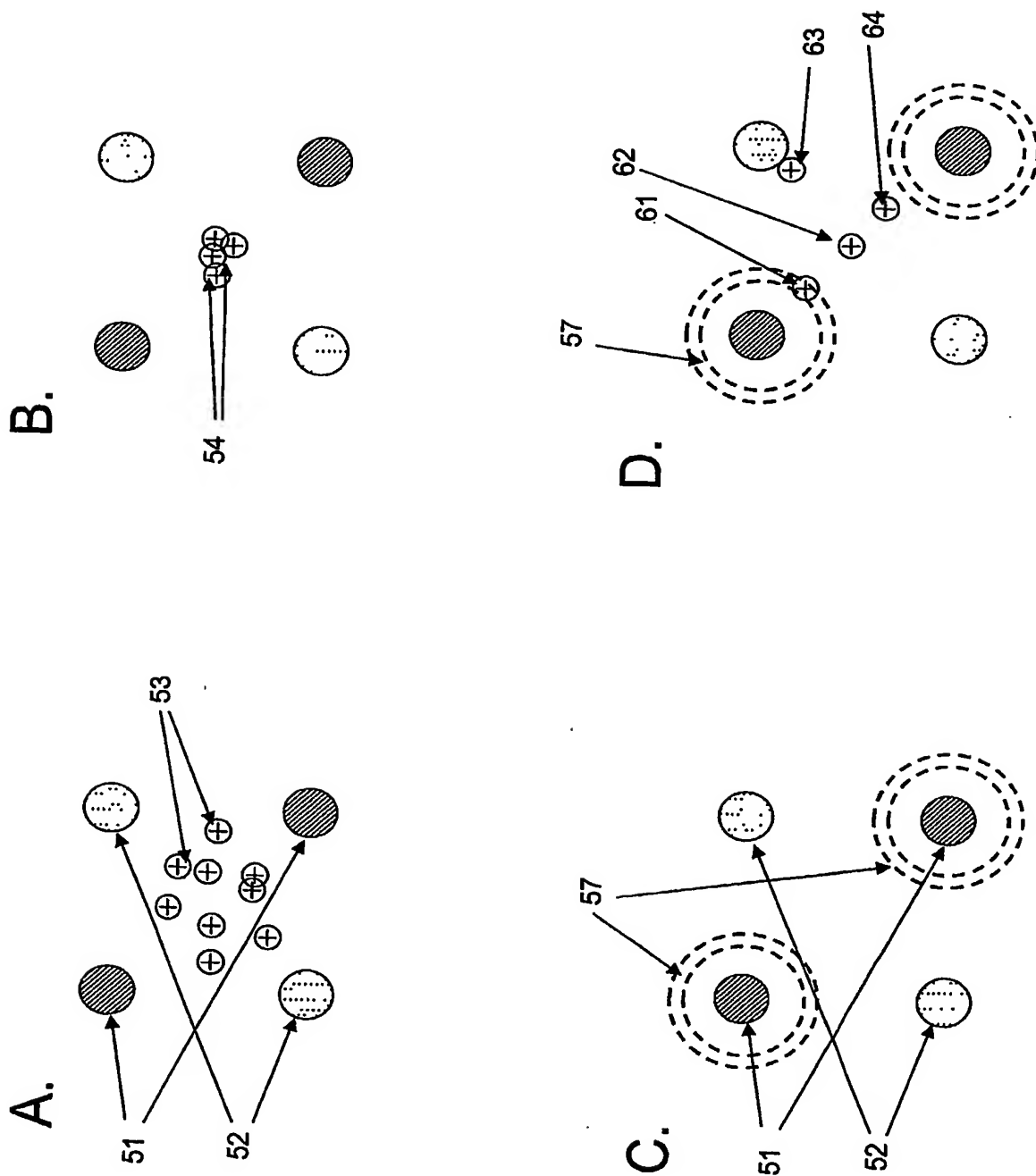


Figure 23



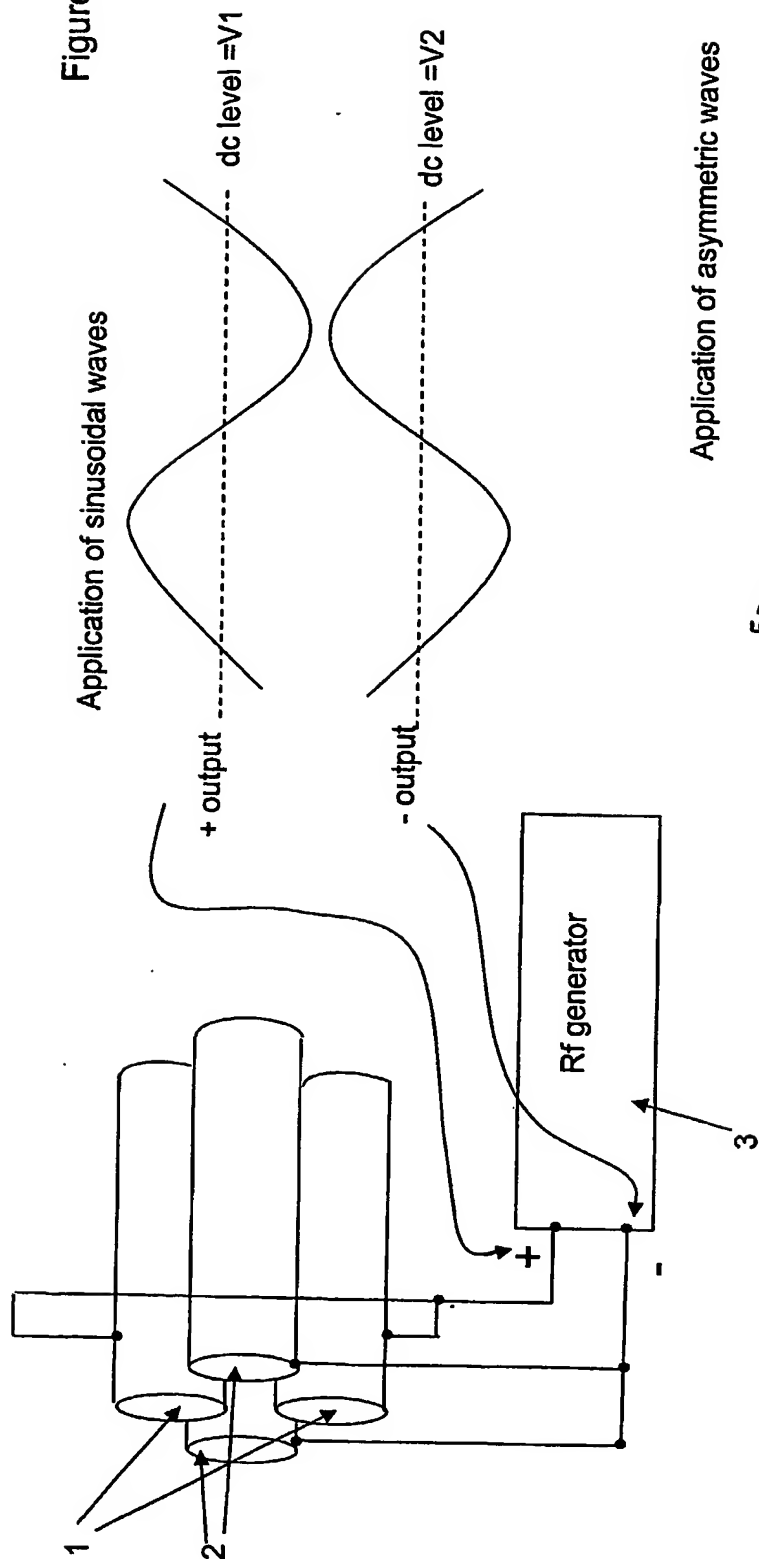
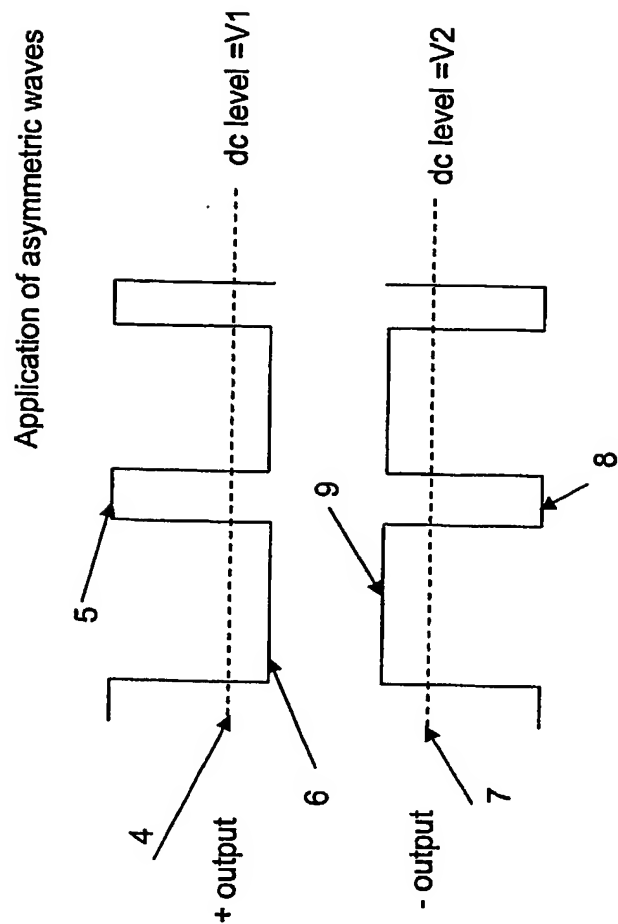
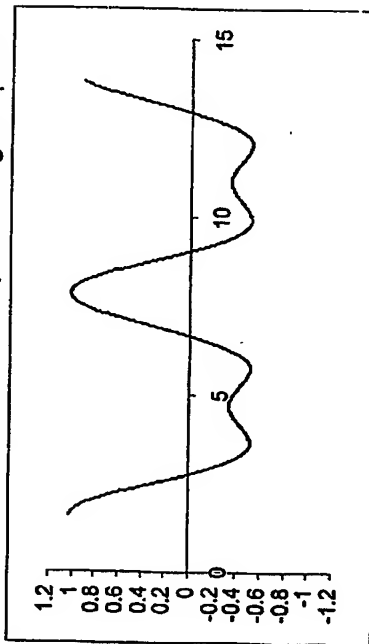


Figure 24

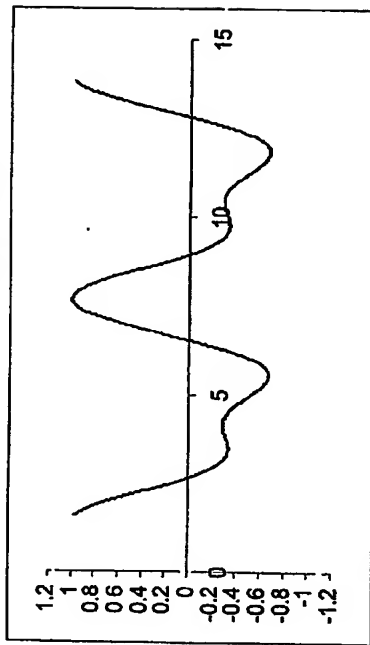


Application of asymmetric waves

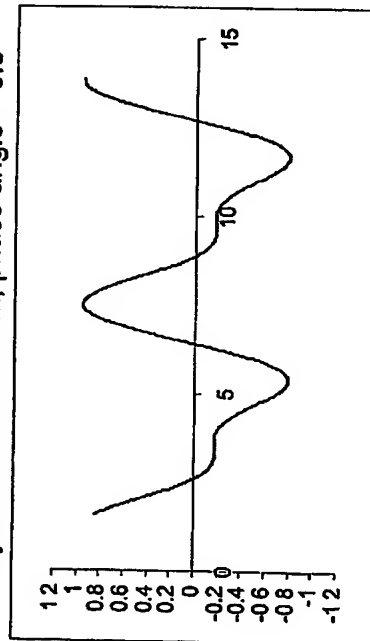
Asymmetric Waveform, phase angle =  $\pi/2$



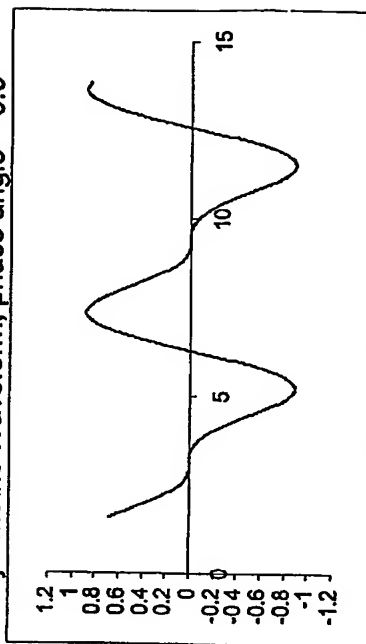
Asymmetric Waveform, phase angle = 1.0



Asymmetric Waveform, phase angle = 0.5



Symmetric Waveform, phase angle = 0.0



All waveforms generated with  $A\sin(\omega t) + B\sin(\omega t - \Phi)$  where  $A/B=2$ ,  $A+B=1$ ,  $\Phi$  is phase shift (radians),  $\omega$  is frequency (radians/s)

**This Page is Inserted by IFW Indexing and Scanning  
Operations and is not part of the Official Record**

**BEST AVAILABLE IMAGES**

Defective images within this document are accurate representations of the original documents submitted by the applicant.

Defects in the images include but are not limited to the items checked:

- ☒ **BLACK BORDERS**
- ☐ **IMAGE CUT OFF AT TOP, BOTTOM OR SIDES**
- ☐ **FADED TEXT OR DRAWING**
- ☐ **BLURRED OR ILLEGIBLE TEXT OR DRAWING**
- ☐ **SKEWED/SLANTED IMAGES**
- ☐ **COLOR OR BLACK AND WHITE PHOTOGRAPHS**
- ☐ **GRAY SCALE DOCUMENTS**
- ☐ **LINES OR MARKS ON ORIGINAL DOCUMENT**
- ☐ **REFERENCE(S) OR EXHIBIT(S) SUBMITTED ARE POOR QUALITY**
- ☐ **OTHER:** \_\_\_\_\_

**IMAGES ARE BEST AVAILABLE COPY.**

**As rescanning these documents will not correct the image problems checked, please do not report these problems to the IFW Image Problem Mailbox.**